UNIVERSIDADE FEDERAL DE MINAS GERAIS

Escola de Veterinária

Programa de Pós-graduação em Ciência Animal

Raquel Rodrigues Soares Santos

LINALOOL, LINALYL ACETATE, AND LAVENDER ESSENTIAL OIL: EVALUATION OF METABOLISM AND DRUG INTERACTIONS IN DOGS USING *IN SILICO* AND *IN VITRO* APPROACHES

Belo Horizonte

2025

Raquel Rodrigues Soares Santos

LINALOOL, LINALYL ACETATE, AND LAVENDER ESSENTIAL OIL: EVALUATION OF METABOLISM AND DRUG INTERACTIONS IN DOGS USING *IN SILICO* AND *IN VITRO* APPROACHES

Thesis presented to the Programa de Pós-graduação em Ciência Animal at the Universidade Federal de Minas Gerais, as a partial requirement for obtaining the title of Doctor in Animal Science.

Advisor: Prof. Dr. Benito Soto Blanco

Co-advisor: Prof. Dr. Michael H. Court

Co-advisor: Prof. Dr. Renata Cristina Mendes Ferreira

Belo Horizonte

202

S237l

Santos, Raquel Rodrigues Soares,1990 -

Linalool, linalyl acetate, and lavender essential oil: evaluation of metabolism and drug interactions in dogs using in silico and in vitro approaches/ Raquel Rodrigues Soares Santos.- 2025.

189f: il.

Orientador: Benito Soto Blanco

Coorientadores: Michael H. Court

Renata Cristina Mendes Ferreira

Tese (Doutorado) apresentada à Faculdade de Medicina Veterinária da UFMG, como requisito parcial para obtenção do título de Doutora em Ciência Animal.

Bibliografia: f. 155 – 189.

1. Cão - Teses - 2. Ciência Animal- Teses – 3. Medicina Veterinária – Teses. I. Soto Blanco, Benito - II. Court, Michael H - III. Ferreira, Renata Cristina Mendes – IV. Universidade Federal de Minas Gerais, Escola de Veterinária - V. Título.

CDD – 636.089

Bibliotecária responsável Cristiane Patrícia Gomes CRB 2569

Biblioteca da Escola de Veterinária, UFMG.

UNIVERSIDADE FEDERAL DE MINAS GERAIS

ESCOLA DE VETERINÁRIA
PROGRAMA DE PÓS-GRADUAÇÃO EM CIÊNCIA ANIMAL

FOLHA DE APROVAÇÃO

RAQUEL RODRIGUES SOARES SANTOS

Tese submetida à banca examinadora designada pelo Programa de Pós Graduação em **CIÊNCIA ANIMAL**, como requisito para obtenção do grau de **DOUTOR(a)** em CIÊNCIA ANIMAL, área de concentração **Medicina e Cirurgia Veterinárias**. Defesa da tese intitulada: **"LINALOOL, LINALYL ACETATE, AND LAVENDER ESSENTIAL OIL: EVALUATION OF METABOLISM AND DRUG INTERACTIONS IN DOGS USING IN SILICO AND IN VITRO APPROACHES."**

Aprovado(a) em 30 de junho de 2025, pela banca constituída pelos membros:

Dr.(a). Benito Soto Blanco - Orientador(a)

Dr.(a). Thiago Roberto Lima Romero

Dr.(a). Raphael Rocha Wenceslau

Dr.(a). Tania Elena Perez Jimenez

Dr.(a). Nicolas Francisco Villarino

Documento assinado eletronicamente por **Nicolas Francisco Villarino**, **Usuário Externo**, em 30/06/2025, às 16:52, conforme horário oficial de Brasília, com fundamento no art. 5º do Decreto nº 10.543, de 13 de novembro de 2020.

Documento assinado eletronicamente por **Tania Elena Perez Jimenez**, **Usuário Externo**, em 30/06/2025, às 16:59, conforme horário oficial de Brasília, com fundamento no art. 5º do Decreto nº 10.543, de 13 de novembro de 2020.

Documento assinado eletronicamente por **Benito Soto Blanco**, **Professor do Magistério Superior**, em 30/06/2025, às 18:22, conforme horário oficial de Brasília, com fundamento no art. 5º do Decreto nº 10.543, de 13 de novembro de 2020.

Documento assinado eletronicamente por **Raphael Rocha Wenceslau**, **Professor do Magistério Superior**, em 30/06/2025, às 18:52, conforme horário oficial de Brasília, com fundamento no art. 5º do Decreto nº 10.543, de 13 de novembro de 2020.

Documento assinado eletronicamente por **Thiago Roberto Lima Romero**, **Professor do Magistério Superior**, em 04/07/2025, às 12:51, conforme horário oficial de Brasília, com fundamento no art. 5º do Decreto nº 10.543, de 13 de novembro de 2020.

A autenticidade deste documento pode ser conferida no site https://sei.ufmg.br/sei/controlador_externo.php?acao=documento_conferir&id_orgao_acesso_externo=0, informando o código verificador **4329096** e o código CRC **C38055A0**.

To Ramona, the reason for the existence of this work.

ACKNOWLEDGMENTS

To God, my spiritual energy, who has never abandoned me.

To Master Jesus, who taught me about kindness and charity.

To the *Orixás*, especially Ogum, tireless warrior, for granting me strength, courage, and protection through every battle fought along this journey; and Exu, lord of crossroads and communication, who opened the paths before me and taught me to trust the movement of life. To both of you, my *axé*, my respect, and my eternal gratitude.

To Dr. Benito Soto Blanco and Dr. Michael Court, who were true father figures throughout this phase of my academic journey. They believed in my work, gave me strength when I felt like giving up, encouraged my projects, and, above all, corrected me, when necessary, always with empathy for my struggles. I could not have asked for better advisors. I also thank Dr. Renata Mendes, not only for trusting my work but especially for sharing her valuable experience with me, acting like a sister and giving me important guidance throughout this path.

To the examination committee, for both qualification and defense, for their contributions and availability.

To CAPES and William R. Jones Endowment, whose financial support made this achievement possible.

To Zhaohui Zhu for her teachings at the Comparative Pharmacogenomics Lab, which allowed me to quickly gain independence in *in vitro* technical procedures. To Arun

Jaiswal, from the Bioinformatics Department at the Institute of Biological Sciences at UFMG, whose help was essential for my *in silico* studies.

To my lifelong friends, Alle, Vitor, and Shayenna, for never abandoning me, even without our daily conversations. To my dear friend Fernanda, always a companion for heartfelt talks. To Igor, who has always remained a close friend and took such good care of Ramona in my absence. To the friends from Pullman, who became my family away from Brazil.

To my family, my roots, my foundation. To my mother Maria, my brother Alex, my sister-in-law Fernanda, and especially my nephews Isabela and Lucca, who help me stay in touch with my inner child while also warmly embracing my adult advises. To my father, who, though physically absent from this realm, remains alive in me through his teachings on ethics, integrity, and, above all, his devotion to learning. These values are deeply rooted in my personality, my memory, and my heart.

To Gomez, who taught me how to face the challenges of living far from my loved ones in my homeland—and who became the one I love most.

Finally, I thank Ramona. More than being a therapy dog, she is the reason this entire journey was possible. She is my companion, my friend, my lifeline. I have no words to thank her enough.

“(…) The safety attributable to (…) natural products is overestimated” (Johnson Afonne and Chinedu Ifediba, 2022).

RESUMO

O uso de óleos essenciais (OEs) na medicina veterinária tem ganhado destaque, especialmente após a pandemia de COVID-19, devido às suas propriedades ansiolíticas, analgésicas e anti-inflamatórias. Dentre eles, o óleo essencial de lavanda (Lavandula angustifolia, LEO) é um dos mais estudados. Seus principais constituintes ativos são o linalol (LIN) e o acetato de linalila (LINAct), compostos com efeitos terapêuticos amplamente descritos. No entanto, há lacunas quanto à farmacocinética desses compostos em cães, especialmente no que se refere à metabolização hepática e ao risco de interações medicamentosas, já que muitos pacientes veterinários recebem múltiplos fármacos concomitantemente. Este estudo visou investigar os mecanismos de metabolização de LIN e LINAct em cães, bem como seu potencial de interação com enzimas do citocromo P450 (CYP450), por meio de abordagens combinadas *in silico* e *in vitro*. As enzimas CYP2B11, CYP2C21 e CYP2D15 foram modeladas com o SWISS-MODEL e validadas com o PROCHECK, apresentando mais de 90% dos resíduos em regiões favoráveis nos gráficos de Ramachandran. O docking molecular com AutoDock Vina e MOE indicou que LIN interage com resíduos catalíticos das três isoformas, enquanto LINAct interagiu majoritariamente com CYP2B11 e CYP2D15. A análise farmacofórica revelou cinco características para LIN (duas regiões hidrofóbicas, uma doadora/aceptora de H+ e duas AtomQ) e sete para LINAct (cinco hidrofóbicas, uma aceptora de H+ e uma AtomQ). Nos estudos *in vitro*, utilizaram-se microssomos hepáticos caninos (pDLMs) e enzimas recombinantes (rCYPs). A quantificação foi feita por HPLC/MS, com tempos de retenção de 1,53 min (LIN) e 1,81 min (LINAct). A CYP2B11 foi a principal enzima metabolizadora do LIN, seguida por CYP2C21. A presença de

NADPH aumentou a depleção de ambos os compostos. LINAct apresentou depleção também em microssomos fervidos, indicando participação de esterases. Os parâmetros cinéticos de LIN indicaram Km de 52 µM e constante de depleção (k) de 0,050 min^{-1}, permitindo o cálculo da depuração intrínseca (CLint). Foram avaliados efeitos inibitórios e indutivos sobre CYP2B11, CYP2C21, CYP2D15 e CYP3A12. LIN, LINAct e LEO inibiram a CYP2B11, mas não as demais. A pré-incubação aumentou a inibição do LIN sobre o metabolismo do tramadol e reduziu a do LINAct. Os achados indicam que LIN é preferencialmente metabolizado pela CYP2B11, enquanto LINAct tem metabolismo mais limitado. Ambos os compostos, assim como o LEO, apresentam potencial de interação medicamentosa. Esses resultados destacam a importância das abordagens *in silico* e *in vitro* na predição do metabolismo e na segurança do uso terapêutico de OEs em cães, ressaltando a necessidade de estudos *in vivo* complementares.

Palavras-chave: *Lavandula angustifolia*; metabolismo; CYP; linalol; acetato de linalila.

ABSTRACT

The use of essential oils (EOs) in veterinary medicine has gained prominence, especially after the COVID-19 pandemic, due to their anxiolytic, analgesic, and anti-inflammatory properties. Among them, lavender essential oil (Lavandula angustifolia, LEO) is one of the most studied. Its main active constituents are linalool (LIN) and linalyl acetate (LINAct), compounds with well-documented therapeutic effects. However, there are still gaps regarding the pharmacokinetics of these compounds in dogs, particularly concerning hepatic metabolism and the risk of drug interactions, an essential aspect considering that many veterinary patients receive multiple medications simultaneously. This study aimed to investigate the metabolic pathways of LIN and LINAct in dogs, as well as their interaction potential with cytochrome P450 (CYP450) enzymes, using a combined *in silico* and *in vitro* approach. The canine enzymes CYP2B11, CYP2C21, and CYP2D15 were modeled using SWISS-MODEL and validated with PROCHECK, showing over 90% of residues in favorable regions of the Ramachandran plots. Molecular docking using AutoDock Vina and MOE revealed that LIN interacts with catalytic residues of all three isoforms, while LINAct interacted mainly with CYP2B11 and CYP2D15. Pharmacophore analysis identified five features for LIN (two hydrophobic regions, one H-bond donor/acceptor, and two AtomQ regions) and seven for LINAct (five hydrophobic, one H-bond acceptor, and one AtomQ). In *in vitro* assays, canine liver microsomes (pDLMs) and recombinant enzymes (rCYPs) were used. Quantification was performed by HPLC/MS, with retention times of 1.53 min (LIN) and 1.81 min (LINAct). CYP2B11 was the primary enzyme responsible for LIN metabolism, followed by CYP2C21. The presence of NADPH increased the depletion of both compounds. LINAct also showed depletion in boiled

microsomes, indicating esterase activity. The kinetic parameters for LIN revealed a Km of 52 µM and a depletion constant (k) of 0.050 min^{-1}, allowing the calculation of intrinsic clearance (CLint). Inhibitory and inductive effects were evaluated using substrates, inhibitors, and inducers of CYP2B11, CYP2C21, CYP2D15, and CYP3A12. LIN, LINAct, and LEO inhibited CYP2B11, but not the other isoforms. Pre-incubation enhanced LIN's inhibitory effect on tramadol metabolism and reduced that of LINAct. These findings indicate that LIN is preferentially metabolized by CYP2B11, while LINAct shows lower metabolic activity. Both compounds, as well as LEO, demonstrated potential drug interaction. These results underscore the relevance of *in silico* and *in vitro* approaches in predicting metabolism and drug interactions and highlight the need for complementary *in vivo* studies to ensure the safe therapeutic use of LEO in dogs.

Keywords: *Lavandula angustifolia*; metabolism; CYP; linalool; linalyl acetate.

FIGURES LIST

TABLE LIST

EQUATION LIST

LIST OF ABBREVIATIONS AND ACRONYMS

3D	Three-dimensional
CLint	Intrinsic clearance
C_{max}	Maximum plasma concentration
CYP	Cytochrome P450
EDDP	2-Ethylidene-1,5-dimethyl-3,3-diphenylpyrrolidine
EO	Essential oil
GMQE	Global Model Quality Estimate
IC_{50}	Half-maximal inhibitory concentration
LEO	Lavender essential oil
LIN	Linalool
LINAct	Linalyl acetate
m-CCP	m-Chlorophenylpiperazine
MOE	Molecular Operating Environment
pDLMs	Canine liver microsomes

TABLE OF CONTENTS

1 INTRODUCTION

1 INTRODUCTION

1.1 DRUG DISCOVERY AND DEVELOPMENT

Literature describes that since prehistory, there has been constant concern about the appearance of diseases in human and animal populations as well as how to treat them (Ramirez Rozzi and Froment, 2018). With advances in medicine and the pharmaceutical industry, human life expectancy has increased. In 1920, the life expectancy in Brazil was 35 years, and by 2010, it had risen to 74, almost double the 90-year mark (Miranda *et al.*, 2016). At the beginning of the twentieth century, in the world, the average age was 31–32 years, with values practically doubled in 2021: 71 years (Dattani *et al.*, 2023). However, these advances in the treatment of diseases do not occur quickly. The slow, standardized, and multidisciplinary process for the discovery and development of new drugs followed by their launch on the market takes at least 10 years, in addition to an investment of thousands of dollars over this time (Figure 1), even though a new drug is usually derived from natural substances with known effects (Rang *et al.*, 2011; Ediriweera *et al.*, 2019; Davanço *et al.*, 2020; Chopra and Dhingra, 2021; Ma *et al.*, 2021), and it depends mainly on the amount invested and is generally linked to an industry or academic institution. This occurs because of several phases of the studies, such as *in silico* processing and clinical trials (Rang *et al.*, 2011; Wohlleben *et al.*, 2016; Ma *et al.*, 2021; Sampathkumar and Kerwin, 2024). Recently, with the advancement of bioinformatics, *in silico* research has gained prominence as a pre-*in vitro* research method (Chopra and Dhingra, 2021), thereby avoiding unnecessary expenses in the other stages of drug development. However, it is often necessary to return to the previous steps or even restart the entire study due to the limitations inherent in each phase (Ma *et al.*, 2021; Xiong *et al.*, 2021).

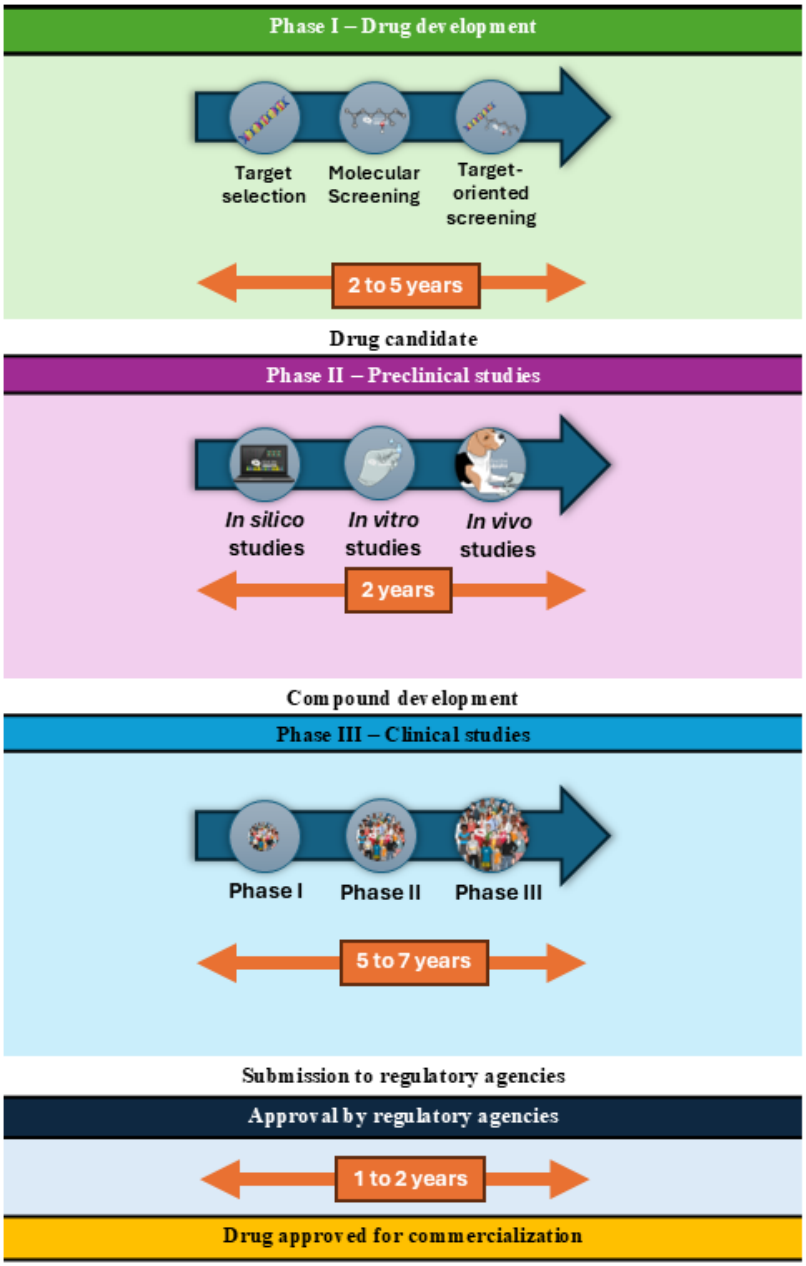

Figure 1 Process of discovery and development of new drugs, based in Rang et al. (2011); Sampathkumar & Kerwin (2024); Wohlleben et al. (2016).

In recent years, approximately 70% of pharmaceutical companies have started preclinical research for drug discovery and development with a study *in silico* (Piñero *et al.*, 2018; Loiodice *et al.*, 2019), in which computer software and bioinformatics tools are used to perform ligand prediction (Chopra and Dhingra, 2021; Fernández-Quintero *et al.*, 2023), study physicochemical characteristics of the molecule, pharmacophoric properties, and, mainly, prediction of pharmacokinetic properties of absorption, distribution, metabolization, and excretion (Piñero *et al.*, 2018; Loiodice *et al.*, 2019; Fernández-Quintero *et al.*, 2023), which help to direct the assays *in vitro* and analyze the profile of the drug in different concentrations and how its kinetics are in the body, often reducing the costs and time of the analyses (Piñero *et al.*, 2018; Chopra and Dhingra, 2021; Kar and Chatterjee, 2021; Ma *et al.*, 2021; Fernández-Quintero *et al.*, 2023). In addition, *in silico* tests make it possible to predict binding to enzymes involved in the metabolization of drugs, such as enzymes of the cytochrome P450 (CYP450) family (Mackenzie *et al.*, 2017; Piñero *et al.*, 2018), the results of which can be used to support in vitro studies on toxicity and drug interactions, in addition to contributing to the reduction of the use of animals in *in vivo* studies (Piñero *et al.*, 2018; Chopra and Dhingra, 2021; Xiong *et al.*, 2021). Molecular screening is a possibility in this phase.

The second stage of the process involves *in vitro* experiments. These relatively simple analyses with relatively fast processing use a cellular environment under controlled conditions to reproduce an organic system (Ediriweera *et al.*, 2019; Davanço *et al.*, 2020; Morofuji and Nakagawa, 2020; Ma *et al.*, 2021). During the study, *in vitro* screening of the pharmacokinetic processes that support and indicates possibilities for the analyses that

will be carried out *in vivo* (Loiodice *et al.*, 2019; Ma *et al.*, 2021). However, due to the less complex characteristics of living organisms, the results were often not the same as those obtained in the *in vivo* study (Mackenzie *et al.*, 2017; Loiodice *et al.*, 2019; Davanço *et al.*, 2020). One of the key pharmacokinetic processes in this phase is metabolization assays, which predict whether a species can eliminate the drug from the body or whether it accumulates (Loiodice *et al.*, 2019; Xing, 2021). This is the first step in organically evaluating the safety of a molecule and the possibility of drug interactions (Mackenzie *et al.*, 2017; Loiodice *et al.*, 2019; Kar and Chatterjee, 2021). Even drugs already on the market can be reevaluated *in vitro* when adverse reactions in the population are described (Morofuji and Nakagawa, 2020).

In vivo studies are those conducted on animals (Ma *et al.*, 2021). In human medicine, several animal models are used, such as rodents, dogs, rabbits and pigs, representing 64% of the studies (Sim and Kauser, 2015; Loiodice *et al.*, 2019; Davanço *et al.*, 2020), due to the similarity with the phenotype and pathophysiology of the disease in relation to humans (Sim and Kauser, 2015), in addition to responding to drug therapies in a similar way to people. In veterinary medicine, models tend to be more species-specific, according to the indication for the drug to be developed (Gronkiewicz *et al.*, 2016; Mueller and Olivry, 2017; Seangseerattanakulchai and Piratae, 2021). Animal studies are considered the "gold standard" for preclinical drug validation (Sim and Kauser, 2015; Ma *et al.*, 2021), once it is possible to obtain data on the safety and efficacy of a drug. This step is crucial for discovering and developing new drugs (Sim and Kauser, 2015). If a compound is not approved at this stage, it is necessary to restart the treatment changing,

for example, the molecular characteristics of the drug. This leads to delays and increased costs associated with bringing a drug to the market (Ma *et al.*, 2021).

All these steps are called preclinical studies. Thus, after these analyses, clinical studies are conducted in humans to determine the appropriateness of the medication. Only after the drug has satisfactory results in clinical studies and passes approval from regulatory agencies can it be authorized to be launched on the market (Loiodice *et al.*, 2019; Ma *et al.*, 2021).

1.2. LIGAND PREDICTION AND BIOINFORMATICS APPLIED TO DRUG DEVELOPMENT

The development of computational technologies, as well as the increase in databases on therapeutic targets and possible ligands, has contributed to the increasing use of *in silico* methodologies and, consequently, to the reduction of the cost of identifying potential drugs (Lohning *et al.*, 2017; Pinzi and Rastelli, 2019).

Molecular modeling (Figure 2) is useful for analyzing data related to the structure of biological targets and ligand activity in the ligand-target complex (Ferreira *et al.*, 2015). In addition, they also provide predicted information on the pharmacodynamic characteristics of ligand potency, efficacy, affinity, and selectivity, as well as the pharmacokinetic and toxicological safety characteristics of the target (ADMET) (Ferreira *et al.*, 2015; Yuan and Xu, 2018; Xia *et al.*, 2023).

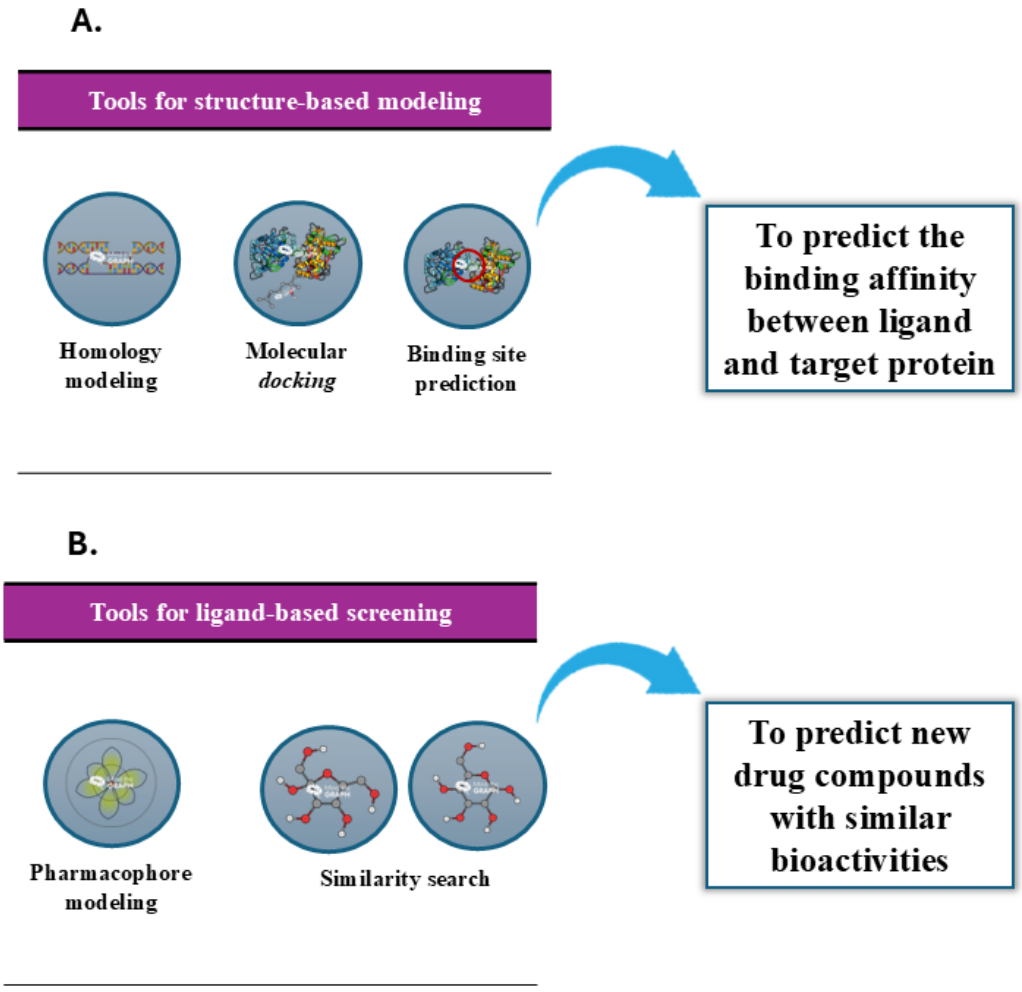

Figure 2 Types of molecular models commonly used in the discovery and development of new drugs. **A.** Examples of computational tools commonly used to predict binding affinity and binding sites in the target protein. Target proteins may be modeled using homology modeling if the structure is not found in the database. **B.** Ligand-based tools are useful for predicting the molecular features of ligands and for searching for similarity between compounds. Note that the *in silico* methodology is not limited to these types of modeling. For a better understanding of the subject, see Xia; Chen; Zhang (2023).

1.2.1 Structure-based modeling

Structure-based methods use the three-dimensional (3D) structure of a biological target, which is crucial for drug development (Muhammed and Aki-Yalcin, 2019; Rebehmed *et al.*, 2022). The classification of the molecules collected in the databases and carried out

according to the structure (Ferreira *et al.*, 2015; Lohning *et al.*, 2017; Pinzi and Rastelli, 2019) and data can inform about the binding energy, molecular interactions, and conformational changes of the target, which are often related to electrostatic and stereochemical properties, that is, how the distribution of charges around that protein occurs, defining, therefore, the binding affinity (Ferreira *et al.*, 2015; Lohning *et al.*, 2017). The greater the affinity of the ligand for the structure, the greater the capacity for cellular changes to occur and therefore, the greater the pharmacological effect (Ferreira *et al.*, 2015).

One such method is molecular modeling, which allows the interactions between molecules and targets to be predicted from databases of already known structures (Ferreira *et al.*, 2015; Pinzi and Rastelli, 2019). These structures can be found in Protein DataBank (PDB) (Berman, 2000) and analyzed using online platforms, such as AlphaFold2 (Jumper *et al.*, 2021; Rebehmed *et al.*, 2022). This technique began in the mid-1970s, but the study by Kuntz et al. (1982) revolutionized molecular modeling by geometrically evaluating the alignment between ligands and receptors in the heme-myoglobin/methemoglobin and thyroxine/prealbumin clusters. This study also made it possible to describe hydrogen bonds in the protein-ligand interaction (Kuntz *et al.*, 1982; Pinzi and Rastelli, 2019). Thus, with the first algorithms being built in the 80s, molecular modeling and docking have become essential tools for the discovery and development of new drugs (Ferreira *et al.*, 2015). Ring et al. (1993) also used structure-based methods for drug development when evaluating the docking between nonpeptide inhibitors and enzymes of the serine and cysteine protease families (Ring *et al.*, 1993; Pinzi and Rastelli, 2019). Thus, docking allows evaluation of the structure-ligand complex and correlation

with biological effects, thereby increasing the ability to identify ligands that have greater affinity with the target protein (Ferreira *et al.*, 2015; Lohning *et al.*, 2017).

Despite their efficiency in studying the structure of biological targets and interactions with possible ligands (Ferreira *et al.*, 2015), these methods have limitations. Due to docking depending on the existence of a database, the sampling of both ligands and receptors is restricted (Pinzi and Rastelli, 2019). In addition, the values obtained from the mathematical functions performed by artificial intelligence may differ from those found in the bench experiments, and even if they are approximate, this can lead to incorrect interpretations of the results (Pinzi and Rastelli, 2019).

1.2.2 Homology Modeling

When the structure under study is not present in the database, homology modeling from an existing model is necessary, which can generate inconsistencies in the result (Lohning *et al.*, 2017; Pinzi and Rastelli, 2019).

This step of *the in silico* analysis builds a 3D structure of the target protein from a model with similar characteristics (Lohning *et al.*, 2017; Muhammed and Aki-Yalcin, 2019), assuming that similar structures tend to exhibit similar biological activities (Muegge and Mukherjee, 2016). The two structures must be practically identical not only in spatial conformation but also in amino acid sequence (Lohning *et al.*, 2017; Muhammed and Aki-Yalcin, 2019), thus respecting the two fundamental principles of homology modeling: (a) the amino acid sequence determines the structure of the protein and (b) the 3D structure of the generated protein must be similar to the 3D structure of the model (Hameduh *et al.*,

2020). The low availability of reliable models is a limitation of homology modeling, despite its common use in drug discovery (Lohning *et al.*, 2017).

Platforms for homology modeling include MODELLER (Webb and Sali, 2016) and (Arnold *et al.*, 2006) SWISS-MODEL, as well as AlphaFold (Hameduh *et al.*, 2020; Jumper *et al.*, 2021).

1.2.3 LIGAND-BASED MODELING

Ligand-based methods can be used to predict optimal conformations for specific ligands that are found in ligand libraries (Ferreira *et al.*, 2015; Pinzi and Rastelli, 2019).

One of these methods is pharmacophoric ligand analysis, which improves the prediction of molecular docking when evaluating the stability of complexes (Ferreira *et al.*, 2015; Pinzi and Rastelli, 2019). According to the International Union of Pure and Applied Chemistry (IUPAC), the pharmacophoric properties of a ligand "is the set of steric and electronic features necessary to ensure optimal supramolecular interactions with a specific biological target structure and to trigger (or block) its biological response" (Wermuth *et al.*, 1998). They show the ability to perform hydrogen bonding, hydrophobic and electrostatic interactions, or charge transfer and are useful for identifying specific regions of interaction with the target protein that can block it (Wolber and Langer, 2005; Jade *et al.*, 2022). Data such as solubility and molecular volume can also be collected (Ferreira *et al.*, 2015). Thus, the goal of pharmacophoric analysis is to identify a good ligand for the target protein and to help define its pharmacological activity (Ferreira *et al.*, 2015; Jade *et al.*, 2022).

Wang et al. (2013) evaluated the pharmacophoric properties and binding stability of a series of compounds with binding potential with the amyloid β-42 protein, which plays a role in the pathophysiology of Alzheimer's disease. Compounds with better binding stability and pharmacophoric properties should be selected for further *in vitro* assays (Wang *et al.*, 2013; Pinzi and Rastelli, 2019). Mohebbi (2023) used the same approach to identify a potential inhibitor of the carcinogenic protein Smoothened (SMO) (Mohebbi, 2023). These are examples of the application of ligand-based *in silico* assay methods.

Some tools, such as MOE (Chemical Computing Group ULC, 2025), can be useful for the 3D modeling of these properties and can help visualize the interaction of the ligand with the target protein (Ferreira *et al.*, 2015). A limitation of this type of methodology is the need to create a tool capable of developing accurate molecular alignment using the proposed algorithm (Ferreira *et al.*, 2015; Lohning *et al.*, 2017).

With structure-based methods, ligand-based methods can be used to predict the ability of a ligand to interact with the target molecule (Pinzi and Rastelli, 2019). When used together, this makes the analysis *in silico* versatile because both methods act synergistically and are integrated in terms of the collection of structural, chemical, and biological data of the target and the ligand under study (Ferreira *et al.*, 2015). The study by Qiao et al. (2024) is an example of this synergy, in which the authors performed structure-based and pharmacophore-based (ligand-based) screening to obtain a dual candidate that could concomitantly inhibit the AXL receptor tyrosine kinase and the histone deacetylase-2 enzyme, which participate in the pathophysiology of colorectal cancer. The results could be used in future *in vitro* and *in vivo* trials (Qiao *et al.*, 2024).

1.3 *IN VITRO* ASSAYS

For a compound to be a drug, it needs to be successful as a biologically active molecule, have pharmacokinetic characteristics (absorption, distribution, metabolization, and excretion) and toxicity (ADMET) (Zhu *et al.*, 2015; Fernández-Quintero *et al.*, 2023). The potency and selectivity of a drug are also evaluated in this phase, and metabolization and potency assays can be performed concomitantly to reduce study time (Xiong *et al.*, 2021; Fernández-Quintero *et al.*, 2023). It is important to notice that in *in vitro* assays it is possible to perform only metabolism assays. Absorption, distribution, and excretion of a given molecule in a specific species are only "indicative of" and can be extrapolated from observed data using specific tools.

In relation to the toxicity of a drug, the *in vitro* assays aim to evaluate hepatotoxicity and cardiotoxicity, which are the main causes of drug withdrawals from the market (Loiodice *et al.*, 2019). These assays are also able to provide information about the metabolization profile of the compound. Metabolization is a crucial part of supporting assays *in vivo*, mainly because it is often species-specific. Anticonvulsant drugs, for example, are toxic to canine hepatocytes, but not to rodents (Nicolas *et al.*, 2014; Loiodice *et al.*, 2019). Dogs can metabolize some compounds well, although cats are not, generating drug poisoning for these animals (Lascelles *et al.*, 2007; Court, 2013b; Martinez *et al.*, 2018). In addition, toxicity testing involves drug interactions, such as assessing a drug's ability to induce or inhibit CYP, which is also often species-specific (Martinez *et al.*, 2013, 2018; Loiodice *et al.*, 2019). If the studies are about drugs used in veterinary medicine, it is also necessary to evaluate the behavior of that compound in relation to breeds, since the genetic profile varies between them, so that one breed may respond

well to one drug and another not (Court, 2013a; Martinez *et al.*, 2013, 2018; Mealey *et al.*, 2019). Thus, the trials *in vitro* can make use of pharmacogenomics, which studies the relationship between genes and the response to drugs, being able to predict whether the results obtained in the cell model are capable of being transposed to the living organism based on results found in DNA analyses (Court, 2007; Relling and Evans, 2015; Roden *et al.*, 2019).

Due to the high cellular variability and the possibility of storage for long periods, *in vitro* tests are useful tools to clarify the permeability of a drug, the role of transporters and enzymes, and cell signaling, in addition to enabling the use of recombinant proteins, mRNA, and gap junction proteins to analyze the behavior of the compound in relation to cellular biochemistry (Martinez *et al.*, 2013; Relling and Evans, 2015; Ediriweera *et al.*, 2019; Morofuji and Nakagawa, 2020), in addition to allowing immunoassays to analyze the role of the immune system in relation to that drug, even when the drug is already available on the market (Fernández-Quintero *et al.*, 2023). These studies involve the use, besides human cells, cattle, pigs, rodents, dogs, and cats cells, making it possible to compare results found among species (Court MH *et al.*, 1997; Court, 2013a; Martinez *et al.*, 2018; Morofuji and Nakagawa, 2020).

1.4 Drug development for humans and animals

1.4.1 Comparative pharmacokinetics

During the *in vivo* phase, drugs intended for human use should be tested on animals (Ward *et al.*, 2005; Martignoni *et al.*, 2006a). The murine model is usually used for this purpose because of the ease of maintaining and handling rats and mice, in addition

to the ease of reproduction (Martignoni *et al.*, 2006a). However, other non-rodent species can also be used. Due to their physiological and genetic similarity to humans, their size and ease of handling, and their long-life expectancy, which allows for longitudinal evaluations, dogs are often the non-rodent model of choice for toxicity and safety testing of human drugs (Martignoni *et al.*, 2006a; Turner, 2011; Hytönen *et al.*, 2016). In addition, veterinary medications for dogs in these species are also evaluated *in vivo* (Mag *et al.*, 2024).

Due to the well-established knowledge about toxicodynamics and toxicokinetics in dogs and the metabolism of both phase I and phase II xenobiotics comparable to that of humans, this species can be used as a model *in vivo* to evaluate the safety of drugs in humans (Dalgaard, 2015; Martinez *et al.*, 2021). In addition, the genome of canines is similar to that of humans. Beagle dogs have pseudogenes related to drug targets that explain the behavior of molecules in humans. Some of these genes encode, for example, the enzyme CYP2D15 (orthologous gene of human CYP2D6), which is the most enzyme found in the canine liver (Roussel *et al.*, 1998) and performs drug metabolization in both species (Martignoni *et al.*, 2006a; Vamathevan *et al.*, 2013; Dalgaard, 2015). Other human CYPs, such as CYP1A2 (Turpeinen *et al.*, 2007) and CYP3A4 (the orthologous gene of canine CYP3A12) (Sharer *et al.*, 1995; Court, 2013a), exhibit activity comparable to that of dogs (Dalgaard, 2015). In addition, some transporters, such as MDR1 and BCRP, which participate in the exocytosis of molecules, have 90% and 83% homology with respect to human orthologous genes, respectively (Zhang *et al.*, 2000; Dalgaard, 2015).

Regarding intrinsic clearance (CLint), the canine model is a good option for studies related to metabolization, including both drugs for human use and those for use in canine therapy. Nishimuta et al. (2013) showed that CLint of drugs by the enzyme CYP3A has a positive correlation with liver microsomes in humans and dogs, although the metabolic activity of these enzymes is lower in the intestinal microsomes of dogs (Ward *et al.*, 2005; Nishimuta *et al.*, 2013).

Human pharmacokinetic data following oral drug exposure can be predicted using canine models, such as the area under the curve (AUC) and half-life time (Ward *et al.*, 2005). However, although there was a higher percentage of positive correlations, the particularities of each species may differ according to the results of clinical trials (Ward *et al.*, 2005). *In vivo* approaches are indicative and comparative to other techniques.

1.4.2 Development of drugs for use in veterinary therapeutics

The development of new drugs for human and veterinary use involves comparative in vivo pharmacokinetic studies, often using animal models to evaluate safety, efficacy, and metabolism. Rodents, particularly rats and mice, are widely used because of their ease of handling and maintenance. However, dogs are the preferred non-rodent species in preclinical toxicology and pharmacokinetics because of their physiological and genetic similarities to humans, manageable size, and longer life expectancy, which allows longitudinal evaluations (Hytönen et al., 2016; Martignoni et al., 2006a; Turner, 2011).

Dogs are not only valuable for testing drugs intended for humans but also serve as primary models for developing veterinary therapeutics. Their metabolic capacity includes phase I and II enzyme systems that closely resemble those of humans. For instance, the

CYP2D15 enzyme in dogs is orthologous to human CYP2D6 and plays a key role in drug metabolism in both species. Other enzymes, such as CYP1A2 and CYP3A4 (orthologous to canine CYP3A12), as well as transporters such as MDR1 and BCRP, also show high genetic homology and comparable activity (Dalgaard, 2015; Court, 2013a; Turpeinen et al., 2007; Zhang et al., 2000).

Canine models are effective for predicting human pharmacokinetic parameters, such as AUC and half-life, despite some interspecies differences. The intrinsic clearance (CLint) of CYP3A substrates shows a strong correlation between dog and human liver microsomes (Nishimuta et al., 2013). This makes dogs a relevant model for assessing drug metabolism for both human and veterinary purposes.

The veterinary drug development process (Figure 3) mirrors that of human pharmaceuticals, beginning with target identification and molecule screening via in silico and in vitro methods, followed by in vivo studies (often in dogs) and clinical trials on affected animals (Mag et al., 2024; Zhou et al., 2021). The evaluation of drug withdrawal periods for food animals is unique to veterinary medicine. A major challenge is the low commercial investment due to a smaller market compared to human medicine. However, increasing demand, a growing pet population, and heightened attention to food safety have driven new interest in veterinary pharmacology (Associação Brasileira da Indústria de Produtos para Animais de Estimação, 2023; Agência Senado, 2024).

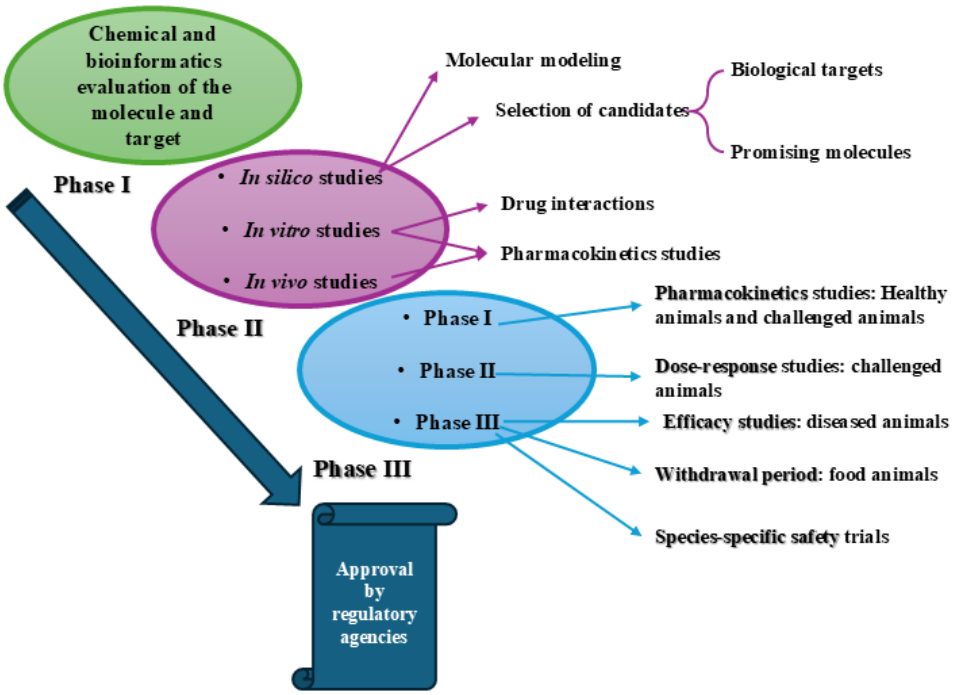

Figure 3 Development flow of a new drug for launch in the veterinary market, based on K. Zhou et al. (2021).

The "One Health" concept emphasizes the interdependence of human, animal, and environmental health. This has expanded the relevance of animal models not only in zoonosis and antimicrobial resistance research but also in the joint development of drugs and vaccines for both human and veterinary use, reinforcing the need for cross-disciplinary collaboration and sustained investment in veterinary therapeutics (CDC, 2024; Mag et al., 2024).

1.5 Essential oils

Herbalism has been practiced since ancient times. The traditional peoples of China, India, Egypt, Rome and the Middle East region combined philosophical principles and family traditions with medical practices (Sakkas and Papadopoulou, 2017; Vora *et al.*, 2024). Ancient Egypt is considered the birthplace of aromatherapy. As early as 3500 BC,

diseases were treated empirically based on magical and theocratic knowledge (Sakkas and Papadopoulou, 2017; Hoffmann, 2020). In China and India, plants are included in traditional Chinese and Ayurvedic medicine, respectively (Hoffmann, 2020; Vora *et al.*, 2024). In ancient Greece, Hippocrates, considered the father of medicine, used medicinal plants based on observation and experimentation at the end of the 5th century BC and cataloged around 300 to 400 plants for medicinal use. In Mesopotamia, around 2600 BC, the use of therapeutic oils derived from plants began, and even the Bible mentions around 30 medicinal plants (Sakkas and Papadopoulou, 2017). In the Middle Ages, great empires controlled the production and sale of medicinal plants, while monks in monasteries studied the therapeutic properties of plants. In Europe, especially during the Renaissance, essential oil (EO) use gained even more attention (Sakkas and Papadopoulou, 2017; Hoffmann, 2020; Vora *et al.*, 2024).

With the advancement of modern medicine, natural medicines have given way to synthetic drugs. However, the search for natural strategies for treating diseases has returned, either due to fear of adverse effects caused by synthetic drugs or due to a greater search for contact with nature, which has increased after the COVID-19 pandemic, from 2019 to 2022 (Hoffmann, 2020; Bartova *et al.*, 2023).

The term "essential oil" was first coined by the Swiss alchemist and physician Paracelsus (1493–1541) in the 16th century. This term comes from the Latin "quinta essentia", which means the fifth element, referring to the spirit, together with the other four elements: fire, air, earth, and water (de Sousa *et al.*, 2023; Sattayakhom *et al.*, 2023; Vora *et al.*, 2024). According to the European Pharmacopeia and the French Association for

Standardization, "essential oil" is defined as a “product obtained from a natural raw material of plant origin, either by distillation with water or steam, or from the epicarp of *Citrus* sp. fruits by a mechanical process, or by ‘dry distillation’. EO is then separated from the aqueous phase by physical means” (AFNOR, 2000; EPC *et al.*, 2009; Do *et al.*, 2015; de Sousa *et al.*, 2023; Vora *et al.*, 2024).

EOs are natural liquid products with low molecular weight (around 300 Da) and high volatility (Sattayakhom *et al.*, 2023; Tan *et al.*, 2023a; Vora *et al.*, 2024) and are part of the plant protection system against diseases and facilitate pollination by attracting insects, among other functions (Vora *et al.*, 2024). They are extracted from flowers, seeds, leaves, fruits, wood, roots and other parts of the plant by breaking down their cell walls and releasing their active components. These molecules could be extracted from plants using solvent extraction, steam distillation, and hydrodistillation (Zhao *et al.*, 2020; Vora *et al.*, 2024; Wang *et al.*, 2024). Other methods include microwave-assisted extraction, green solvent extraction, supercritical fluid extraction, and mechanical extraction. These other methods, which are considered less polluting, are called "green" methods (Zhao *et al.*, 2020; Wang *et al.*, 2024).

EOs are mixtures of terpenoids (mainly alcohols monoterpenes and sesquiterpenes), which are major components, and other compounds, such as ethers, ketones, aldehydes, oxides, phenols, amines, amides and aromatic compounds (Sattayakhom *et al.*, 2023; Vora *et al.*, 2024; Wang *et al.*, 2024). These compounds give the oil its aromatic characteristic and its therapeutic effects. They are highly lipophilic, allowing

it to easily cross biological membranes, such as the blood-brain barrier and cell membranes (Zhang *et al.*, 2021).

Several clinical applications of EOs have been described, both in veterinary and human medicine. Among them, antiseptic, anti-inflammatory, antinociceptive, antidepressant, anticonvulsant, and anxiolytic effects stand out (Brito *et al.*, 2013; Baldinger *et al.*, 2015; Brnawi *et al.*, 2018; Zhang *et al.*, 2021; Vora *et al.*, 2024). Depending on the composition of the EO, it may cause changes in both the central and peripheral nervous systems, generating mydriasis, blood pressure changes, and muscle tone (Igarashi *et al.*, 2014; Baldinger *et al.*, 2015; Kawai *et al.*, 2020; Sattayakhom *et al.*, 2023), resulting in a physical, mental, and emotional response in the patient (Sattayakhom *et al.*, 2023).

Common sense holds that “natural” substances have no side effects and are therefore considered completely beneficial. However, plants may contain toxic components that, if not used correctly, could lead to acute or chronic poisoning, in addition to being responsible for the worsening or emergence of various pathologies (Dosoky and Setzer, 2021). The molecules present in EOs could be toxic at high concentrations, causing hepatic, renal, pulmonary, and central nervous system damage. In the liver, these compounds may cause acute damage, leading to enzyme leakage into the vascular bed and finally to hepatic encephalopathy. In addition, they may act as CYP inhibitors and inducers, generating important drug interactions. Some monoterpenes, especially those derived from citrus fruits, may cause skin irritation (Jimenez *et al.*, 1983; Anderson, 1996; Khojasteh *et al.*, 2010; Ramos *et al.*, 2015; Zárybnický *et al.*, 2018). Although the literature

describes the safety or toxicity of EOs in humans and *in vitro*, in veterinary medicine, it is scarce and presents, for the most part, case reports or applications in experimental animals, most of which use much higher doses than those used therapeutically (Mondal et al., 2023).

1.5.1 LAVENDER ESSENTIAL OIL

Lavender is a plant whose name comes from the Latin "lavare", which means to wash, to bathe, and it got its name because it was commonly used by the ancient Arabs, Greeks, and Romans during bathing (Miastkowska *et al.*, 2021; Pokajewicz *et al.*, 2022). The genus *Lavandula* in the Lamiaceae family, has around 39 species and 400 registered cultivars (Figure 4), with the most important species commercially being *Lavandula angustifolia* (true lavender or English lavender) and *Lavandula latifolia* (spike lavender), in addition to the hybrid of these two, *Lavandula* × *intermedia* (known as lavandin) (Miastkowska *et al.*, 2021; Pokajewicz *et al.*, 2022; Crișan *et al.*, 2023). It occurs naturally on the islands of the North Atlantic and mountainous regions of the Mediterranean, especially in Bulgaria and France, and in the regions of Spain and Italy (Miastkowska *et al.*, 2021; Pokajewicz *et al.*, 2022; Crișan *et al.*, 2023). The region in which the lavender plant is grown determines its chemical composition (Crișan *et al.*, 2023).

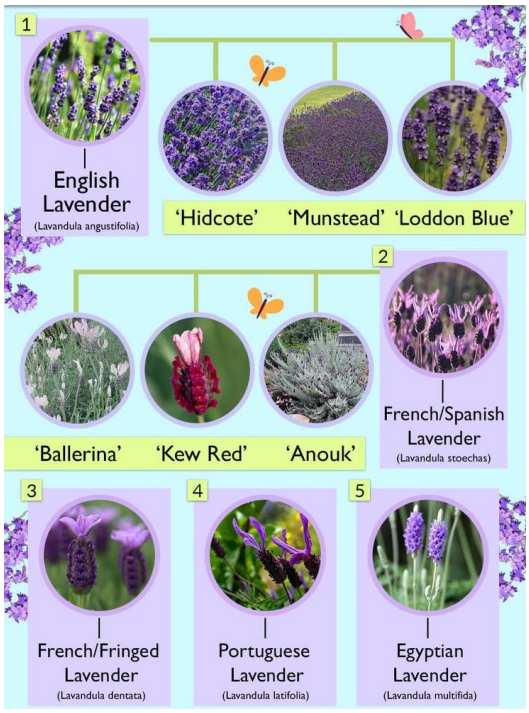

Figure 4 Primary types of lavender (extracted from https://www.gardenmandy.com/)

Lavandula angustifolia, the most commercially important species, is used to produce lavender essential oil (LEO). The chemical composition of LEO is responsible for its aroma, floral notes, and therapeutic action. *Lavandula. angustifolia* may provide 8–30 kg of EO per hectare, with a worldwide production of 300–500 tons per year (Pokajewicz *et al.*, 2022; Crișan *et al.*, 2023).

LEO is obtained mainly from the distillation of flowers, which epidermal structures contain 100-300 volatile substances, including monoterpenoid and other oxygenated compounds, with emphasis on linalool (LIN) and linalyl acetate (LINAct) (Figure 5) (Miastkowska *et al.*, 2021; Pokajewicz *et al.*, 2022; Crișan *et al.*, 2023). It is a clear, pale-yellow liquid with a density between 0.878 % and 0.892 %, refractive index between 1.457 and 1.466 and an optical rotation between 12.5º and 6º. The acidity index should be between 1.0 and 1.2. The concentration of LINAct determines the quality of the EO, which,

according to the European Pharmacopeia, should have a concentration of 25-47 % v/v, and the concentration of LIN should be between 20-45 % v/v (EPC *et al.*, 2009; Miastkowska *et al.*, 2021; Pokajewicz *et al.*, 2022; Crișan *et al.*, 2023). Among the other constituents, 1,8-cineole and camphor are also present (Pokajewicz *et al.*, 2022).

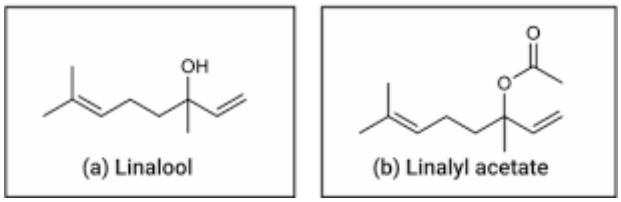

Figure 5 Chemical structures of (a) linalool and (b) linalyl acetate.

LEO is one of the most popular EOs with clinical utility (López *et al.*, 2017; de Melo Alves Silva *et al.*, 2023). It could be administered in several ways, for example by inhalation, transdermal application, or oral administration (Rai *et al.*, 2020; Sayed *et al.*, 2020; de Melo Alves Silva *et al.*, 2023). By inhalation, volatile molecules bind to receptors in the nasal cavity, which transduce and send signals to the limbic system and hypothalamus, which release neurotransmitters responsible for the effects on the central and peripheral nervous systems (de Melo Alves Silva *et al.*, 2023). The antidepressant effect occurs by inhibiting the serotonin transporter, which is also attributed to LIN when administered alone. The anxiolytic, sedative, and relaxing effects are due to the inhibition of voltage-dependent calcium channels, serotonergic transporter inhibition, and activation of the parasympathetic nervous system (de Melo Alves Silva *et al.*, 2023). These terpenoids may cause antinociception by modulating cholinergic, opioid, and dopaminergic transmission, in addition to acting on the mechanism of inflammatory cytokine release and, bind to the NMDA glutamate receptor, thereby reducing excitatory discharge (Batista *et al.*, 2010;

López *et al.*, 2017; Montibeler *et al.*, 2018; Rai *et al.*, 2020; Miastkowska *et al.*, 2021; de Melo Alves Silva *et al.*, 2023). Furthermore, LEO is neuroprotective and prevents neuronal oxidation (López *et al.*, 2017). In wounds, LEO promotes collagen synthesis, fibroblast differentiation, and the reduction of perilesional area, making it a good healing agent. Other therapeutic effects of LEO include antiemesis, neuroprotection, antineoplastic, and control of mood disorders (Rai *et al.*, 2020; Miastkowska *et al.*, 2021; de Melo Alves Silva *et al.*, 2023).

Therapeutic use of LEO in humans has led to increased use of LEO in animals (Fitzi *et al.*, 2002), especially after the COVID-19 pandemic (Bartova *et al.*, 2023). LEO is used in veterinary medicine to control ectoparasites, reduce external bacterial contamination, and treat dermatological pathologies (Vercelli *et al.*, 2021), but its use to control behavioral disorders in animals, such as anxiety, has increased in recent years. In addition, pet owners have sought natural resources as alternatives to synthetic medications because of their known side effects (Fitzi *et al.*, 2002). However, the use of EOs in animals has been largely extrapolated from human medicine because of limited specific studies.

In a study on rabbits (Mekonnen *et al.*, 2019), lavender oil in a concentration of 10 % p/p was applied only once and the area was evaluated every 24 h for 3 days. It did not alter their skin's appearance, with no erythema or edema. On the other hand, Jenner et al. (1964) reported skin irritation using 8000 mg/kg of LIN in a single oral dose. Furthermore, in rats, the administration of 250–4000 mg/kg of LIN for more than 21 days transcutaneous may cause weight loss, discomfort, piloerection, lethargy, and ataxia. Systemically, it could increase alkaline phosphatase, glucose, and cholesterol levels,

indicating liver damage (Marnett *et al.*, 2014). In mice (Mekonnen *et al.*, 2019), a single oral dose of 2000 mg/kg did not cause death, or any central or peripheral changes, such as behavioral changes, salivation, diarrhea, or skin or ocular mucosa irritation. Therefore, the lethal dose (LD_{50}) of oral lavender oil is over 2000 mg/kg in male rats and mice (Jenner *et al.*, 1964; Marnett *et al.*, 2014; Mekonnen *et al.*, 2019). When repeated doses of 2000 mg/kg were administered for 21 days in male mice, the animals did not exhibit any changes in internal organs, with liver and kidney functions remaining unchanged (Mekonnen *et al.*, 2019). Thus, given the high dose required to cause lethality in animals or any adverse reaction, both LIN and LINAct, as well as LEO, could be considered safe for use in veterinary medicine. According to the European Food Safety Authority, LIN and LINAct are safe for ingesting by all animal species (Bampidis *et al.*, 2020; Villa *et al.*, 2024) and could be added to feed and drinking water at doses of up to 30 mg/kg, including in food animals. There are no reports of accumulation in animal tissues or milk and eggs, so a withdrawal period is not necessary. (Villa *et al.*, 2024). There is no evidence that LIN and LINAct have carcinogenic or teratogenic effects based on long-term studies in animals, so they are safe for oral ingestion, according to Fukushima et al. (2020).

1.6 Pharmacokinetics of bioactive compounds in mammals

Pharmacokinetics is the part of pharmacology that studies the movement of drugs through the body, i.e., the profile of the drug over time. It could be divided didactically into four phases: absorption, distribution, metabolism, and excretion. Absorption is the passage of the drug from the site of administration to the systemic circulation and involves the ability of a drug to cross biological membranes (Starkey and Sammons, 2015; Currie, 2018). Common routes of administration are oral, subcutaneous, intramuscular, and

intravenous. The other routes include the percutaneous, intrarectal, and intrathecal routes (Starkey and Sammons, 2015; Currie, 2018). Distribution is the passage of the drug from the systemic circulation to the tissues. It is the only reversible pharmacokinetic movement, i.e., the drug may return from the tissue to the systemic circulation. Because it is difficult to measure the concentration of a drug in tissues, plasma concentration is used to estimate this concentration (Currie, 2018). Both metabolism and excretion are ways of eliminating the drug from the body, with metabolism (also called biotransformation) being the conversion of lipophilic molecules into molecules that are more soluble in water and then eliminated by the kidneys or biliary tract, and excretion being the elimination of the drug, as such, from the body, with renal excretion being the most common (Starkey and Sammons, 2015; Currie, 2018).

Elimination of the drug from the body is closely linked to the concept of clearance, which is one of the most important parameters of pharmacokinetics (van den Anker *et al.*, 2018). Clearance is the intrinsic ability to remove a drug from a volume of blood or plasma per unit of time. Clearance may occur by metabolism and/or excretion (Starkey and Sammons, 2015; Currie, 2018; van den Anker *et al.*, 2018). Hepatic clearance is biotransformation itself, being a combination of metabolism and biliary excretion, whereas renal clearance is urinary excretion (Starkey and Sammons, 2015).

Drug metabolism may occur in the gastrointestinal tract (especially the small intestine mucosa), kidneys, respiratory tract, skin, and some other tissues; however, the main organ responsible for this process is the liver (Starkey and Sammons, 2015; Currie, 2018). Hepatic drug metabolism could be divided into two phases: phase I (catabolic), in which reactions occur to break down the molecule. Among these reactions, hydrolysis and

oxidation stand out, with the participation of enzymes from the CYP family and esterases (Figure 6). Phase II (anabolic) reactions involve the synthesis of new, more polar molecules. The most common reaction involves conjugation with UDP-glucuronic acid (glucuronidation) by the UDP-glucuronosyltransferase enzymes. Other reactions, such as sulfation by the sulfotransferase enzymes and glutathionylation by the glutathione transferase enzymes, may also occur (Starkey and Sammons, 2015; Currie, 2018). When there is a balance between the concentration of the drug in the blood and the rate of drug clearance, this is called first-order kinetics, or linear kinetics. The amount of drug that is eliminated is proportional to the amount of intake. On the other hand, when this balance is disrupted, the enzymes responsible for metabolism may become saturated. This process is referred to as zero-order kinetics or saturation kinetics, wherein the rate of drug elimination remains constant and is independent of its plasma concentration (Wagner, 1973; Cederbaum, 2012; Starkey and Sammons, 2015; Currie, 2018).

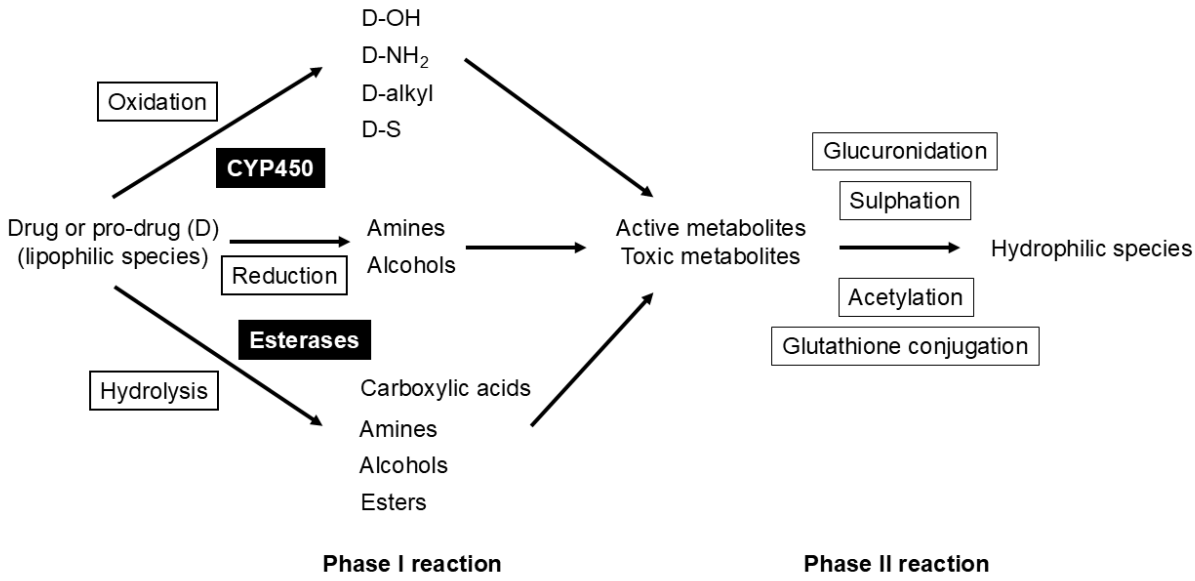

Figure 6 Didactic diagram of the phases of hepatic metabolism of drugs and prodrugs. Phase I is catabolic, and oxidation, reduction, or hydrolysis reactions may occur. CYP enzyme isoforms play an important role in this process, producing active or potentially toxic metabolites. Other enzymes, like esterases, also catalyze ester-containing drugs and prodrugs in phase I. Phase II reactions are anabolic, with the participation of the enzymes glucuronosyltransferase (glucuronidation), sulfotransferase (sulphation), N-acetyltransferase (acetylation), and glutathione S-transferase (glutathione conjugation) producing inactive and polar metabolites to be excreted mainly by the renal system.

The main organ of excretion is the kidneys. Other organs may excrete compounds too, like gall bladder, but it is difficult to measure this excretion. Three processes are involved: glomerular filtration, tubular secretion, and tubular reabsorption. These three processes must be balanced for excretion to occur satisfactorily (Starkey and Sammons, 2015).

1.6.1 CYP-MEDIATED METABOLISM

One of the most important groups of enzymes involved in phase I metabolism is CYP450, that were discovered in the early 1960s (Guengerich *et al.*, 2016; Waring, 2020). CYPs are found in many living creatures (primarily eukaryotes), and their genes encode up to 50,000 proteins. In humans, the 57 genes and 58 pseudogenes encode 18 protein families and 43 subfamilies, and their names are based on genetic identity. CYP2, CYP3, and CYP4 families are the most abundant human enzymes. It is a determinant of metabolic efficiency in humans and dogs (Mealey *et al.*, 2019; Waring, 2020). In dogs, according to Martinez et al. (2019), the most abundant enzymes in liver microsomes are CYP2D15 and CYP3A12, followed by CYP1A2, CYP2B11, CYP2E1, and CYP2C21 in an intermediary amount. CYP2A13, CYP2A25, CYP2C41, CYP3A26 and CYP1A1 are the least abundant in dog liver.

These mammalian enzymes are present in the endoplasmic reticulum and mitochondria, mainly in the liver and intestinal mucosa, and in smaller quantities in the brain, kidneys, lungs, and skin (Guengerich *et al.*, 2016; Mealey *et al.*, 2019; Waring, 2020). CYP family enzymes could metabolize drugs into active and inactive compounds, which are metabolized by phase II enzymes (especially glucuronosyltransferases) or excreted by the kidneys (Visser *et al.*, 2019).

CYPs are responsible for the oxidation of 75 % to 80 % of drugs, with human CYP2D6 (ortholog of CYP2D15 in dogs) being the most important in the metabolism of 20 % of prescription drugs in humans (Guengerich *et al.*, 2016; Mealey *et al.*, 2019; Waring, 2020). The CYP family of enzymes primarily function as monooxygenases, that is, they

transfer electrons to oxygen and catalyze the oxidation of organic molecules. In general, NADPH is required for the reaction to proceed satisfactorily according to the following equation:

$$NADPH + H^+ + RH + O_2 \xrightarrow[CYP]{} NADP^+ + H_2O + ROH$$

where RH is the substrate (Guengerich *et al.*, 2016).

In vitro assays have made it possible to perform studies involving CYPs, with the prediction of pharmacokinetic parameters, drug interactions, and interindividual varia8tions (Guengerich *et al.*, 2016). These tests are performed with hepatocytes, recombinant CYPs, or liver microsomes, which are obtained by serial centrifugation, and then the CYPs are isolated together with the endoplasmic reticulum. In these tests, it is possible to determine the CLint of a drug and its hepatic clearance, which is an essential step in drug development (Visser *et al.*, 2019).

The major hepatic CYPs that are capable of metabolizing drugs in dogs are described in Table 1.

Table 1 Major drug metabolizing CYPs in canine liver.

Canine CYP	Human ortholog CYP	Substrates	Inducers	Inhibitors	Notes	References
1A2	1A2	Caffeine, theophylline, theobromine and other methylxanthines	Diet, omeprazole, and β-naphthoflavone	Ciprofloxacin, cimetidine	It is estimated that 10-15% of beagles are deficient in this enzyme, and this is due to a mutation in the gene that causes interruption in the synthesis of this protein	(Eguchi *et al.*, 1996; Tenmizu *et al.*, 2004; Kamimura, 2006; Trepanier, 2006; Court, 2013a; Gagliardi *et al.*, 2015)
2B11	2B6	Midazolam, ketamine, propofol, bupropion	Phenobarbital (strong) Rifampicin (weak)	Medetomidine, chloramphenicol, ketoconazole, diazepam, fluoxetine	Interact with benzodiazepines. Greyhounds have a deficiency in this CYP, due to an aberrant mRNA or reduced translational efficiency.	(Eguchi *et al.*, 1996; Graham *et al.*, 2006; Baratta MT *et al.*, 2010; Court, 2013a; Martinez *et al.*, 2020)
2C21	2C9	Diclofenac, testosterone, midazolam, tramadol	Phenobarbital (strong) Rifampicin (weak)	Clopidogrel, fluoxetine, clomipramine		(Nishibe Y *et al.*, 1998; Shou *et al.*, 2003; Mills *et al.*, 2010a; Mössner *et al.*, 2011; Court, 2013a; Jimenez *et al.*, 2018; Martinez *et al.*, 2019)
2D15	2D6	Celecoxib, desipramine, dextromethorphan, imipramine, tramadol	None	Quinidine		(Tasaki *et al.*, 1998; Court, 2013a; Jimenez *et al.*, 2018)
2E1	2E1	Chlorzoxazone, acetaminophen, caffeine	Ethanol, other alcohols including propylene glycol	Disulfiram, diethyldithiocarbamate	Participation in physiological detoxification and nutritional support; induction and inhibition are protective effects	(Court MH *et al.*, 1997; Martignoni *et al.*, 2006b; Court, 2013a)
3A12 3A26	3A4	Midazolam, testosterone, dextromethorphan, diazepam, tramadol	Rifampicin (strong) Phenobarbital (weak)	Ketoconazole, ketamine		(Nishibe Y *et al.*, 1998; Shou *et al.*, 2003; Lu *et al.*, 2005; Graham *et al.*, 2006; Mealey *et al.*, 2008; KuKanich B and Hubin M, 2010; Haller *et al.*, 2012; Perez *et al.*, 2016; Martinez *et al.*, 2019)

1.7 LAVENDER ESSENTIAL OIL AS AN ADJUVANT TREATMENT FOR ANXIETY

In human medicine, studies have investigated the effects of linalool (LIN), linalyl acetate (LINAct), and/or LEO on anxiety. Randomized clinical trials have shown that administering LIN and LINAct at a dose of 80 mg/day orally had an anxiolytic effect comparable to that of lorazepam (0.5 mg/day) after eight weeks of treatment (Kasper *et al.*, 2010; Woelk and Schläfke, 2010; Heger-Mahn *et al.*, 2014). In another study, both LEO and its main components exerted an analgesic effect in patients with postherpetic pain when used a single time orally (You *et al.*, 2024). This effect may be a consequence of relieving the emotional component of the pain.

Silexan® is a drug patented in Germany that is made from LEO distilled from the flowers (*Lavandula angustifolia*) and is indicated for treating anxiety in humans (Müliner et al., 2015). In Europe, it is sold under the trade name Lasea®, and in the United States, it is marketed under the name CalmAid®. The capsule contains 80 mg of oil and is administered orally once daily (Kasper *et al.*, 2018). Absorption studies in humans and rats have shown that LIN, the main active ingredient in this formula, is present in plasma in a very small amount after ingestion at single or multiple doses, whereas LINAct is not detected (Müliner et al., 2015). In addition to treating anxiety, Silexan® is also indicated for treatment of depression, mood disorders, and sleep disorders (Uehleke *et al.*, 2012; Bartova *et al.*, 2023).

1.8 METABOLISM AND DRUG INTERACTIONS INVOLVING LAVENDER ESSENTIAL OIL AND ITS MAIN CONSTITUENTS

The metabolism of LIN in mammals occurs via oxidation by CYPs. According to Meesters et al. (2007), the main enzymes capable of performing this metabolism in

humans are CYP2C19 and CYP2D6, with CYP2C19 having greater enzymatic affinity than CYP2D6. The major metabolites of LIN are cis- and trans-8-hydroxyllalool (Meesters *et al.*, 2007). CYP2C19 and CYP2D6 in humans metabolize LIN to form 8-hydroxyllalool. Similarly, murine liver microsomes may hydroxylate LIN (Chadha and Madyastha, 1982, 1984; Meesters *et al.*, 2007). Bacteria like *Pseudomonas incognita* may also metabolize LIN, although differently from mammals. LIN in these microorganisms is used as an energy source and is converted to linalool-8-carboxylic acid by linalool dehydrogenase with the aid of NADH rather than NADPH, which is used in mammals. LINAct, in turn, is converted into linalyl acetate-8-carboxylic acid (Renganathan and Madyastha, 1983). However, the metabolism of LINAct may not be exclusively dependent on CYP. Schlacher et al (1998), in their work with bacteria, identified esterases capable of hydrolyzing LINAct into LIN and acetic acid. This raises a plausible hypothesis that this ester in mammals could be metabolized not only by CYP enzymes but also by hepatic esterases (Schlacher *et al.*, 1998).

Doroshyenko et al. (2013) evaluated the potential for herbal-drug interactions between LEO and pharmaceutical substrates of CYP1A2, CYP2C9, CYP2C19, CYP2D6, and CYP3A4 at clinical doses. In this study, healthy volunteers received a cocktail of specific substrates for each CYP enzyme and LEO, enabling the evaluation of drug interactions and CYP activity. Heger-Mahn et al. (2014) also reported similar results when studying the interaction of LEO with CYP3A4 drug substrates. The authors used a randomized, double-blind, crossover clinical study with healthy women to evaluate the possible drug interaction between LEO and oral contraceptives. They concluded that LEO, from a pharmacokinetic perspective, has a low capacity for drug interaction in humans (Doroshyenko *et al.*, 2013; Heger-Mahn *et al.*, 2014). On the other hand, in an *in vitro* study

using human liver microsomes, Mondal et al. (2023) found that LEO is capable of inhibiting CYP3A4 and CYP1A2 in a dose-dependent manner and that LINAct (but not LIN) is also capable of inhibiting CYP3A4 (Mondal *et al.*, 2023). Noskova et al. demonstrated that LIN could increase the metabolic activity of CYP2A in murine hepatic microsomes (Samojlik *et al.*, 2012, 2016; Nosková K *et al.*, 2016; Mondal *et al.*, 2023).

Many studies have demonstrated the effectiveness of LEO when administered orally, but nothing has been published regarding the potential for interactions between LEO and its constituents with medications used in veterinary medicine to control anxiety in dogs. Considering this gap in canine pharmacology and therapeutics, some hypotheses are raised. (1) Both linalool and linalyl acetate are metabolized by canine CYP450 enzymes. (2) Since CYP450 enzymes metabolize many medications used to treat anxiety disorders in dogs, there is the possibility of drug interactions between linalool, linalyl acetate, and these drugs. (3) Since LEO is composed mainly of linalool and linalyl acetate, the use of this EO as an adjuvant in the control of anxiety in dogs may alter the metabolism of other drugs used concomitantly. These studies were performed to characterize the metabolism of LEO and its main compounds and determine the potential for drug interactions using *in silico* and *in vitro* approaches: structure-based and ligand-based modeling, dog liver microsomes and recombinant CYP enzymes.

2 AIMS

2 AIMS

2.1 MAIN AIMS

- To evaluate the hepatic metabolism and potential drug interactions of linalool, linalyl acetate, and lavender essential oil (Lavandula angustifolia) in the canine liver;
- To elucidate the mechanisms of hepatic biotransformation in dogs, with a focus on isoenzymes of the cytochrome P450 (CYP450) system;
- To investigate the potential for drug interactions involving linalool, linalyl acetate, and lavender essential oil in canine liver microsomes using substrates commonly used in clinical practice.

2.2 SPECIFIC AIMS

- To model the canine enzymes CYP2B11, CYP2C21, and CYP2D15 in a three-dimensional manner using bioinformatics tools and validate the obtained structures regarding stereochemical quality;
- To investigate the possible interactions between linalool, linalyl acetate, and canine cytochrome P450 isoforms, molecular docking and pharmacophoric analyses were performed to predict the site and type of molecular binding;
- To evaluate the metabolism rate of linalool and linalyl acetate in vitro, canine liver microsomes (pDLMs) and recombinant enzymes (rCYPs) were used to quantify the depletion of the compounds over time;

- To evaluate the metabolism rate of linalool and linalyl acetate in vitro, canine liver microsomes (pDLMs) and recombinant enzymes (rCYPs) were used to quantify the depletion of the compounds over time.
- To determine the kinetic parameters of linalool metabolism, including the Michaelis-Menten constant (Km), depletion constant (k), and intrinsic clearance (CLint), to better characterize the metabolic pathway;
- To evaluate the metabolism rate of linalool and linalyl acetate in vitro, canine liver microsomes (pDLMs) and recombinant enzymes (rCYPs) were used to quantify the depletion of the compounds over time.
- To determine the kinetic parameters of linalool metabolism, including the Michaelis-Menten constant (Km), depletion constant (k), and intrinsic clearance (CLint), to better characterize the metabolic pathway.
- To identify the enzymes most involved in the metabolism of linalol;
- To investigate the inhibitory effects of linalool, linalyl acetate, and lavender essential oil on the enzymes CYP2B11, CYP2C21, CYP2D15, and CYP3A12, with emphasis on the risk of drug interactions with drugs metabolized by the same pathways;
- To compare the *in silico* findings with the *in vitro* results to identify correlations that may reinforce the predictive validity of computational methods in veterinary pharmacology.

3 MATERIALS AND METHODS

3 MATERIALS AND METHODS

3.1 IN SILICO ASSAYS

3.1.1 MOLECULAR MODELING OF TARGET PROTEINS

To identify the 3D structure of proteins CYP2B11, CYP2C21, and CYP2D15 SWISS-MODEL (https://swissmodel.expasy.org) (Waterhouse et al., 2018) homology protein Modeling server was used. The procedure was first conducted by obtaining the target sequences. The sequences of the studied isoforms were obtained in FASTA format from the National Center for Biotechnology Information (NCBI protein) database (https://www.ncbi.nlm.nih.gov/protein/). The identification codes NP_001006653.1, NP_001183973.1, and BAA20357.1 were used for CYP2B11, CYP2C21 and CYP2D15, respectively. The sequences were then submitted to SWISS-MODEL to align the target sequence with structures available in the Protein Data Bank (PDB) (https://www.rcsb.org). The platform automatically selects the best templates based on sequence identity, coverage, and structural quality, thus generating a three-dimensional model of the target protein. For each protein, the following quality criteria were evaluated: Global Model Quality Estimation (GMQE), which estimates model reliability based on similarity and coverage, and the QMEAN Z-score, which assesses the stereochemical and structural plausibility of the model. The models were then exported to a pdb format for subsequent molecular docking analysis with linalool and linalyl acetate.

3.1.2 Structure-Based Drug Designing

3.1.2.1 Preparation of Proteins and Ligand Compound Molecule for Docking Analysis

After the prediction of 3D protein structure of proteins CYP2B11, CYP2C21, and CYP2D15, we used MGLTool suite (version 1.5.7), Autodock tool (ADT) (Morris et al., 2009). The PDB files were loaded, and structural cleaning was performed by removing water molecules and any residual ligands or cofactors from the structural template. Next, charge correction and assignment were performed by adding polar hydrogens to the proteins to simulate the interactions. Kollman partial charges were assigned to all protein atoms. Subsequently, visual inspection of the structure and molecular topology checking were performed in ADT as a scan for structural errors.

The search space (grid box) was defined without considering the heme cluster (the active site of CYP enzymes). The position and dimensions of the box were defined to include the entire volume of the receptors. The prepared protein was saved in. pdbqt format and loaded into AutoDock Vina software.

Ligand molecule LIN and LINAct were prepared and saved in. mol or .sdf format from the PubChem database (https://pubchem.ncbi.nlm.nih.gov/). The structures were optimized and converted to. pdb format from OpenBabel software, version 3.1.1 (https://openbabel.org/index.html) (O'Boyle et al., 2011) via the command line

```
obabel entrada.mol -O saida.pdb --gen3d
```

The ligand geometries were optimized by adding hydrogen atoms and generating 3D conformations.

Using AutoDock Vina (version 1.1.2) (Trott and Olson, 2010), the .pdb files were converted to. pdbqt, with the addition of Gasteiger charges and the definition of the rotatable atoms. Molecular docking was also performed in ADT using the default Vina settings, with flexibility in the ligands and rigidity in the receptor.

The resulting protein-ligand complexes were visualized using the UCSF Chimera visualization tool (Pettersen et al., 2004), which was also used for image extraction and identification of interacting residues and hydrogen bonds.

3.1.3 Ligand-Based Drug Designing

MOE (Molecular Operating Environment) (http://www.chemcomp.com/) software package was used to carry out the pharmacophore properties of the compounds LIN and LINAct and molecular docking. MOE is designed by the Chemical Computing Group to support Cheminformatics, Molecular Modeling, Bioinformatics, Virtual Screening, Structure and Ligand-based-drug-design and could be used to build new applications based on SVL (Scientific Vector Language). To predict the interaction between CYP2B11, CYP2C21, and CYP2D15 with ligand molecules, LigPlot implementation in MOE was used (KITCHEN et al., 2004; WADOOD et al., 2014).

3.1.3.1 Ligands Preparation

The ligands for CYP2B11, CYP2C21 and CYP2D15 were constructed using MOE Builder application (Riasat et al., 2022). The molecular structures of LIN and LINAct were imported into the MOE using mol or sdf format. The energies of all the ligand molecules were minimized using the Energy minimization algorithm of MOE tool. The following parameters were used for energy minimization; gradient: 0.05, force field: MMFF94X,

Chiral Constraint: Current Geometry. Addition of explicit hydrogen and stereochemistry correction was performed, if necessary. The basic physicochemical properties were inspected, including molecular mass, logP, PSA, and number of H-bond donors/acceptors.

The MOE Pharmacophore Query Editor tool was used to identify and graphically represent the main pharmacophoric elements of the compounds: hydrogen bond donor and acceptor groups, hydrophobic centers, aromatic rings and cationic or anionic centers. The pharmacophoric model was then exported for use in virtual screening or comparative analyses with other structures.

All the minimized molecules were saved in the (.mdb) file format. In the next step, the prepared ligands were used as input files for MOE-Dock (Wadood, Jamal, et al., 2014; Faheem and Jamal, 2020).

3.1.3.2 Protein Preparation

The 3D protonation of the protein molecules was carried out. The target proteins CYP2B11, CYP2C21, and CYP2D15 were loaded into the MOE (in .pdb format).

The energies of the protein molecules were minimized using the energy minimization algorithm of MOE tool. The following parameters were used for energy minimization; gradient: 0.05, force field: MMFF94X+Solvation, Chiral Constraint: Current Geometry. Energy minimization was terminated when the root mean square gradient falls below 0.05. The minimized structures were used as the template for docking (Wadood, Jamal, et al., 2014).

3.1.3.3 MOLECULAR DOCKING

The protein-ligand complexes generated previously (via AutoDock Vina) were imported and used as the basis for the interaction analysis. The LigPlot implementation integrated with MOE was used to generate 2D diagrams of protein-ligand interactions, identifies residues via hydrogen bonds and hydrophobic interactions, visualize interaction distances and geometries and then images of the interactions generated by LigPlot were used for documentation and qualitative analysis.

The binding of the ligand molecules with the protein molecules were analyzed using MOE docking program to find the correct conformation of the ligands, so, as to obtain minimum energy structure. After the completion of docking, we analyze the best poses for hydrogen bonding/π-π interactions and root mean square deviation (RMSD) calculation by using MOE applications (Wadood, Riaz, et al., 2014). The RMSD was used to assess the similarity between different molecular conformations, allowing us to quantify the degree of spatial overlap between the corresponding atoms in the two structures. Low RMSD values indicate high structural similarity and are commonly used to validate docking poses and analyze conformational variations.

Material and methods of the *in silico* approach *are* summarized in Figure 7.

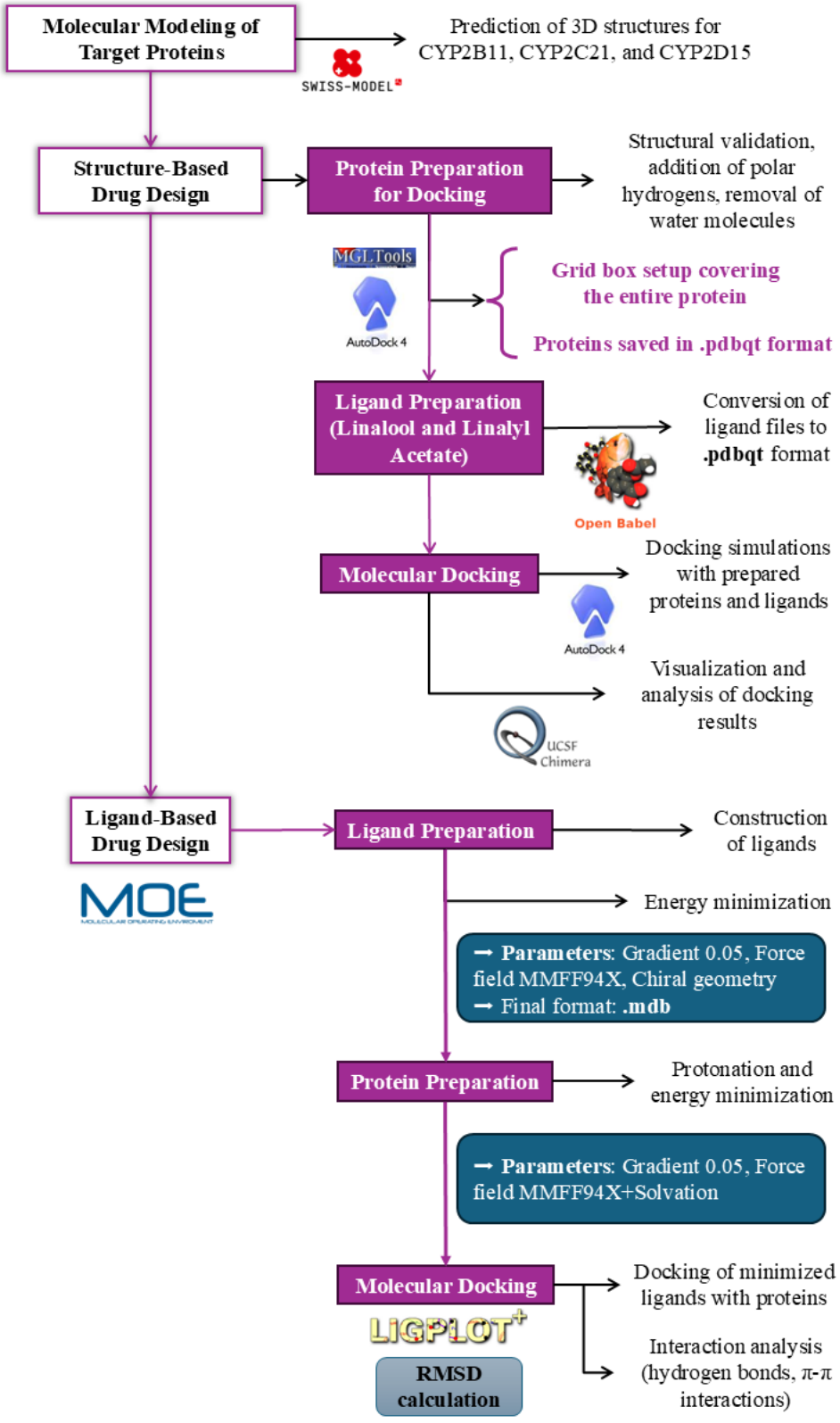

Figure 7 Summary of materials and methods of *in silico* assays.

3.2 *IN VITRO* APPROACH

3.2.1 REAGENTS

Linalool (L2602-5G), linalyl acetate (W263605-SAMPLE-K), LEO (W262218-SAMPLE-K), NADPH, UDP-glucuronic acid, and bovine serum albumin were from Sigma-Aldrich. P450 substrates, linalool-d3 (TRC-L465951-5MG), and alamethicin were obtained from Cayman Chemicals, Cerilliant, and Toronto Research Chemicals. Other chemical supplies were from J.T Baker, Sigma-Aldrich, and Fisher Chemical. Recombinant canine P450 enzymes (CYP1A1, CYP1A2, CYP2B11, CYP2C21, CYP2C41, CYP2D15, CYP3A12, and CYP3A26) and liver microsomes from male beagle dogs treated with corn oil, rifampin, β-naphthoflavone, saline, phenobarbital, or clofibric acid were supplied by Xenotech LLC. Pooled dog liver microsomes (pDLMs) were prepared as described by Court et al. (1997), using a collection of 59 frozen dog livers stored in the Pharmacogenomics Laboratory at Washington State University. These livers were obtained from 59 healthy adult dogs, comprising 25 beagles (19 males and 6 females), 5 male greyhounds, 12 female hounds, 12 mixed breeds (6 males and 6 females), 4 chihuahuas (3 males and 1 female), and 1 male labrador retriever. All dogs were euthanized for reasons unrelated to this research. The Institutional Animal Care and Use Committee of Washington State University and the Institutional Animal Care and Use Committee of Universidade Federal de Minas Gerais judged prior approval was not required, in accordance with the current ethical guidelines for the use of biological material obtained *post mortem*. Protein concentrations in dog liver microsomes were quantified using the bicinchoninic acid assay (Thermo Scientific Pierce).

3.2.2 MEASUREMENT OF LINALOOL AND LINALYL ACETATE DEPLETION RATES

Experiments were conducted to measure the depletion rates of LIN, LINAct, and LIN and LINAct from lavender oil in *in vitro* incubations. Canine liver microsomes (pDLMs) were incubated with and without cofactors at 37°C in a final volume of 500 µL. The 2 mL polypropylene tubes were prepared on ice containing 50 mM (pH 7.4) phosphate buffer, 0.1 mg/ml pDLMs, and the cofactors NADPH or UDPGA. Enzyme cofactors (or phosphate buffer for negative control samples) NADPH or UDPGA were added before incubating the samples. For P450 enzymes, mixtures contained NADPH (0.5 mM final concentration) and magnesium chloride (5 mM). For the cofactors that participated in glucuronidation, the mixture contained UDP-glucuronic acid (5 mM), magnesium chloride (5 mM) and alamethicin (50 µg/mL). Reactions were initiated by the addition of substrate dissolved in methanol (5 µM LIN, LINAct or LEO final concentration). The concentration of LEO was a combination of LIN (2.5 µM) and LINAct (2.5 µM) concentrations. The final methanol solvent concentration in incubations was 1%. Immediately after addition of the substrate (time 0 min), a 50-µL aliquot was removed and immediately added to a 1.5 mL polypropylene tube on ice containing 100 µL of 1 µM linalool-D3 in acetonitrile and 100 µL of 1 µM diazepam in methanol and vortex. Then, the incubation tubes were placed in an incubator containing water at a temperature of 37 °C, and an aliquot of 50 µL was removed at 5, 10, 15, 20, 30, 40, 50, and 60 min after the start of incubation and transferred to tubes containing the internal standards and vortexed. The mixture was centrifuged at 15,000 rcf for 10 minutes, and 200 µL of supernatant was diluted in 400 µL of water and analyzed via HPLC-MS. To verify the participation of esterases in the

depletion of LINAct and lavender oil, the same method was performed using pDLMs previously boiled for 5 min to inactivate these enzymes.

The concentrations of LIN and LINAct were measured by HPLC (Agilent 1100, Agilent Technologies) coupled to a triple-quadrupole mass spectrometer (AB-Sciex API4000, Applied Biosystems Life Technologies) operated in positive ion mode. The mobile phases consisted of a mixture of 0.1% formic acid in water (mobile A) and 100% acetonitrile (mobile B) and were pumped at 1.1 mL/min through a 2.1 x 50 mm 5 µ C18 column (Agilent Zorbax Eclipse XDB-C18). A linear gradient method was used, starting at 75:25 (A:B v/v), changing to 5:95 after 1 min, and returning to 75:25 at 2 min to complete the 5 min run. The mass transitions monitored included m/z+ 137.2→81 (LIN and LINAct), m/z+ 140.2→83 (linalool-d3, internal standard for LIN), and m/z+ 285→193 (diazepam, internal standard for LINAct). Chromatographic retention times for pure LIN, linalool-d3, LINAct, and diazepam were 1.53 min, 1.53 min, 1.81 min, and 1.46 min, respectively.

All stock concentrations of LIN and LINAct dissolved in methanol were stored at -20 °C. Preliminary experiments showed that 10 µM LIN and LINAct diluted in phosphate buffer (pH 7.4) at room temperature were stable (less than 20% decrease of concentration) up to 12 h and 6h, respectively. Consequently, the experiments were completed within 6h after dilution of LIN, LINAct, and lavender oil in phosphate buffer.

The LIN and LINAct concentrations in incubations were calculated using a standard curve which was generated adding different concentrations of pure compounds dissolved in incubation buffer and a fixed concentration of the internal standard. The concentration of pure LIN and LINAct ranged from 1 to 5 µM. The standard curves were linear ($R^2 > 0.9$)

over this range of concentrations. Unknown concentrations of analytes were calculated using the slope of ratios of analyte and internal standard peak areas. All experiments were repeated at least 3 times on different days, and the results were reported as the average with standard deviations. For the LIN assay, the inter- and intra-assay coefficients of variation (CV%) were 15.7 and 9.6, respectively, and for LINAct, the CV% were 14.1 for inter-assay and 13.1 for intra-assay. For lavender oil assay, LIN depletion had inter-assay CV% of 12.9, and for LINAct depletion, the inter-assay CV% was 17.9.

LIN depletion rates over 30 min in liver microsomes and recombinant P450 enzymes were used to determine CLint values that can be used to predict in vivo drug clearance (pharmacokinetic scaling). We employed the previously described "in vitro $T_{1/2}$" methodology (Obach, 1999)with slight variations. For each assayed time point in the experiment, a spreadsheet program (Excel, Microsoft) was used to calculate the remaining percentage of substrate. The natural logarithm of the remaining substrate percentage was plotted against time. The elimination rate constant (k) was identified as the negative slope of the fitted line in linear regression analysis. The elimination rate constant divided by the liver microsomal protein concentration yields the liver microsomal CLint values (µL/min/mg microsomal protein).

LIN depletion rates were determined using different pDLMs protein concentrations and different substrate concentrations. The same methodology was used to evaluate the influence of cofactors on LIN depletion rates, but only NADPH was added to the incubation. The following pDLMs protein concentrations were used: 1, 0.8, 0.4, 0.2, and 0.1 mg/mL with 5 µM of LIN. LIN concentrations used in these experiments were 2, 5, 10, 20, 50, 100 µM with 0.4 mg/mL pDLMs protein concentration.

CLint values for recombinant enzymes were determined using 5 µM of LIN and 160 pmoles/mL of recombinant P450 for most enzymes. For CYP2B11, 40 pmoles/mL was used and for CY2C21 80 pmoles/mL. In incubations with liver microsomes, the protein concentration was 0.4 mg/mL. Recombinant P450 CLint values were calculated by dividing the elimination rate constant by the P450 concentration (µL/min/pmole P450). Recombinant P450 CLint values were also extrapolated to liver microsomal CLint values by multiplying each P450 CLint value by the average abundance of each P450 measured in the same set of liver microsomes as reported previously (Martinez *et al.*, 2019).

3.2.3 Enzyme kinetic parameter determination

The Michaelis-Menten formula was used to derive the kinetic parameters (k and k_m) for LIN depletion by pDLMs (equation 2) (Nath and Atkins, 2006). k_{dep} is the substrate depletion rate constant; $k_{dep[S]\rightarrow 0}$ is the theoretical maximal depletion rate, also known as k_{max}. [S] is the concentration of LIN, and k_m is the Michaelis-Menten constant, which is the substrate concentration at half the theoretical maximal depletion rate.

Equation 1 Equation to obtain the Michaelis-Menten constant and consequently derives the enzyme kinetic parameters (Nath and Atkins, 2006).

$$k_{dep} = k_{\mathrm{dep[S]}\rightarrow 0} \times \left(1 - \frac{[S]}{[S] + k_m}\right)$$

The fit of the experimental data to the Michaelis-Menten model was assessed by nonlinear regression using SigmaPlot software, applying the integrated enzyme depletion kinetics equation. The goodness of fit was analyzed based on the coefficient of determination (R^2), distribution of residuals, and standard error of the estimated parameters. The adequacy of the model was visually verified by inspecting the depletion

versus concentration plot, confirming the hyperbolic behavior typical of saturation-modulated first-order enzyme kinetics.

3.2.4 Inhibition of P450 activities in liver microsomes

The inhibition assay methods are summarized in table 11. LIN, LINAct, and lavender oil were evaluated as inhibitors of tramadol N-demethylation (by CYP2B11) O-demethylation (by CYP2D15), midazolam 1′-hydroxylation (by CYP3A12), cannabidiol 6-hydroxylation (by CYP2C21), methadone N-demethylation to 2-ethylidene-1,5-dimethyl-3,3-diphenylpyrrolidine (EDDP) (by CYP2B11) and trazodone N-dealkylation to m-chlorophenylpiperazine (m-CPP) (by CYP3A12) (Perez *et al.*, 2016; Zeng *et al.*, 2021; Court *et al.*, 2024). In humans, tramadol is metabolized by CYP2D6 (ortholog of canine CYP2D15), CYP2B6 (ortholog of canine CYP2B11) and CYP3A4 (orthologue of canine CYP3A12) (Roussel *et al.*, 1998; Hay Kraus *et al.*, 2000; Lee *et al.*, 2019; Martinez *et al.*, 2020). Methadone is metabolized by human liver *in vitro* and *in vivo* mainly by CYP3A4, CYP2B6, CYP2D6 (Volpe *et al.*, 2018). Midazolam and trazodone are highly selective probes for human CYP3A4 isoform as well as trazodone (Court, 2013a; Yang *et al.*, 2018; Matos *et al.*, 2020). In human liver microsomes, cannabidiol is metabolized to 6-hydroxycannabidiol by CYP3A4 and CYP2C19 (Jiang *et al.*, 2011). According to Karakus et al. (2021), humans and dogs share similar chromosomal locations for CYP2C. Thus, cannabidiol can be metabolized by both CYP2C19 in humans and CYP2C21 in dogs.

Table 2 Inhibition assays of the activities of CYP2B11, CYP2D15, CYP3A12 and CYP2C21 enzymes.

Assay	CYP involved	Positive control	Substrate	Internal standard	Measured metabolites
Tramadol N-demethylation inhibition	CYP2B11	Chloramphenicol	10 µM Tramadol	N-desmethyltramadol-d3 (m/z+ 253→47)	N-desmethyltramadol (m/z+ 250 → 44)
Tramadol O-demethylation inhibition	CYP2D15	Quinidine	10 µM Tramadol	O-desmethyltramadol-d6 (m/z+ 256→64)	O-desmethyltramadol (m/z+ 250 → 58)
Methadone N-demethylation inhibition	CYP2B11	Chloramphenicol	0.5 µM Methadone	EDDP-d3 (m/z+ 281.4→234)	EDDP (m/z+ 278.4→234)
Midazolam 1′-hydroxylation inhibition	CYP3A12	Ketoconazole	200 µM Midazolam	1′-Hydroxymidazolam-d4 (m/z+ 346 → 301)	1′-Hydroxymidazolam (m/z+ 342 → 297)
Trazodone N-dealkylation inhibition	CYP3A12	Ketoconazole	50 µM Trazodone	Diazepam (m/z+ 285.0→193.2)	m-CCP (m/z+ 197.2→118.1)
Cannabidiol 6-hydroxylation inhibition	CYP2C21	Fluconazole	5 µM Cannabidiol	Diazepam (m/z+ 285.0 → 193.2)	6-Hydroxycannabidiol (m/z+ 315.4→193.2)

Note: The concentrations of linalool, linalyl acetate, and lavender oil were 0.3, 1, 3, 10 and 30 µM, as well as the concentrations of the positive controls. In each incubation, 0.1 mg/mL of pDLMs and NADPH, as enzyme cofactor, were used, and 50 mM phosphate buffer (pH 7.4) was used as the diluent. After incubation, samples were vortexed briefly and centrifuged at 15000 rcf for 10 min. The supernatants were collected and diluted in water or a mixture of 0.1% formic acid and 2 mM ammonium formate. The final methanol concentration during incubation was 1%. m-CCP: meta-chlorophenylpiperazine.

For tramadol N-demethylation and O-demethylation inhibition assays and methadone N-demethylation inhibition assay, 100 µL incubations containing LIN, LINAct, or lavender oil (0.3, 1, 3, 10, and 30 µM), pDLMs at 0.1 mg/mL, 50 mM phosphate buffer at pH 7.4, and the enzyme cofactor NADPH were used. Chloramphenicol (N-demethylation, 0.3, 1, 3, 10, and 30 µM) and quinidine (O-demethylation, 0.3, 1, 3, 10, and 30 µM) were used as positive controls inhibitors. The final methanol solvent concentration in the incubations was 1%. The reactions were initiated by the addition of 10 µM (final concentration) tramadol or 0.5 µM (final concentration) methadone, and after 10 min (or 30 minutes in the case of the methadone assay), the reactions were stopped by the addition of 100 nM N-desmethyltramadol-d3 and O-desmethyltramadol-d6 mix in

acetonitrile (internal standard) or 0.25 μM 2-Ethylidene-1,5-dimethyl-3,3-diphenylpyrrolidine-d3 (EDDP-d3) in HCl. The reaction was vortexed briefly and centrifuged at 15,000 RCF for 10 min. 350 μL or 140 μL of the supernatant was added to 350 μL water or 100 μL of a 0.1% formic acid/2 mM ammonium formate solution before HPLC/MS measurement of N,O-desmethyltramadol, and EDDP concentration. For measuring tramadol metabolites, the mobile phases were 0.1% formic acid and methanol, in the ratio of 65:35 (v/v) at the flow rate of 300 μL/min for 5 min, with separations on a 4 μ C18 150 × 2.0 mm Synergi Fusion RP column (Phenomenex). The positive mass transitions were m/z+ 250 → 44 (N-desmethyltramadol), m/z+ 253 → 47 (N-desmethyltramadol-d3), m/z+ 250 → 58 (O-desmethyltramadol), and m/z+ 256 → 64 (O-desmethyltramadol-d6). The mobile phases for methadone assay were a blend of 0.1% formic acid and 2 mM ammonium formate in water (mobile A) and acetonitrile (mobile B) pumped at 1100 μL/min through a 2.1 mm × 50 mm 5 μ C18 column (Agilent, Phenomenex). A linear gradient method was used that started at 95:5 (A:B v/v), changed to 10:90 over 1.5 min, and returned to 95:5 at 2.5 min until the completion of the run at 4.5 min. The monitored positive-ion mass transitions included m/z+ 310.4 → 105 (methadone), m/z+ 278.4 → 234 (EDDP), and m/z+ 281.4 → 234 (EDDP-d3, internal standard).

For the midazolam 1′-hydroxylation and trazodone N-dealkylation inhibition experiments, a similar approach was used with some differences. The final concentration of midazolam used to initiate the reaction was 200 μM, that of trazodone was 50 μM and the positive control inhibitor was ketoconazole (0.3, 1, 3, 10, and 30 μM). The internal standard 1′-hydroxymidazolam-d4 (200 ng/mL in acetonitrile) for midazolam assay or

diazepam (10 µM in methanol mixed with 1 N HCl) for trazodone assay were used. The HPLC setup consisted of a mixture of 0.1% formic acid with 2 mM ammonium formate in water (mobile A) and 100% acetonitrile (mobile B), which was pumped at 450 µL/min through a 2 mm × 150 mm 4 µ C18 column (Synergi Fusion RP, Phenomenex) for midazolam. For trazodone, mobile phases were pumped at a rate of 1000 µL/min through a 50 mm × 2.1 mm 4 µ C18 column (Agilent Zorbax Eclipse XDB, Phenomenex). A linear gradient method was used that started at 70:30 (A:B v/v), changed to 10:90 over 1.5 min, and returned to 70:30 at 3 min until the completion of the run at 6 min (midazolam). For trazodone, the run was started at 95:5 (A:B v/v), changed to 50:50 over 2.5 min, returned to 95:5 at 3 min, and continued until the completion of the run at 4 min. The monitored positive-ion mass transitions included m/z+ 342 → 297 (1′- hydroxymidazolam), m/z+ 346 → 301 (1′- hydroxymidazolam- d4, internal standard), m/z+ 372.2 → 176.2 (trazodone), m/ z+ 197.2 → 118.1 (m-CCP), and m/z+ 285.0 → 193.2 (diazepam, internal standard).

For the cannabidiol 6-hydroxylation inhibition assay, bovine serum albumin (0.2 mg/mL) was added to the incubation tube, and fluconazole (0.3, 1, 3, 10 and 30 µM) was used as a positive control inhibitor. The reaction was initiated by adding 5 µM cannabidiol and lasted for 30 minutes. Acetonitrile (200 µL) and 10 µM diazepam (internal standard) in methanol (100 µL) were added to terminate the reaction and gently vortexed. The mobile phases, consisting of 0.1% formic acid in water (mobile A) and 100% acetonitrile (mobile B) were pumped at 1.1 mL/min through a 2.1 mm × 50 mm 5 µ C18 column (Zorbax Eclipse XDB-C18, Phenomenex). A linear gradient method was used that started at 80:20 (A:B v/v), changed to 10:90 over 1.5 min, returned to 80:20 at 2.5 min, and was

completed at 5 min. The mass transitions monitored included m/z+ 315.4 → 193.2 (6-hydroxycannabidiol) and m/z+ 285.0 → 193.2 (diazepam, internal standard).

The cannabidiol, methadone, and trazodone metabolism inhibition experiments were repeated by replacing the pDLMs with the recombinant enzymes CYP2C21 (40 pmoles/mL), CYP2B11 (20 pmoles/mL), and CYP3A12 (10 pmoles/mL), respectively.

3.2.5 CALCULATION OF IC_{50} VALUES

Inhibitor concentrations resulting in a 50% reduction in enzyme activity – half maximal inhibitory concentration (IC_{50}) – values were determined for each activity and inhibitor as follows. The slope of the log10-transformed of the inhibitor concentrations, the point at which this line intersects the *Y* axis in a linear regression, and the substrate depletion (expressed as percentage of control) values for each concentration were determined. This calculation was performed using the following formulas:

Equation 2 Calculation of IC50 using linear regression.

(a)

$$y = a + bx$$

(b)

$$IC_{50} = 10^{\frac{bx \times 50}{a}}, y < 50\%$$

(a) Linear regression, where *y* is the substrate depletion value expressed as a percentage of the control (incubation without inhibitor); *a* is the value of *y* when there is no inhibitor (*x=0*); b is the slope; *x* is the value of the base 10 logarithm of the inhibitor concentration (log10[inhibitor]). (b) Calculation of IC_{50} using linear regression. The formula is applicable only when the substrate

depletion value at a concentration of 30 µM is less than 50%. Values lower than 50% depletion when using 30 µM inhibitor were considered. Values higher than 50% depletion after incubation with 30 µM of inhibitor were classified as IC_{50} > 30 µM.

The reported IC_{50} values represent the mean and standard deviation of four separate inhibition experiments.

3.2.6 STATISTICAL ANALYSIS

IC_{50} values of LIN, LINAct, and lavender oil were tested for normality using the Shapiro-Wilk test and compared using the one-way ANOVA followed by the Holm-Sidak post-test. P-values lower than 0.05 were considered significant.

4 RESULTS

4 RESULTS

4.1 *IN SILICO* APPROACH

4.1.1 MOLECULAR MODELING OF THE TARGET PROTEINS CYP2B11, CYP2C21, AND CYP2D15

We used the SWISS-MODEL server to perform homology modeling of our protein targets, and the server identified the templates against the CYP2B11, CYP2C21, and CYP2D15 proteins from AlphaFoldDB to generate the 3D structure of our proteins (Figure 7), and further generation of super imposed structures (Figure 7). For CYP2B11, the best template structure was A0A836CX50.1.A (cytochrome P450 of *Ovis aries* (sheep)) and showed sequence identity 81.30 (Figure 8) and sequence similarity 0.56 with the template structure. For protein CYP2C21, the best template structure identified was A0A6P3GP28.1.A (cytochrome P450 of *Bison bison* (North American plains bison)) and showed sequence identity 79.18 (Figure 9) and sequence similarity 0.55 with the template structure. For the protein CYP2D15, the best identified template was E3VVY0.1.A (cytochrome P450 of *Panthera tigris altaica* (Siberian tiger)) and showed a sequence identity of 80.20 (Figure 10) and sequence similarity of 0.56 with the template structure.

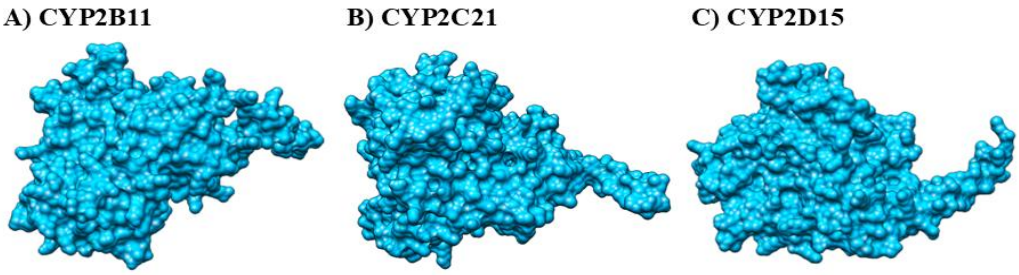

Figure 8 Modeled 3D structure of canine proteins CYP2B11, CYP2C21, and CYP2D15 from SWISS-MODEL server against: (A) template A0A836CX50.1.A (Cytochrome P450 of Ovis aries (Sheep)). GMQE = 0.94. (B) A0A6P3GP28.1.A (Cytochrome P450 of Bison bison (North American plains bison)). GMQE = 0.94, and (C) E3VVY0.1.A (Cytochrome P450 of *Panthera tigris altaica* (Siberian tiger)). GMQE = 0.93, respectively.

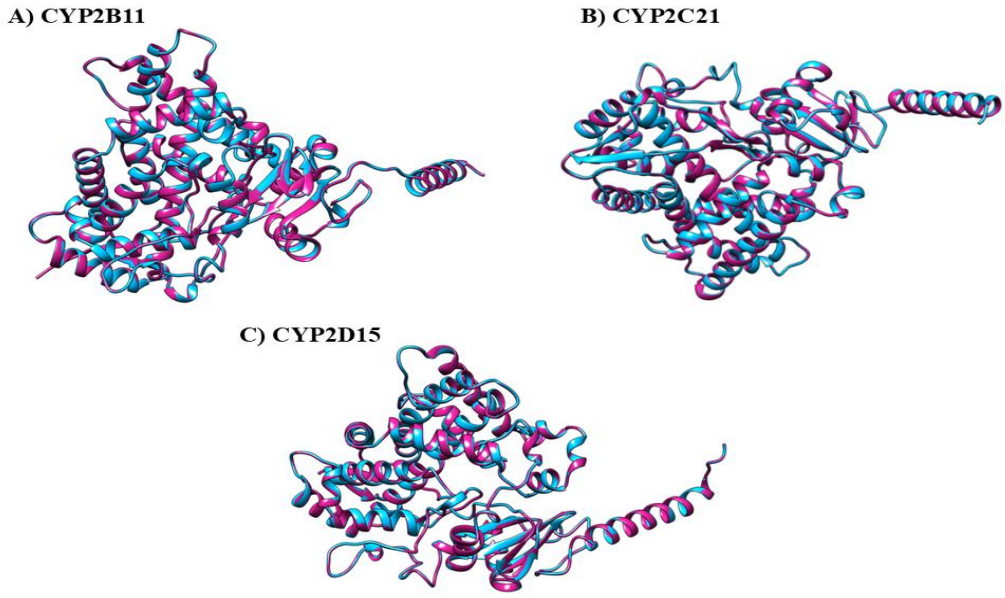

Figure 91 Super imposed structure of: (A) modeled protein CYP2B11 (blue) with template A0A836CX50.1.A (Cytochrome P450 of *Ovis aries* (Sheep)) (red). GMQE = 0.94, (B) Super imposed structure of modeled protein CYP2C21 (blue) with template A0A6P3GP28.1.A (Cytochrome P450 of North American plains bison (*Bison bison*) (red)). GMQE = 0.94, and (C)

protein CYP2D15 (blue) with template E3VVY0.1.A (Cytochrome P450 of *Panthera tigris altaica* (Siberian tiger)) in red). GMQE = 0.93.

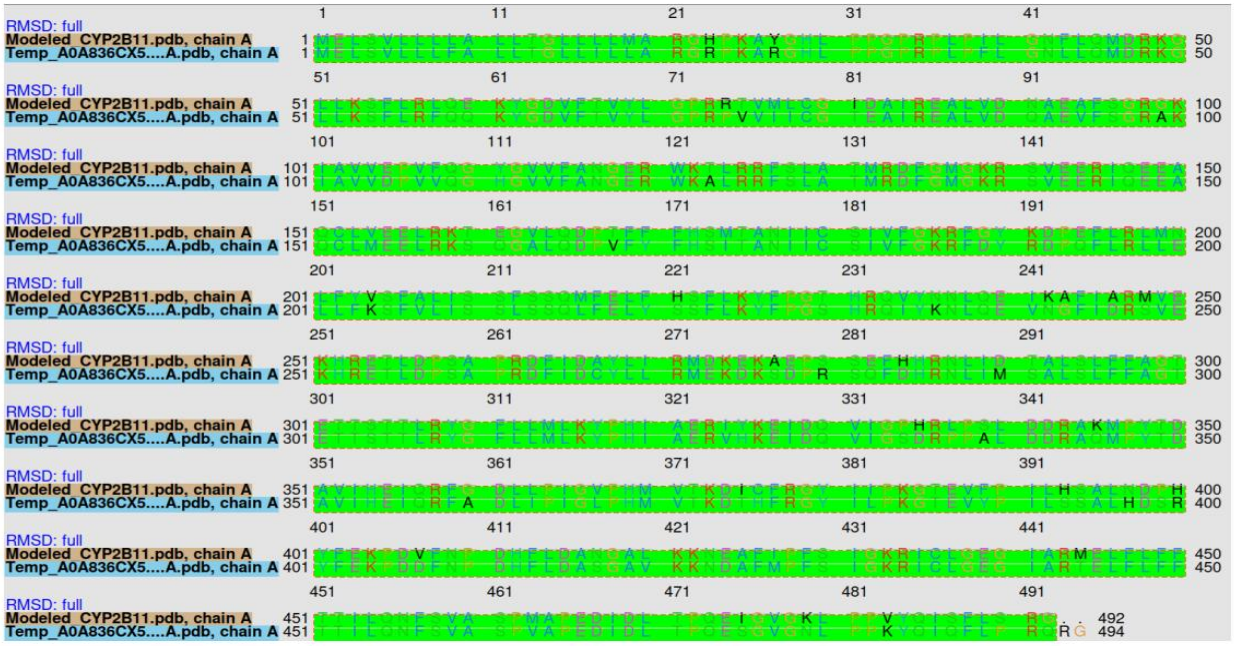

Figure 102 Structure alignment of modeled protein CYP2B11 with template A0A836CX50.1.A (Cytochrome P450 of Ovis aries (Sheep)). Percentage Identity between modeled structure and template 81.30 %.

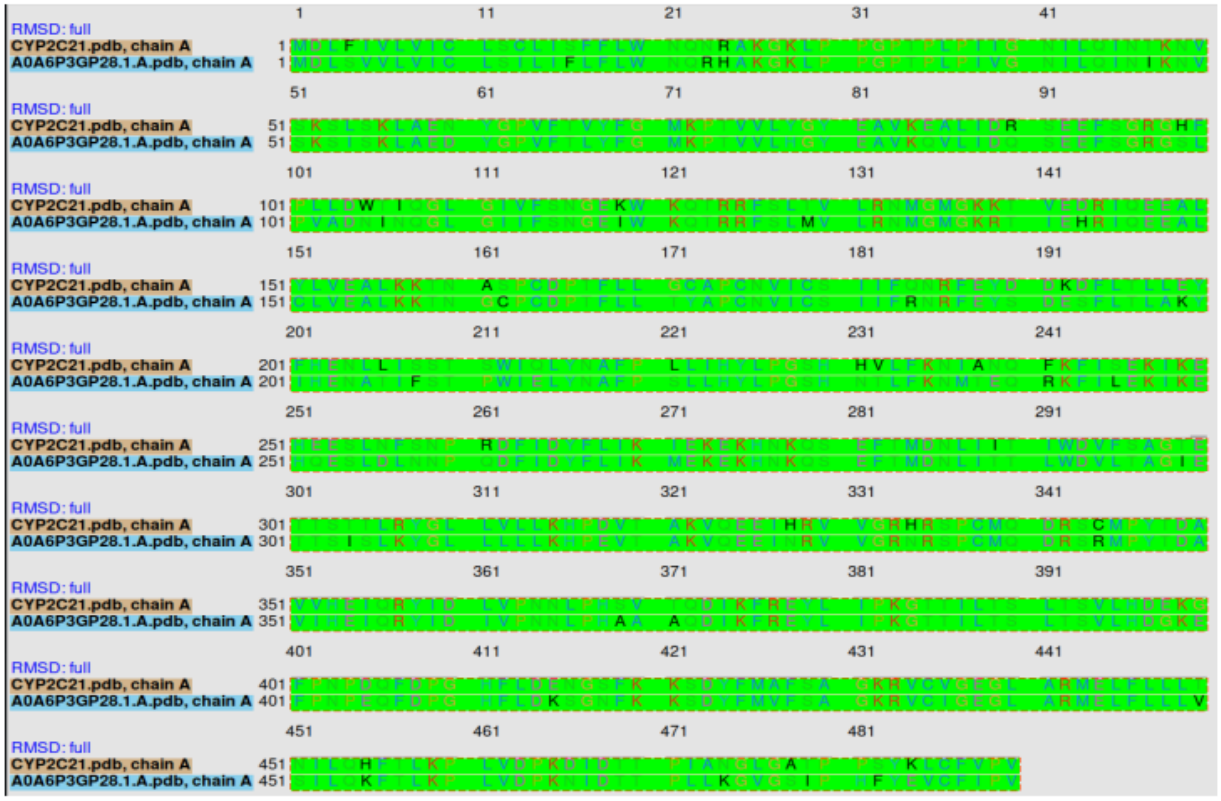

Figure 11 Structure alignment of modeled protein CYP2C21 with template A0A6P3GP28.1.A (Cytochrome P450 of North American plains bison (Bison bison)). Percentage Identity between modeled structure and template 79.18 %.

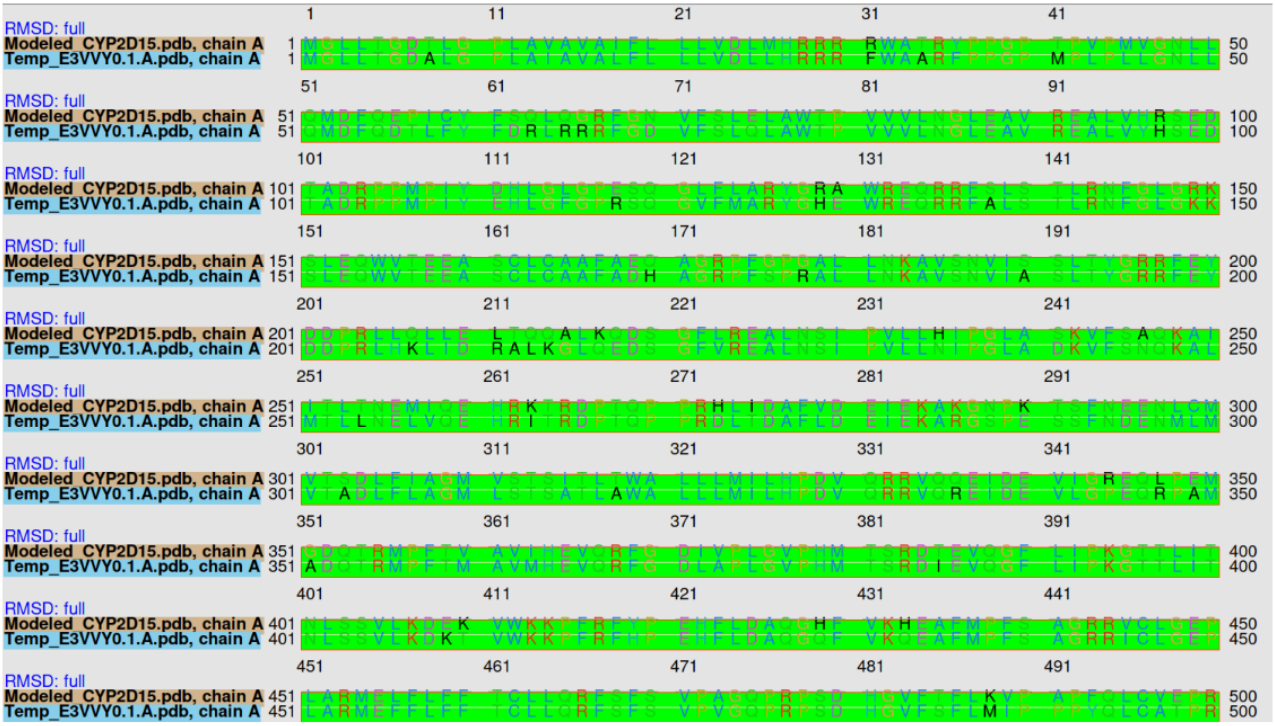

Figure 12 Structure alignment of modeled protein CYP2D15 with template E3VVY0.1.A (Cytochrome P450 of Panthera tigris altaica (Siberian tiger)). Percentage Identity between modeled structure and template 80.20 %.

Figures 7 to 10 reveal that the modeled proteins were highly similar to the template. After generating the 3D structure of proteins, we further performed structure validation analysis to generate the Ramachandran graph from Procheck SAVES server (Graphic 1) and identified for modeled protein structure of CYP2B11 showed 92.5 % residues were in most favored regions; residues in additional allowed regions (a, b, l, p): 30 (7.0 %); residues in generously allowed regions (-a, -b, -l, -p): 1 (0.2 %); residues in disallowed regions: 1 (0.2 %); number of non-glycine and non-proline residues: 426; number of end-residues (except Gly and Pro): 1; number of glycine residues (shown as triangles): 34; number of proline residues: 31; total number of residues: 492. (Graphic 1a), for modeled protein structure of CYP2C21 showed 92.1 % residues were in most favored regions; residues in additional

allowed regions (a, b, l, p): 30 (6.9 %); residues in generously allowed regions (-a, -b, -l, -p): 3 (0.7 %); residues in disallowed regions: 1 (0.2 %); number of non-glycine and non-proline residues: 432; number of end-residues (except Gly and Pro): 2; number of glycine residues (shown as triangles): 27; number of proline residues: 29; total number of residues: 490. (Graphic 1b), and for modeled protein structure of CYP2D15 showed 92.1 % residues were in most favored regions; residues in additional allowed regions (a, b, l, p): 32 (7.5 %); residues in generously allowed regions (-a, -b, -l, -p): 0 (0.0 %); residues in disallowed regions: 2 (0.5 %); number of non-glycine and non-proline residues: 428; number of end-residues (except Gly and Pro): 2; number of glycine residues (shown as triangles): 33; number of proline residues: 37; total number of residues: 500. (Graphic 1c), which shows our modeled proteins structure are good of good quality.

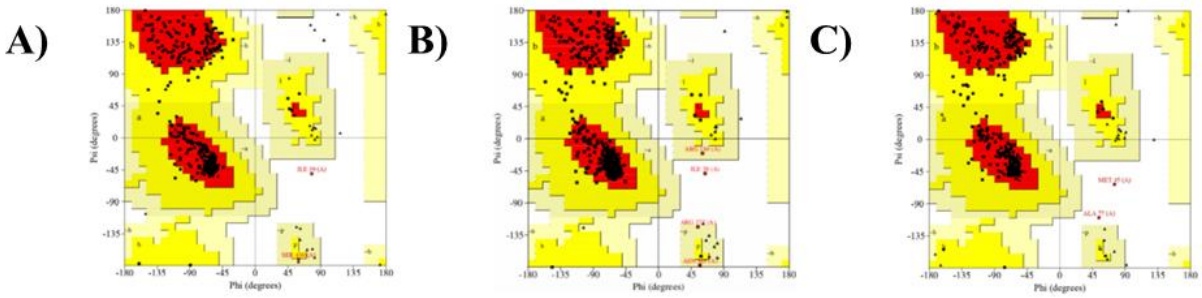

Figure 13 Structure validation Ramachandran graph of modeled protein from Procheck SAVES server. (A) CYP2B11. Residues in the most favored regions (A, B, L): 394 (92.5%) (B) CYP2C21. Residues in the most favored regions (A, B, L): 398 (92.1%) (C) CYP2D15. Residues in the most favored regions (A, B, L): 394 (92.1%).

4.1.2 Molecular Docking Analysis

Molecular docking analysis was performed using AutoDock Vina to identify the binding energy between the modeled protein targets and the ligand compounds LIN and LINAct.

Based on our docking analysis, we identified that the protein target CYP2B11 binds to residues LYS 122 and ARG 126 and forms a hydrogen bond with the ligand compound LIN (Figure 11, Table 2). The protein also showed a binding interaction and formed hydrogen bonds with residues ASN 397 and LYS 479 against the ligand compound LINAct (Figure 11). Similarly, LIN and LINAct were docked against the CYP2C21 protein (Figure 12, Table 3). Based on our docking analysis, we identified that CYP2C21 showed a binding interaction with residues ASN 474 and SER 51 and formed a hydrogen bond against LIN and LINAct, respectively (Figure 12). Protein CYP2D15 showed a binding interaction and formed a hydrogen bond with residues SER 62, GLN 65, ASN 85, and ASN 401 against ligand compound LIN (Figure 13). Additionally, protein CYP2D15 showed interaction with residues ARG 197 and TYR 200 and formed a hydrogen bond against ligand compound LINAct (Figure 13, Table 4).

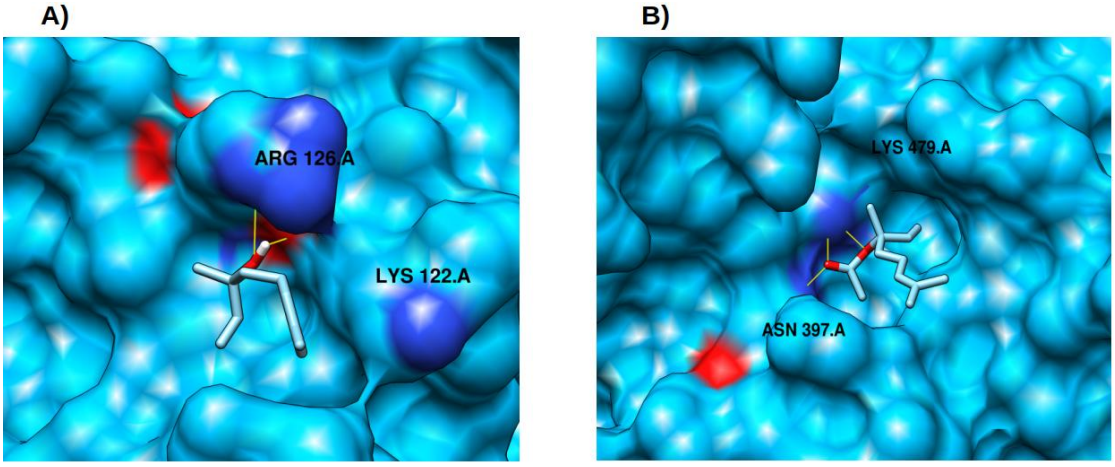

Figure 14 Molecular docking analysis of the CYP2B11 protein using the MOE tool. (A) Binding interaction with the ligand compound linalool. Represented by a yellow line, a hydrogen bond between the molecule and the residue ARG.A. (B) Binding interaction with the ligand compound linalyl acetate. Represented by a yellow line, a hydrogen bond between the molecule and residue ASN 397.A. CYP2B11 is represented in blue. The electronegative zone of the protein is indicated

in red. In purple, amino acids with potential interactions with each molecule are represented. ARG 126.A = arginine; LYS 122.A = lysine.

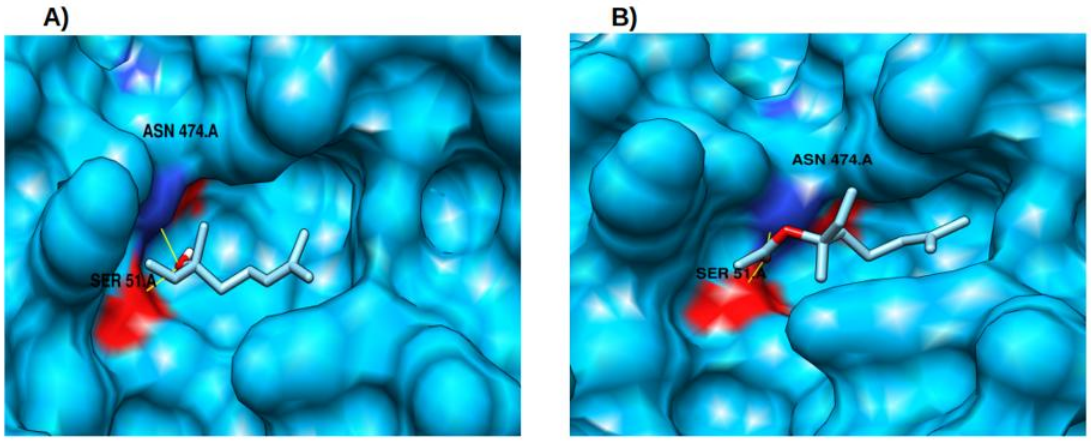

Figure 15 Molecular docking analysis of the CYP2C21 protein using the MOE tool. (A) Binding interaction with the ligand compound linalool. Represented by a yellow line, a hydrogen bond between the molecule and the residue SER 51.A. and ASN 474.A. (B) Binding interaction with the ligand compound linalyl acetate. Represented by a yellow line, a hydrogen bond between the molecule and residue SER 51.A and ASN 474.A. CYP2C21 is represented in deep sky blue. The electronegative zone of the protein is indicated in red. In purple, amino acids with potential interactions with each molecule are represented. SER 51.A = serine; ASN 474.A = asparagine.

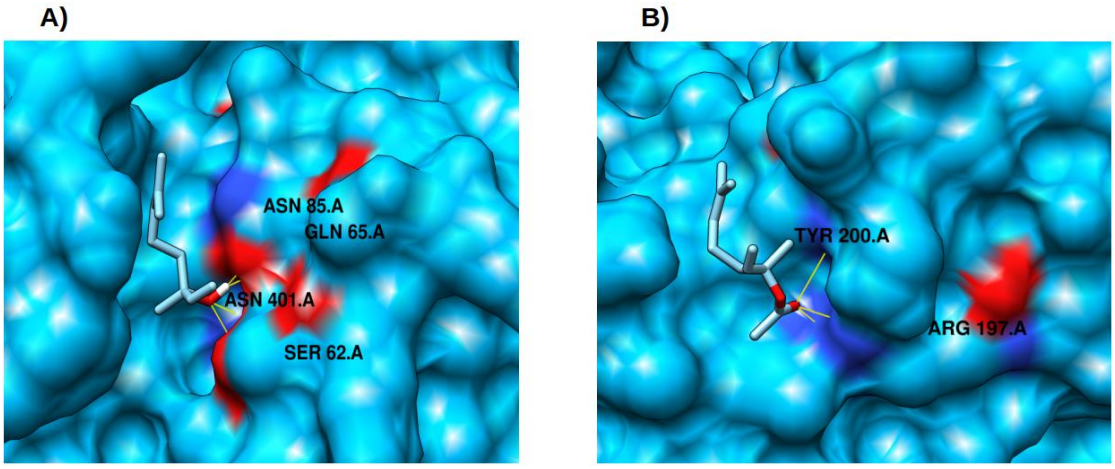

Figure 16 Molecular docking analysis of the CYP2D15 protein using the MOE tool. (A) Binding interaction with the ligand compound linalool. Represented by a yellow line, a hydrogen bond between the molecule and the residue ASN 401.A. and SER 62.A. (B) Binding interaction with the ligand compound linalyl acetate. Represented by a yellow line, a hydrogen bond between the molecule and residue TYR 200.A. CYP2D15 is represented in deep sky blue. The electronegative

zone of the protein is indicated in red. In purple, amino acids with potential interactions with each molecule are represented. ASN 401.A = asparagine; SER 62.A = serine; TYR 200.A; = tyrosine; GLN 65.A = glutamine; ASN 85.A = asparagine; ARG 197.A = arginine.

Table 3 Molecular docking binding energy with interacted residues of protein CYP2B11 with ligand compound linalool and linalyl acetate.

	Compound Ligand Name	Autodock Vina Binding Affinity (kcal/mol)	Binding Residues/Number of Hydrogen Bonds
1	Linalool	-4.096	LYS 122, ARG 126/2
2	Linalyl Acetate	-4.643	ASN 397, LYS 479/3

Table 4 Molecular docking binding energy with interacted residues of Protein CYP2C21 with ligand compound Linalool and linalyl acetate.

	Compound Ligand Name	Autodock Vina Binding Affinity (kcal/mol)	Binding Residues/Number of Hydrogen Bonds
1	Linalool	-4.487	ASN 474, SER 51/2
2	Linalyl Acetate	-4.998	ASN 474, SER 51/2

Table 5 Molecular docking binding energy with interacted residues of protein CYP2D15 with ligand compound linalool and linalyl acetate.

	Compound Ligand Name	Autodock Vina Binding Affinity (kcal/mol)	Binding Residues/Number of Hydrogen Bonds
1	Linalool	-4.144	SER 62, GLN 65, ASN 85 and ASN 401/4
2	Linalyl Acetate	-4.199	TYR 200/3

4.1.3 Ligand-Based Drug Design

4.1.3.1 Pharmacophore properties of linalool and linalyl acetate

For LIN, 5 pharmacophoric characteristics were identified, being 2 hydrophobic groups located in the terpene side chain, a dual region (i.e., hydrogen bond acceptor or donor) located in one of the terminal zones of the molecule and 2 AtomQ in the other

terminal zone (Figure 14). AtomQ is a generic pharmacophoric region that does not fit as a hydrogen-bond donor or acceptor but is relevant for interactions with biological targets. LINAct, on the other hand, has very different pharmacophoric characteristics. Five hydrophobic regions distributed throughout the terpene structure, one hydrogen-bond acceptor region located at the opposite end to the terpene nucleus, and one AtomQ between the acceptor and hydrophobic regions were identified, totaling seven pharmacophoric characteristics (Figure 15).

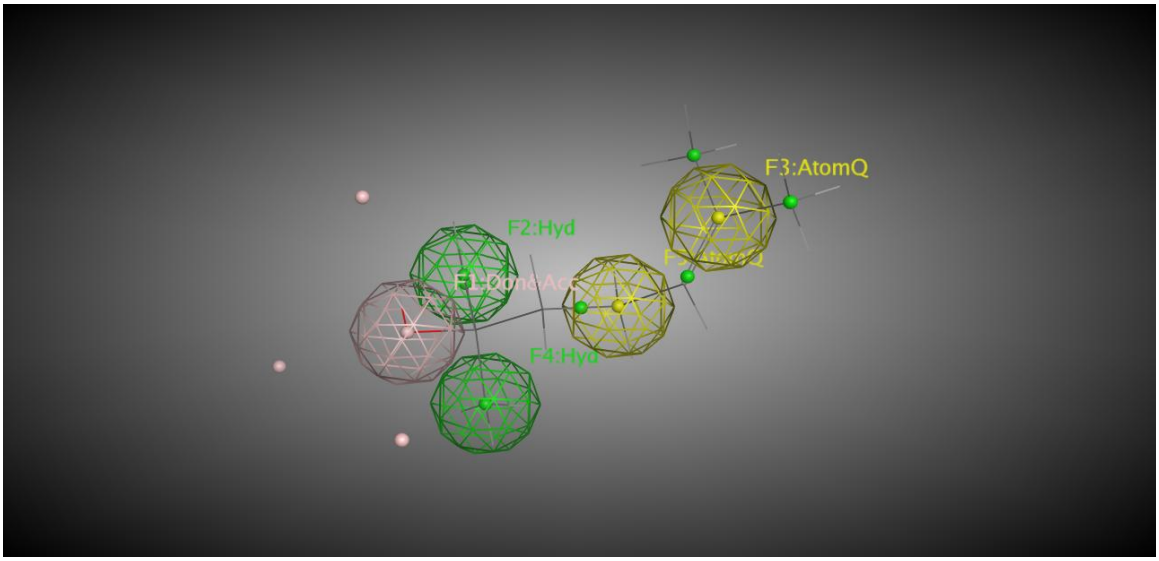

Figure 17 Mapping of the pharmacophoric properties of linalool using the MOE tool. The molecule has 2 hydrophobic groups, represented in green (F2:Hyd and F4:Hyd) and 1 hydrogen bond donor region, represented in pink (F1:DonAcc). Two AtomQ are observed in yellow. F = feature number; Hyd = Hydrophobic region; DonAcc = Dual donor/acceptor; AtomQ = Qualifying Atom.

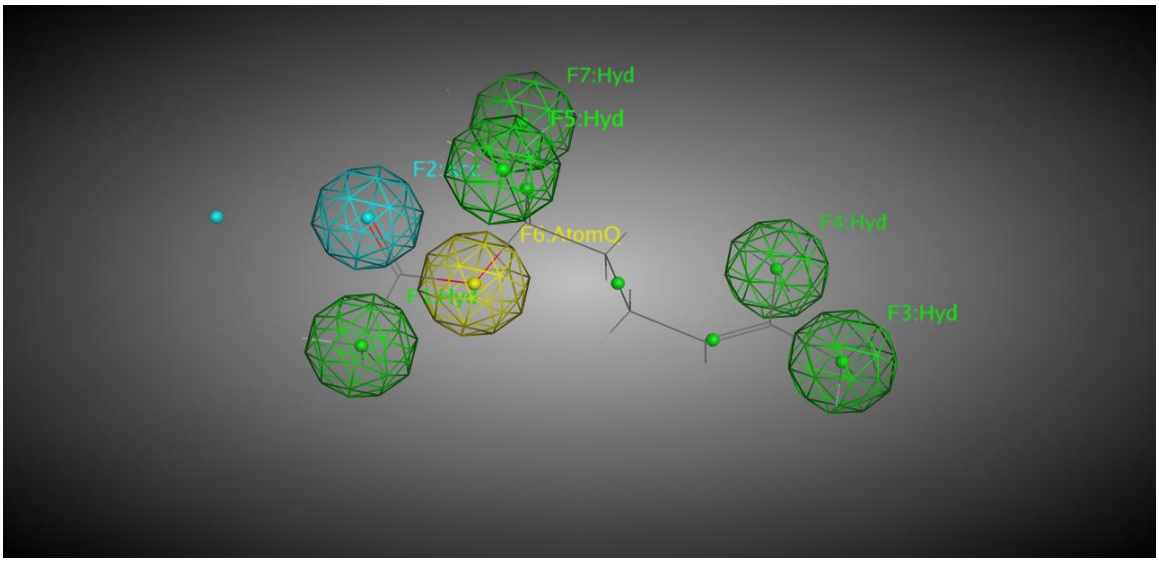

Figure 18 Mapping of the pharmacophoric properties of linalyl acetate using the MOE tool. The molecule has 5 hydrophobic groups, represented in green (F1, F3, F4, F5 and F7:Hyd) and 1 hydrogen bond acceptor region, represented in blue (F2:Acc). A AtomQ are observed in yellow. F = feature number; Hyd = Hydrophobic region; Acc = Dual Hydrogen bond acceptor; AtomQ = Qualifying Atom.

4.1.4 MOLECULAR DOCKING

No experimental data were manually manipulated in this study. The results presented were based on computational predictions made using MOE's internal algorithms without modifying the tool's default parameterization.

Docking was performed for CYP2B11 against LIN and LINAct. The complete docking results are shown in table 5. In the case of LIN, two interactions were observed. The predicted hydrogen bond donor and acceptor features of LIN were found to interact with GLN 59 and ASP 64 residue of CYP2B11 protein. However, in the case of LINAct, the predicted hydrogen-bond acceptor feature was observed to interact with HIS 400 residues of the CYP2B11 protein (Figure 16, Table 5).

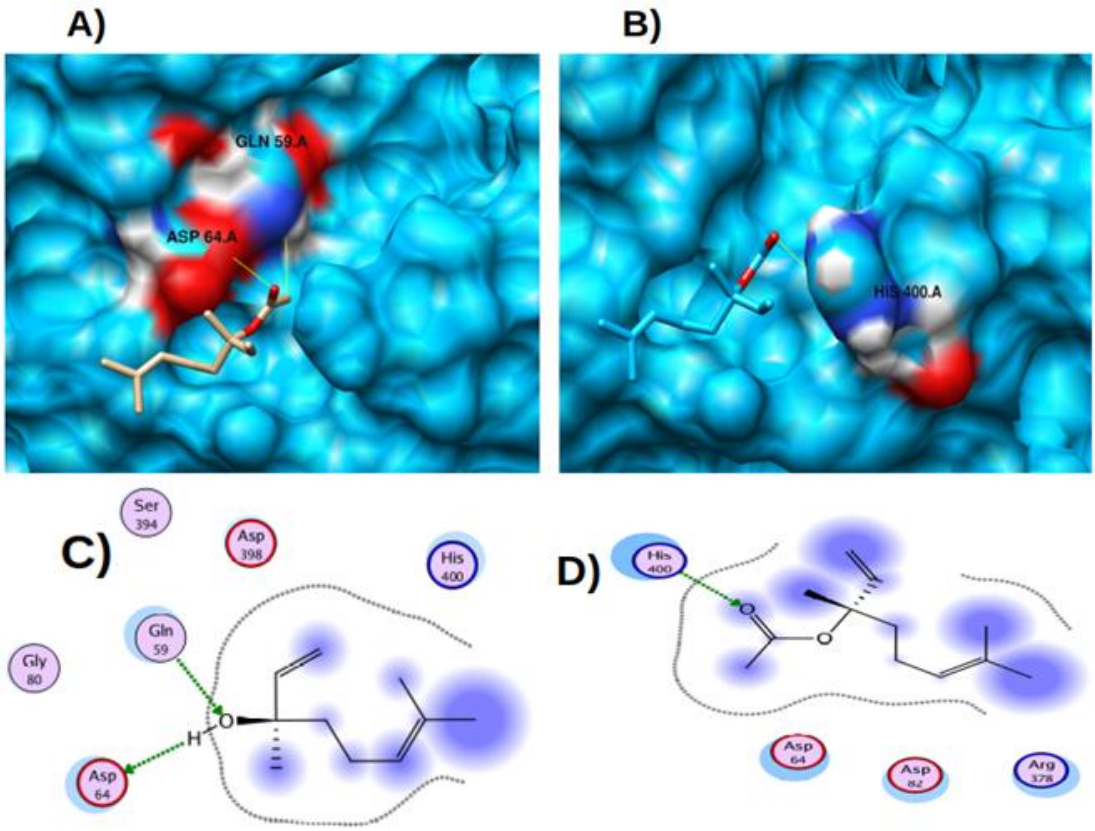

Figure 19 Molecular docking analysis and binding map between linalool, linalyl acetate, and CYP2B11 using the MOE tool. (A) 3D representation of the molecular docking between linalool and CYP2B11. The yellow lines indicate that the ligand interacts with hydrogen bonds with the amino acids GLY (glycine) and ASP (asparagine). (B) 3D representation of molecular docking between linalyl acetate and CYP2B11. The yellow lines indicate that the ligand has hydrogen interactions with the amino acid HIS 400 (histidine). (C) 2D representation of the binding map between linalool and the main amino acids involved in the interactions between the compound and CYP2B11. (D) 2D representation of the bond map between linalyl acetate and the main amino acids involved in the interactions between the compound and CYP2B11. The red color represents the electronegative regions in the 3D representation. Blue represents positive regions in the 3D representation. In the 2D representation, the green dotted line represents hydrogen bonds, red halos represent possible hydrogen bonds, and blue halos represent nonpolar interactions. ARG = Arginine; ASP = Aspartic acid; GLN = Glutamine; SER = Serine.

Table 6 Molecular docking binding score and energy of ligand compound linalool and linalyl acetate against protein CYP2B11.

	Ligand Name	Docking Scores	GBVI/WSA	Binding Residues/Number of Hydrogen Bonds
1	Linalool	-7.624	-15.8441	GLN 59 and ASP 64/2
2	Linalyl acetate	-6.917	-13.7862	HIS 400/1

Similarly, LIN and LINAct were docked against CYP2C21 protein (Figure 17, Table 6). LIN exhibited two interactions with CYP2C21 protein. The same features of LIN were observed to contribute to interactions (Figures 17a and 17c). Interactions were observed between compound and ASN 204 and SER 208. However, LINAct showed no interaction with CYP2C21 protein.

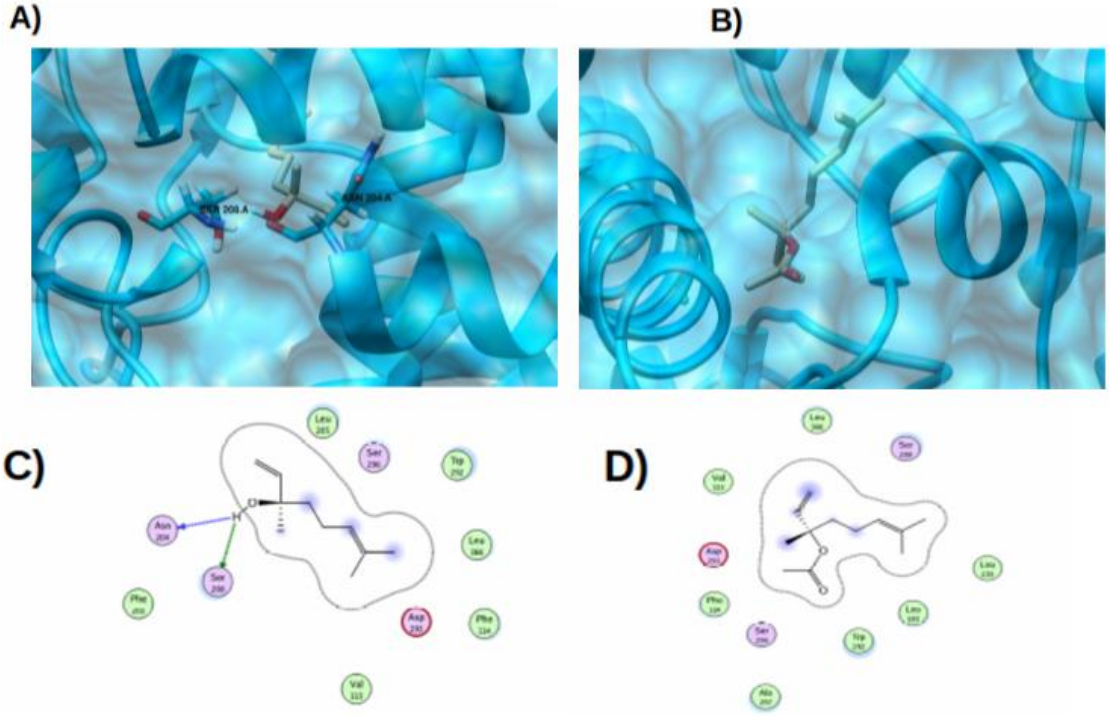

Figure 20 Molecular docking analysis and binding map between linalool, linalyl acetate, and CYP2C21 using the MOE tool. (A) 3D representation of the molecular docking between linalool and CYP2C21. The yellow lines indicate that the ligand interacts with hydrogen bonds with the amino acids SER (serine) and ASN (asparagine). (B) 3D representation of molecular docking between linalyl acetate and CYP2C21. The absence of yellow lines indicates that there are no hydrogen interactions with the protein. (C) 2D representation of the binding map between linalool and the main amino acids involved in the interactions between the compound and CYP2C21. (D) 2D representation of the bond map between linalyl acetate and the main amino acids involved in the interactions between the compound and CYP2C21. Blue represents positive regions in the 3D representation (50% transparency). In the 2D representation, the green dotted line represents hydrogen bonds, and blue dotted line represents a weak hydrogen bond. Red halos represent possible hydrogen bonds. ASP = Aspartic acid; GLU = Glutamic acid; ILE = Isoleucine; LEU = Leucine; PHE = Phenylalanine; THR = Threonine; TYR = Tyrosine; VAL = Valine.

Table 7 Molecular docking binding energy with interacted residues of Protein CYP2C21 with ligand compound linalool and linalyl acetate

	Ligand Name	Docking Scores	GBVI/WSA	Binding Residues/Number of Hydrogen Bonds
1	Linalool	-7.612	-13.345	ASN 204, SER 208/2
2	Linalyl acetate	-6.983	-12.722	No interaction

LIN and LINAct were docked against the CYP2D15 protein (Table 7). Both ligands exhibited a single interaction with the CYP2D15 protein. Interestingly, the same features of both ligands were observed to contribute to interactions (Figure 18). LIN interacts with HIS 112, and LINAct interacts with residue ASN 255.

Table 8 Molecular docking binding score and energy of ligand compound linalool and linalyl acetate against protein CYP2D15

	Ligand Name	Docking Scores	GBVI/WSA	Binding Residues/Number of Hydrogen Bonds
1	Linalool	-6.533	-13.6314	HIS 112/1
2	Linalyl acetate	-6.711	-13.2242	ASN 255/1

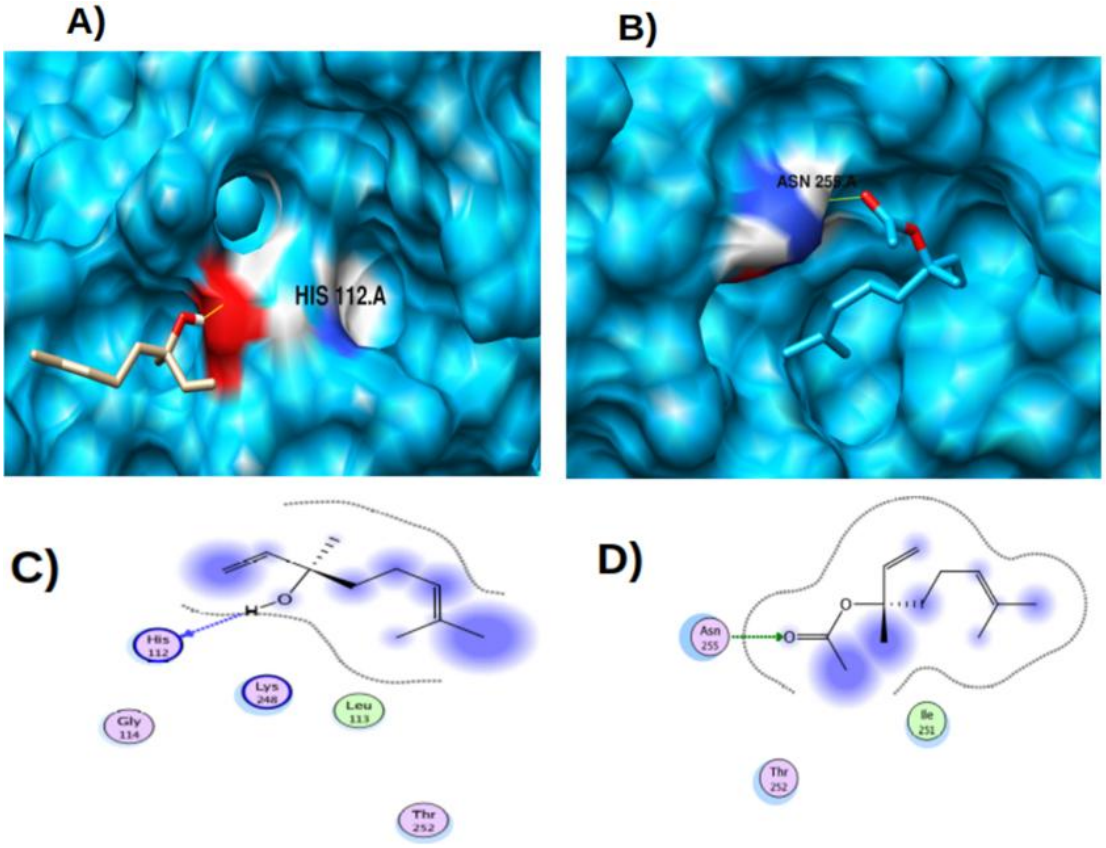

Figure 21 Molecular docking analysis and binding map between linalool, linalyl acetate, and CYP2D15 using the MOE tool. (A) 3D representation of the molecular docking between linalool and CYP2D15. The yellow lines indicate that the ligand interacts with hydrogen bonds with the amino acids HIS (histidine). (B) 3D representation of molecular docking between linalyl acetate and CYP2D15. (C) 2D representation of the binding map between linalool and the main amino acids involved in the interactions between the compound and CYP2D15. The yellow lines indicate that the ligand has hydrogen interactions with the amino acid ASN (asparagine). (D) 2D representation of the bond map between linalyl acetate and the main amino acids involved in the interactions between the compound and CYP2D15. The red color represents the electronegative regions in the 3D representation. Blue represents positive regions in the 3D representation. In the 2D representation, the green dotted line represents hydrogen bonds and blue dotted line represents a weak hydrogen bond. Blue halos represent nonpolar interactions. GLY = Glycine; ILE = Isoleucine; LEU = Leucine; LYS = Lysine; THR = Threonine.

4.2 *IN VITRO* APPROACH

4.2.1 CHROMATOGRAPHIC IDENTIFICATION AND QUANIFICATION OF LINALOOL AND LINALYL ACETATE IN INCUBATIONS

Figure 19 shows representative HPLC tandem mass spectrometry chromatograms used to quantify LIN and LINActCT concentrations in liver microsomal incubations. Since the positive ion mass transitions used to detect both LIN and LINActCT were identical (m/z+ 137.2→81), it was essential to ensure adequate chromatographic separation of the LIN peak at 1.53 minutes and the LINActCT peak at 1.81 minutes, as shown in Figure 19a. The positive ion mass transitions used for the internal standards, linalool-d3 (m/z+ 140.2→83; Figure 1b) and diazepam (m/z+ 285→193; Figure 1c) were unique for each compound. Figure 20 shows representative standard curves for LIN (Figure 20a) and LINActCT (Figure 20b) generated using varied concentrations of these analytes and fixed concentrations of the respective internal standards (linalool-d3 for LIN and diazepam for LINAct).

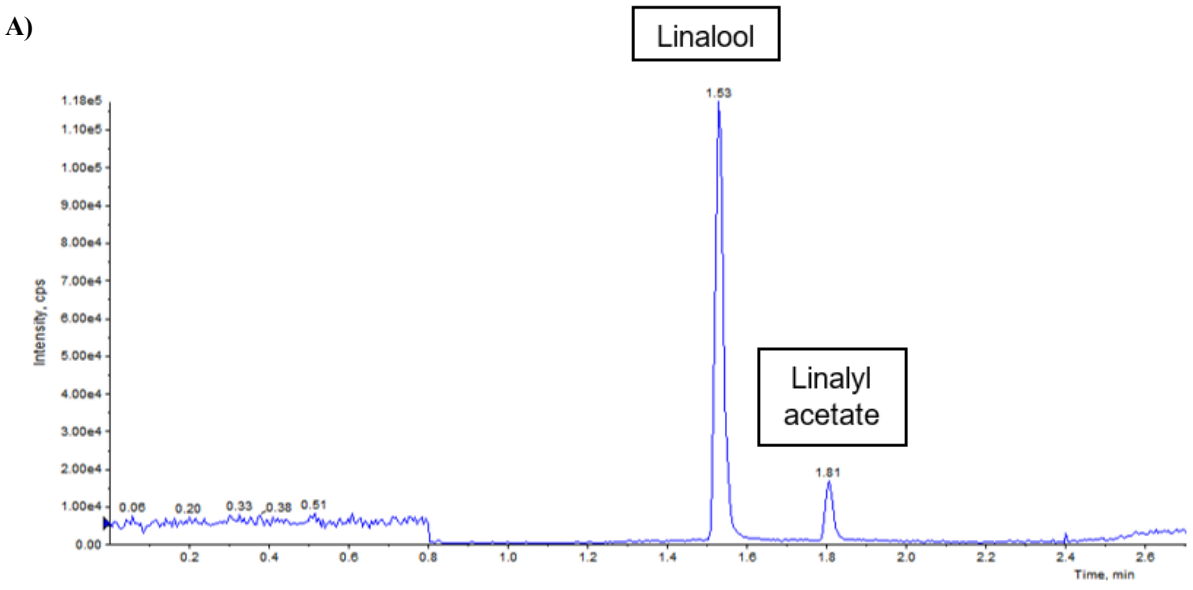

B)

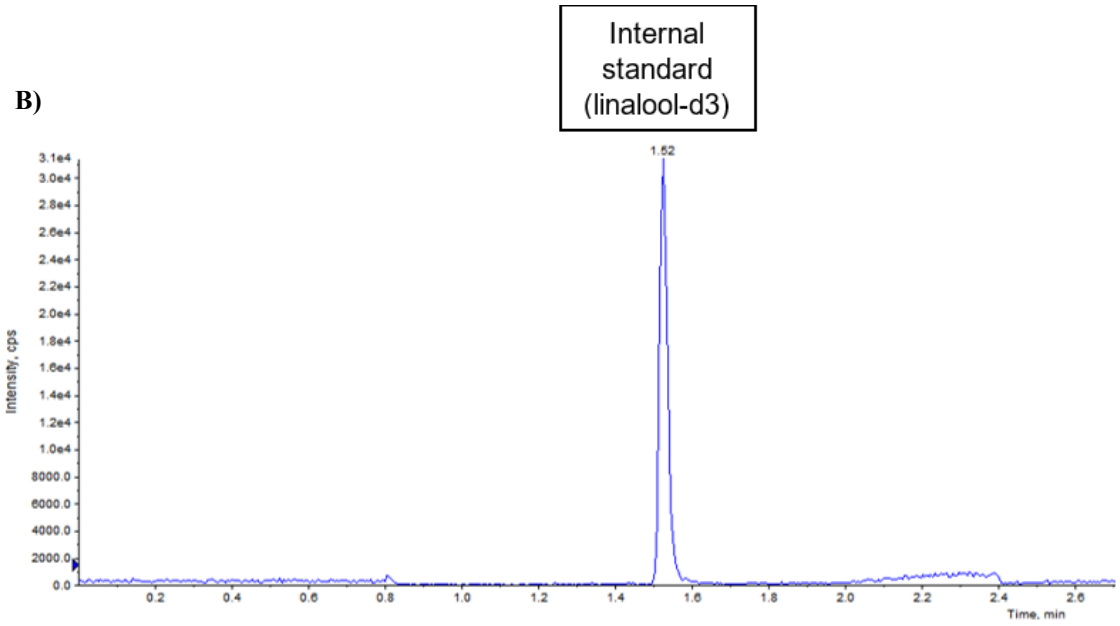
Internal standard (linalool-d3)
1.52
Intensity, cps
Time, min

C)

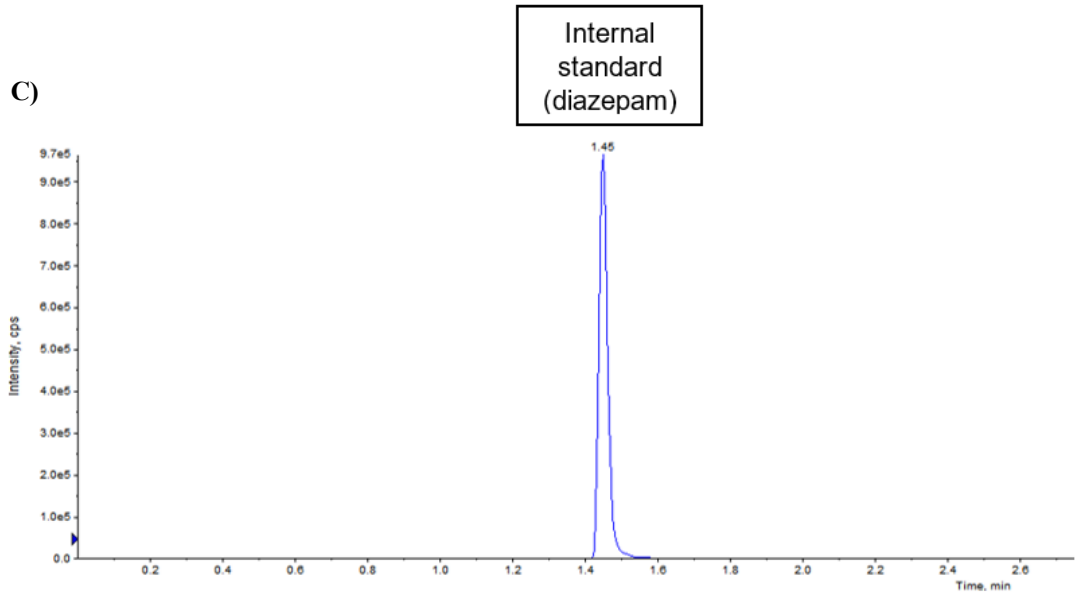
Internal standard (diazepam)
1.45
Intensity, cps
Time, min

D)

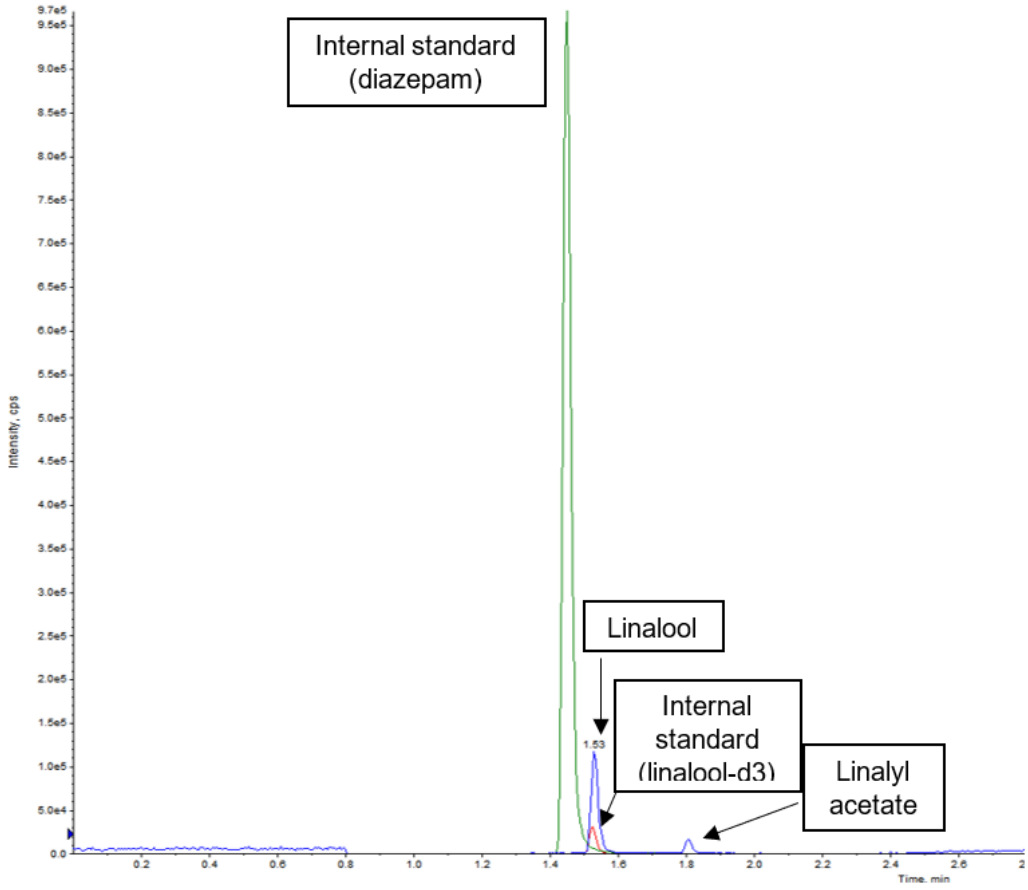

Figure 22 Representative chromatograms of linalool, linalool-d3 (internal standard for linalool), linalyl acetate and diazepam (internal standard for linalyl acetate) analyzed by HPLC tandem mass spectrometry. (a) Chromatogram showing separation of positive ion transition mass peaks corresponding to linalool (m/z+ 137.2→81 at 1.53 minutes) and linalyl acetate (m/z+ 137.2→81 at 1.81 minutes). (b) Chromatogram of linalool-d3 (m/z+ 140.2→83 at 1.53 minutes). (c) Chromatogram of diazepam (m/z+ 285→193 at 1.46 minutes). (d) Merged chromatograms.

A)

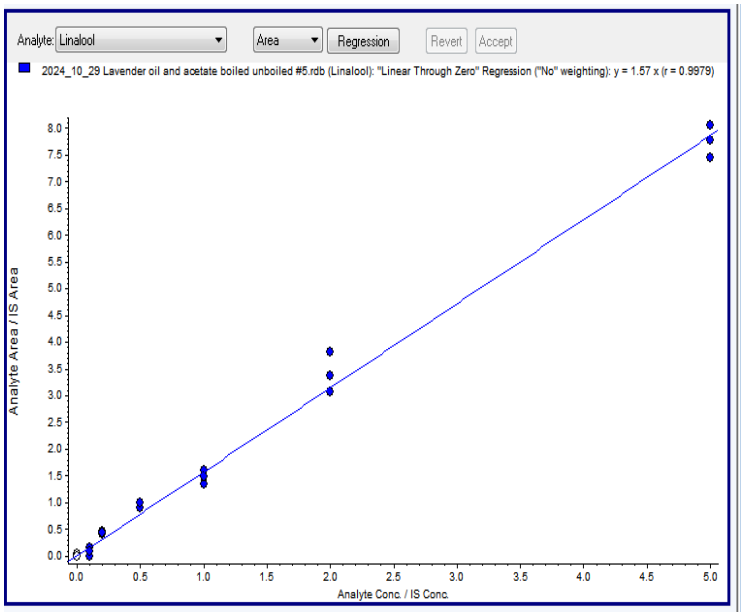

B)

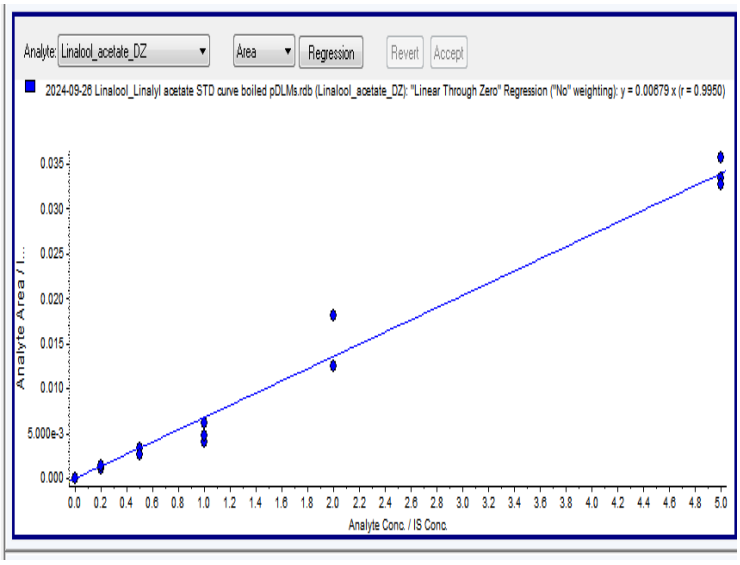

Figure 23 Representative standard curves measurement of linalool (a) and linalyl acetate (b) concentrations in liver microsome incubations. The curve was generated from the comparison between the areas of the analytes and their respective internal standards (linalool-d3 for linalool and diazepam for linalyl acetate) at different concentrations (0, 0.1, 0.2, 0.5, 1, 2, and 5 µM for each analyte). Linear regression was used for the analysis (r^2>0.99 for both analytes). The lowest limits of quantification (LLOQ) were 0.08 µM for linalool and 0.19 µM for linalyl acetate (±SD). These curves were used to determine the concentration of analytes in incubations with canine liver microsomes and to calculate the metabolic parameters.

4.2.2 LINALOOL, LINALYL ACETATE, AND LAVENDER OIL METABOLISM BY POOLED DOG LIVER MICROSOMES

To evaluate the participation of the cofactors NADPH and UDPGA in the metabolism of LIN, LINAct, and lavender oil (containing both LIN and LINAct) by canine liver, incubations were performed using pDLMs with and without each cofactor. Graphic 2 shows the influence of adding each cofactor on the depletion of LIN (a) and LINAct (b), and on the appearance of LIN during the LINAct depletion experiment (c). LIN depletion was observed only in incubations containing NADPH (Graphic 2a). LINAct depletion was observed with or without cofactor addition (Graphic 2b). However, LINAct depletion was somewhat faster in incubations containing NADPH compared to those without NADPH.

LIN concentrations in LINAct incubations linearly increased with time up to about 20 minutes with or without cofactor addition (Graphic 2c). After 20 minutes, LIN concentrations continued to increase in incubations with or without UDPGA, while LIN concentrations in incubations containing NADPH decreased.

Graphic 3 shows the change in LIN and LINAct concentrations in incubations containing lavender oil and pDLMs with and without added cofactor (NADPH or UDPGA). LIN depletion was observed only in incubations containing NADPH (Graphic 3a). Rapid LINAct depletion was observed in all incubations but appeared to be much faster with NADPH inclusion since LINAct was not detected 5 minutes after the start of incubation, while LINAct concentrations were essentially unchanged at 5 minutes for incubations with or without UDPGA.

A)

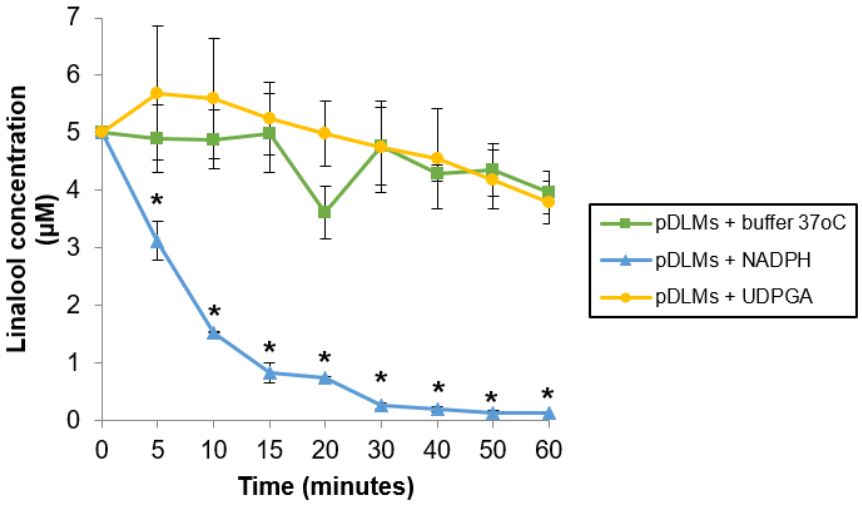
Linalool concentration (µM)
Time (minutes)
pDLMs + buffer 37oC
pDLMs + NADPH
pDLMs + UDPGA

B)

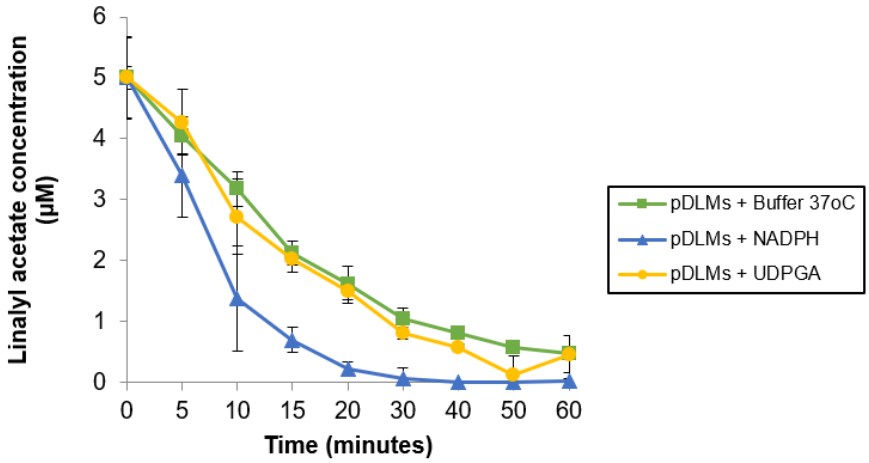
Linalyl acetate concentration (µM)
Time (minutes)
pDLMs + Buffer 37oC
pDLMs + NADPH
pDLMs + UDPGA

C)

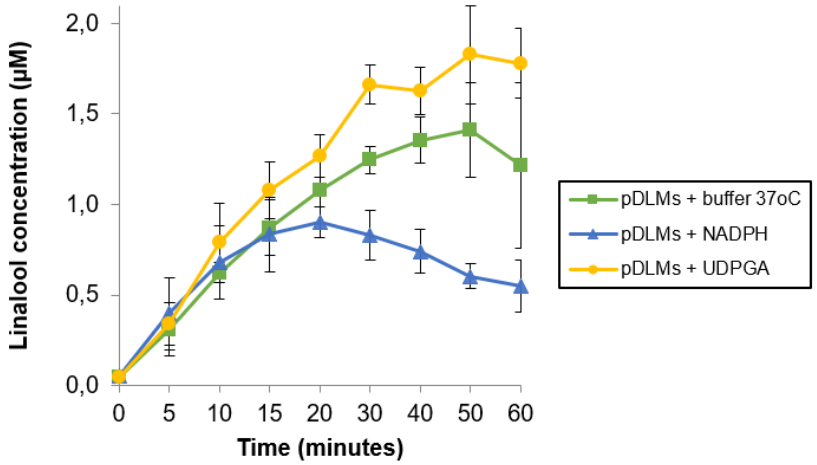

Figure 24 Influence of enzyme cofactors on the depletion and formation of linalool and on the depletion of linalyl acetate. Linalool (a, c) and linalyl acetate (b) concentrations were measured at intervals of 5–60 min in incubations of liver microsomes in the presence or absence of the enzyme cofactors NADPH and UDPGA. The initial concentrations of linalool and linalyl acetate were 5 µM, and the microsomal protein concentration was 0.1 mg/mL. Each point represents the mean (±SD) of three independent experiments. Results were analyzed by one-way ANOVA on Ranks and Dunn's test between the cofactor group and the no cofactor group ("*" $p<0.05$ was considered statistically significant).

A)

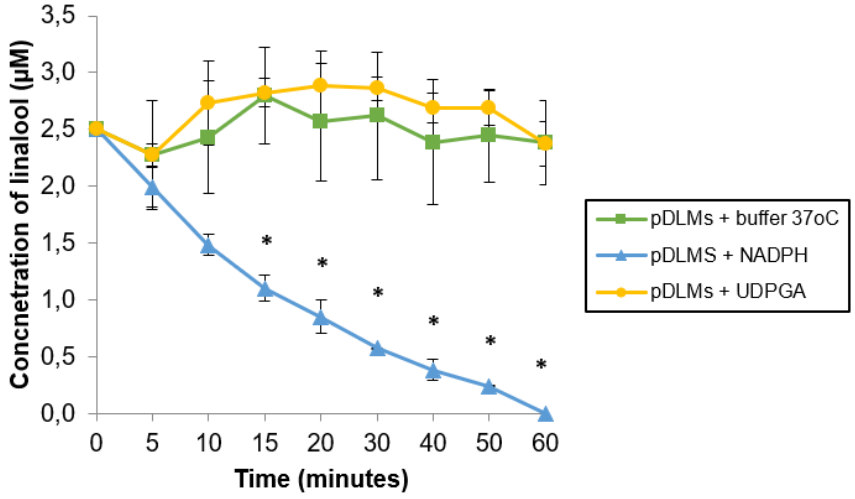

B)

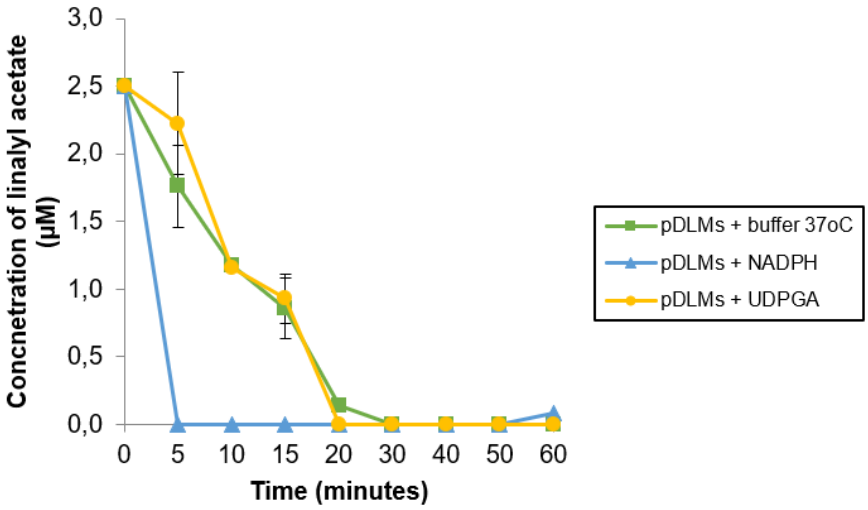

Figure 25 Influence of enzyme cofactors on the depletion of linalool and linalyl acetate from lavender oil. Linalool (a) and linalyl acetate (b) concentrations were measured at intervals of 5–60 min in incubations of liver microsomes in the presence or absence of the enzyme cofactors NADPH and UDPGA. The initial concentrations of linalool and linalyl acetate were 2.5 µM, and the microsomal protein concentration was 0.1 mg/mL. Results expressed as absolute concentrations of linalyl acetate and linalool. Each point represents the mean (±SD) of three independent experiments. Results were analyzed by one-way ANOVA on Ranks and Dunn's test

between the cofactor group and no cofactor group ("*" $p<0.05$ was considered statistically significant).

4.2.3 Effect of enzyme inactivation on linalyl acetate metabolism by pooled dog liver microsomes

Since LINAct depletion and LIN formation occurred by adding pDLMs without P450 or UGT cofactor, the enzyme dependence of this conversion was determined by evaluating the effect of protein denaturation via boiling the pDLMs. Both pure LINAct (Graphic 4a and 4b) and lavender oil (Graphic 4c and 4d) were evaluated. As shown in Graphic 4a, incubation of pure LINAct with unboiled pDLMs resulted in a progressive decrease in LINAct concentrations from 5 µM to almost 0 µM at 60 minutes. At the same time, LIN concentrations increased from 0 µM to about 1 µM (Graphic 4b). By comparison, incubations with boiled pDLMs still resulted in decreased LINAct concentrations, although to a slightly smaller extent than with unboiled pDLMs (Graphic 4a). In contrast there was no detectable formation of LIN with boiled pDLMs (Graphic 4b) despite the noted depletion of LINAct in the same incubation (Graphic 4a). The depletion of LINAct from lavender oil with boiled or unboiled pDLMs (Graphic 4c) were quite similar to those results observed when depletion of pure LINAct was evaluated (Graphic 4a). In the same incubations, LIN concentrations started at about 2.5 µM (from the lavender oil) and then either stayed unchanged with boiled pDLMs, or slightly increased (with unboiled pDLMs).

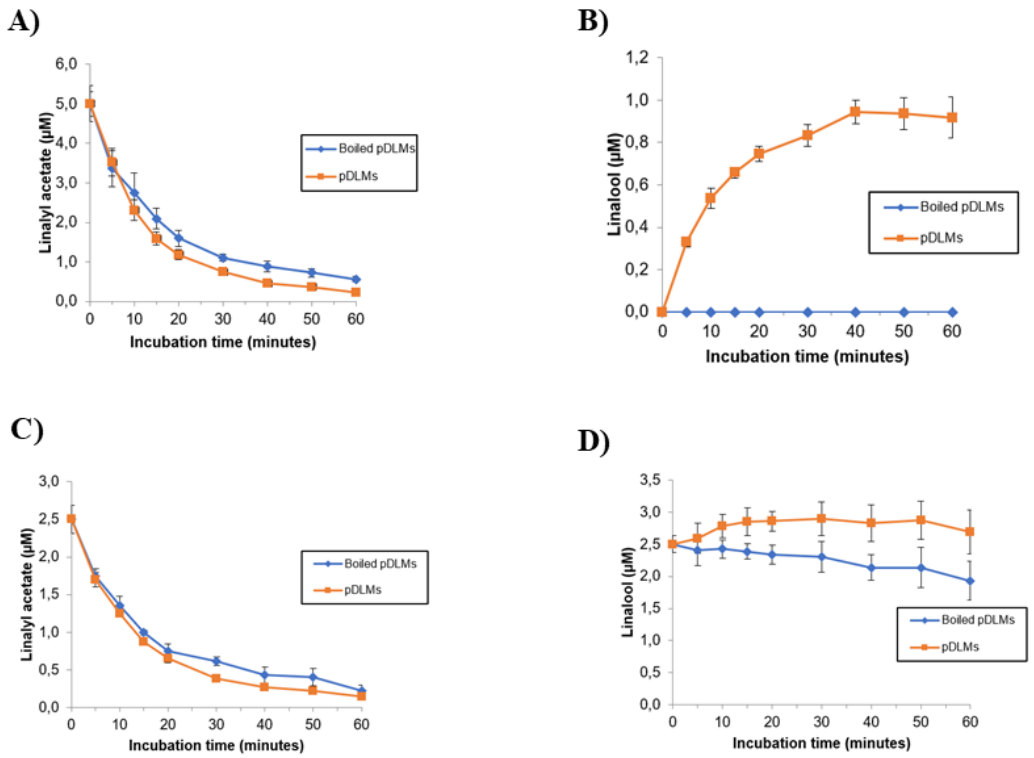

Figure 26 Effect of inactivation of enzymes in pDLMs by boiling on depletion of linalyl acetate (a and c) and formation of linalool (b and d) from pure linalyl acetate and lavender oil. Linalyl acetate and linalool concentrations were measured at intervals from 0–60 min in incubations of boiled or untreated pDLMs with NADPH and linalyl acetate (a and b) or lavender oil (c and d). The initial concentration was 5 µM of linalyl acetate (no linalool) for the pure preparation incubation, and 2.5 µM of linalyl acetate with 2.5 µM of linalool for the lavender oil incubation, and the microsomal protein concentration was 0.1 mg / mL. Results are expressed as absolute concentrations of linalyl acetate and linalool. Each point represents the mean (±SD) of four independent experiments.

4.2.4 Dependence of linalool depletion rate on pDLMs protein concentration

A preliminary study was conducted to evaluate the effect of increasing pDLMs protein concentrations on LIN depletion rate in incubations containing NADPH and 5 µM

LIN. Graphic 5a shows the decrease in LIN concentration (expressed as a percentage of initial concentration) in incubations containing from 0 to 1 mg / mL pDLMs, incubated with NADPH for up to 30 minutes. Depletion rate constant values calculated from these data plotted against pDLMs protein concentration are shown in Graphic 5b. LIN depletion rates increased linearly (R^2 = 1.00; linear regression) with respect to pDLMs concentration over the concentration range tested (0.1 – 1.0 mg / mL).

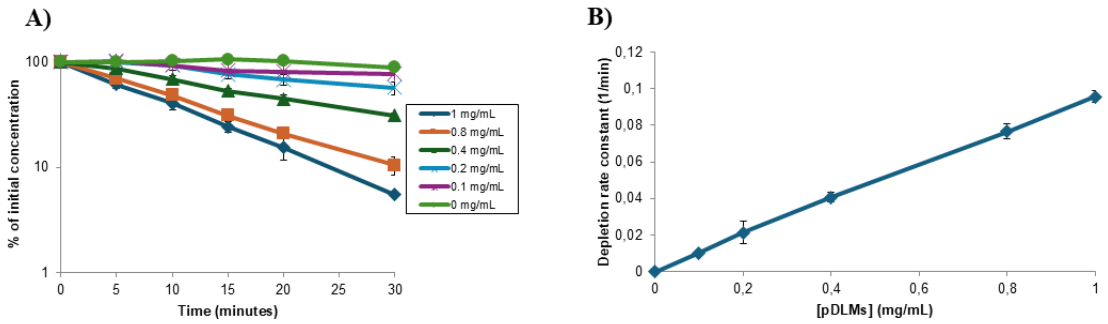

Figure 27 Effect of increasing pDLMs protein concentration on linalool depletion rate constants. (a) Linalool concentrations were measured at intervals from 0–30 min in incubations containing 0, 0.1, 0.2, 0.4, 0.8, and 1 mg/mL of pDLMs, NADPH, and linalool. Concentrations (plotted on a log scale) are expressed as the percentage remaining of the initial linalool concentration (5 µM) in each incubation at each time point. (b) Linalool depletion rate constants calculated from data shown in (a) are plotted against pDLMs protein concentration in each incubation. Depletion rate constants were directly proportional to pDLMs protein concentration (R2 = 1.00; linear regression). Values are shown as mean (±SD) of three independent experiments.

4.2.5 Michaelis-Menten enzyme kinetics of linalool depletion

The effect of increasing LIN concentration on depletion rate was determined to evaluate whether LIN depletion followed Michaelis-Menten (saturable) enzyme kinetics in pDLMs and estimate the Michaelis-Menten constant (k_m) and the maximal depletion rate constant at substrate concentrations approaching zero ($k_{dep([S]\rightarrow 0)}$). Graphic 6a shows the decrease in LIN concentration (expressed as a percentage of initial concentration) in

incubations containing from 2 to 100 µM of LIN, 0.4 mg / mL pDLMs, and NADPH for up to 30 minutes. Depletion rate constant values calculated from these data, plotted against initial LIN concentration, are shown in graphic 6b. Depletion rate constants tended to decrease with increasing LIN concentrations. Nonlinear regression analysis indicated that the data were well described by the modified Michaelis-Menten equation (R^2 = 0.94; P = 0.002). The K_m of LIN was estimated to be 52 ± 11 µM, and $k_{dep([S]\rightarrow 0)}$ was estimated to be 0.050 ± 0.03 min^{-1}.

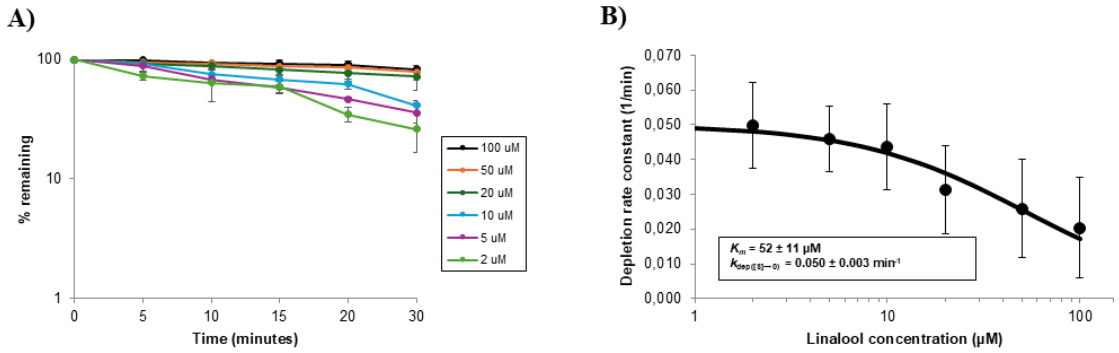

Figure 28 Effect of increasing linalool concentration on linalool depletion rate constants. (a) Linalool concentrations were measured at intervals from 0–30 min in incubations containing 2, 5, 10, 20, 50, 100 µM linalool, NADPH, and 0.4 mg/mL of pDLMs. Concentrations (plotted on a log scale) are expressed as the percentage remaining of the initial linalool concentration in each incubation. (b) Linalool depletion rate constants calculated from data shown in (a) plotted against the initial linalool concentration in the incubation. The Michaelis-Menten constant (km) and maximal depletion rate constant at substrate concentrations approaching zero (kdep([S]→0)) were estimated by non-linear regression fitting of the modified Michaelis-Menten equation to these data (see Materials and Methods). Also shown is the curve of best fit for these data calculated using the fitted parameters (R2 = 0.94; P = 0.002). Values are shown as mean (±SD) of three independent experiments.

4.2.6 LINALOOL METABOLISM BY CANINE RECOMBINANT P450 ENZYMES

LIN depletion assays were performed to evaluate the ability of commercially available canine recombinant P450 enzymes to metabolize LIN, and the results were compared with those of canine liver microsomes (Graphic 7a). As shown in Figure 7b, CLint values were highest for CYP2B11, intermediate for CYP2C21, and lowest for CYP2C41. The remaining enzymes exhibited minimal or no depletion capacity. Because the abundance of P450 enzymes varies in the livers of dogs, the CLint values for each recombinant P450 were extrapolated to liver microsomes using the average abundance values (pmoles/mg of microsomal protein) for each P450 enzyme previously reported for the same set of dog liver microsomes used in this study (Martinez et al). The analyses indicated that CYP2B11 exhibited a 1.6-fold higher capacity to metabolize LIN compared to CYP2C21, and more than seven times greater capacity than other enzymes (Figure 27b). In comparison, the average CLint for pDLMs was intermediate between values for CYP2B11 and CYP2C21.

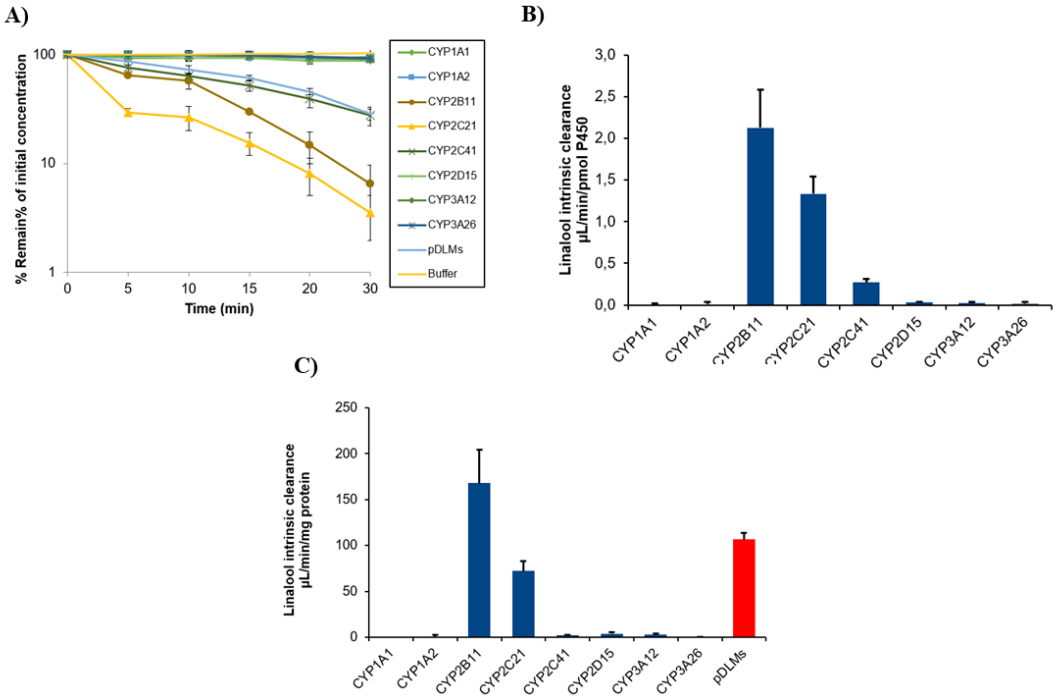

Figure 29 Linalool metabolism by commercially available recombinant P450 enzymes and pooled dog liver microsomes. The values are expressed as the CLint of each recombinant enzyme and pooled liver microsomes. 5 µM of linalool and 160 pmoles/mL recombinant P450 were used for incubation. For CYP2B11, 40 pmoles/mL was used, and for CY2C21 80 pmoles/mL. In incubations with liver microsomes, the concentration was 0.4 mg/mL. (a) Depletion of linalool by pooled dog liver microsomes or recombinant P450. (b) CLint values for each recombinant protein are normalized to P450 concentrations. (c) Intrinsic linalool clearance of each recombinant P450 was adjusted using average abundance values for each P450 enzyme previously reported in dog liver microsomes (pmoles/mg of microsomal protein). These liver microsome-adjusted P450 abundance CLint values of linalool were also compared with those of pooled dog liver microsomes measured under the same experimental conditions. Each bar represents the mean (±SD) of three independent experiments.

4.2.7 LINALOOL METABOLISM BY POOLED DOG LIVER MICROSOMES FROM DOGS TREATED WITH P450 ENZYME INDUCERS

To obtain further evidence for the participation of specific P450 enzymes in the hepatic metabolism of LIN, CLint values were measured using liver microsomes from dogs treated with known P450 inducers and compared with CLint values for dogs treated with the respective vehicles. The inducing drugs included clofibric acid, phenobarbital, rifampicin and β-naphthoflavone. The vehicles were saline (clofibric acid and phenobarbital) and corn oil (rifampin and β-naphthoflavone). The CLint value of LIN incubated with phenobarbital was significantly higher (more than 5-fold) compared with the incubation containing saline ($p<0.001$). Incubations containing the other inducers did not differ significantly in relation to their respective vehicles (Graphic 8).

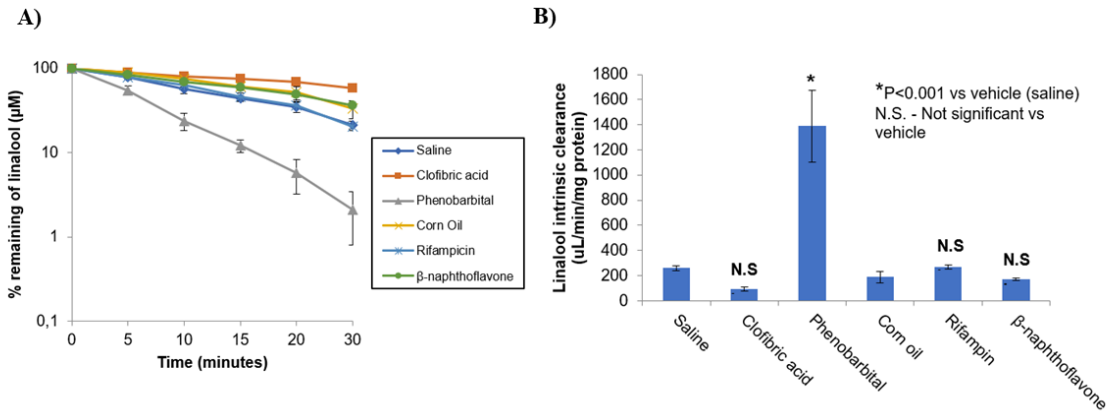

Figure 30 Effects of P450 enzyme induction on linalool metabolism. Linalool depletion rates expressed as percentage remaining linalool (a) and CLint rates (b) were measured using pooled microsomes from dogs treated with known P450 enzyme inducers (clofibric acid, phenobarbital, rifampin, or b-naphthoflavone) or vehicle (saline or corn oil). Incubations contained 2 µM linalool and 0.2 mg/mL microsomal protein (0.1 mg/mL in incubations containing phenobarbital). Each bar represents the mean (±SD) of three independent experiments. Results were analyzed by one-way ANOVA for multiple comparisons and Holm-Sidak post-hoc test between treatment and vehicle ($p<0.05$ was considered statistically significant).

4.2.8 INHIBITION OF P450 ENZYME ACTIVITY BY LINALOOL, LINALYL ACETATE, AND LAVENDER OIL

The inhibitory effects of LIN, LINAct, and lavender oil on drug metabolism by four majors hepatic P450 enzymes (CYP2B11, CYP2C21, CYP2D15, and CYP3A12) were evaluated using canine liver microsomes (Graphic 9). Data are expressed as percentages of enzymatic activity in the absence of inhibitors for each substrate. These data were used to calculate the IC_{50} values given in Table 12. The positive control inhibitors that were used (chloramphenicol, fluconazole, quinidine, and ketoconazole) inhibited the enzymatic activity of the CYP2B11, CYP2C21, CYP2D15, and CYP3A12 isoforms, respectively. All terpenoids inhibited the N-demethylation of tramadol and methadone mediated by CYP2B11, with mean IC_{50} values between 2.5 and 13.9 µM. LIN exhibited less potency of inhibition (higher IC_{50} values) than LINAct and lavender oil (3 times-fold for tramadol and 2 times-fold for methadone, $p<0.001$ and $p=0.013$).

None of the terpenoids investigated inhibited reactions mediated by the CYP2C21, CYP2D15, or CY3A12 isoforms (IC_{50} >30 µM).

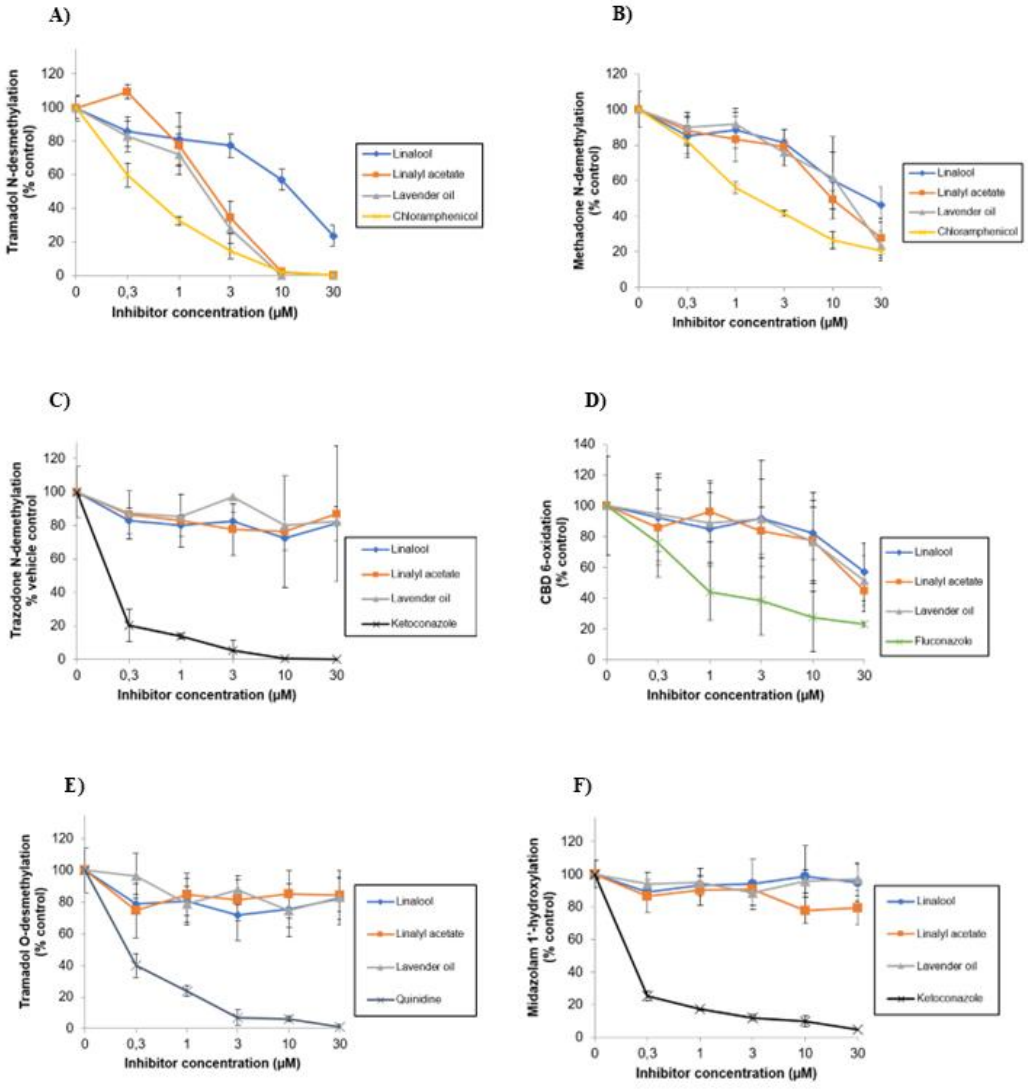

Figure 31 Inhibition of P450 enzymes by linalool, linalyl acetate, and lavender oil. The enzymatic activities studied were N-demethylation of tramadol (a), methadone (b), and trazodone (c), 6-oxidation of CBD (d), O-demethylation of tramadol (e), and 1′-hydroxylation of midazolam (f), which are mainly mediated by the enzymes CYP2B11 (N-demethylation of tramadol and methadone), CYP2C21 (6-oxidation of CBD), CYP2D15 (O-demethylation of tramadol), and CYP3A12 (N-demethylation of trazodone and 1'-hydroxylation of midazolam). Incubations contained 0.3, 1, 3, 10, and 30 µM of inhibitor or no inhibitor (control group). The results are expressed as a percentage of the enzyme activity of the control group for each evaluated inhibitor concentration. Each point represents the mean (±SD) of four independent experiments. The inhibitory concentrations required for the enzyme activity to decrease by 50% were derived from these data and are presented in Table 12.

Table 9 The concentrations required to reduce enzyme activity by half (IC50) of linalool, linalyl acetate, and lavender oil were measured using canine liver microsomes. Chloramphenicol, quinidine, ketoconazole, and fluconazole were included as positive controls for CYP2B11, CYP2D15, CYP3A12, and CYP2C21, respectively. Results expressed as mean (±SD) of four independent experiments and analyzed by one-way ANOVA with Holm-Sidak post-hoc test. "*" $p<0.05$, value considered statistically significant compared with linalool values. "-" not determined.

	IC_{50} (µM)					
Inhibitor	**Tramadol N-demethylation (CYP2B11)**	**Tramadol O-demethylation (CYP2D15)**	**Midazolam 1'-hydroxylation (CYP3A12)**	**CBD 6-oxidation (CYP2C21)**	**Methadone N-demethylation (CYP2B11)**	**Trazodone N-demethylation (CYP3A12)**
Linalool	7.1 ± 1.8	>30	>30	>30	13.9 ± 3.3	>30
Linalyl acetate	2.7 ± 0.8 *	>30	>30	>30	8.0 ± 1.8 *	>30
Lavender oil	2.5 ± 0.8 *	>30	>30	>30	8.6 ± 2.8 *	>30
Chloramphenicol	0.4 ± 0.2	-	-	-	2.2 ± 0.7	-
Quinidine	-	0.1 ± 0.1	-	-	-	-
Ketoconazole	-	-	<0.3	-	-	<0.3
Fluconazole	-	-	-	5.1 ± 6.6	-	-

4.2.9 Inhibition of recombinant P450 enzyme activity by linalool, linalyl acetate, and lavender oil

To clarify the inhibitory effect of LIN, LINAct, and lavender oil on P450 enzymes, the same inhibition protocol was used, but replacing pDLMs with recombinant CYP2B11, CYP2C21, and CYP3A12 enzymes using methadone, CBD, and trazodone as substrates. Consistent with the pDLMs inhibition data (Table 13), none of the terpenoids inhibited recombinant CYP2C21 or CYP3A12-mediated metabolism (IC_{50} >30 µM) (Graphic 10 and Table 14). However, in contrast to the pDLMs inhibition data (Table 3), none of the terpenoids inhibited methadone metabolism by recombinant CYP2B11 (IC_{50} >30 µM) (Graphic 10 and Table 14).

Table 10 Concentrations of linalool, LINAct, and lavender oil required to reduce recombinant enzyme activity by half (IC50). The enzymes used were rCYP2B11, rCYP2C21, and rCYP3A12, with their respective inhibitory controls (chloramphenicol, fluconazole, and ketoconazole). Results expressed as the mean of four independent experiments. "-" not determined.

	IC50 (µM)		
Inhibitor	**CBD 6-oxidation (rCYP2C21)**	**Methadone N-demethylation (rCYP2B11)**	**Trazodone N-demethylation (rCYP3A12)**
Linalool	>30	>30	>30
Linalyl acetate	>30	>30	>30
Lavender oil	>30	>30	>30
Chloramphenicol	-	8.1	-
Fluconazole	<0.3	-	-
Ketoconazole	-	-	<0.3

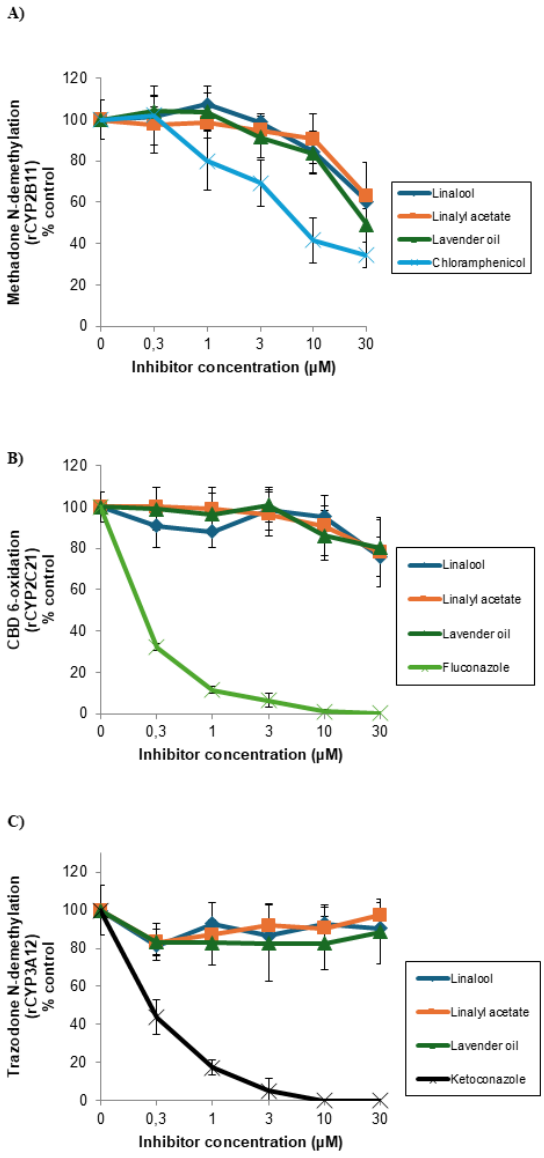

Figure 32 Inhibition of recombinant enzymes by linalool, linalyl acetate, and lavender oil. The enzymes studied were rCYP2B11 (a), rCYP2C21 (b), and rCYP3A12 (c), with their respective substrates methadone, CBD, and trazodone, and positive controls chloramphenicol, fluconazole, and ketoconazole. Incubations containing 0.3, 1, 3, 10, and 30 µM of inhibitor or the absence of inhibitor (negative control). The protein concentrations used were 20 pmoles/mL of rCYP2B11, 40 pmoles/mL of rCYP2C21, and 10 pmoles/mL of rCYP3A12. The results are expressed as a percentage of the enzymatic activity of the negative control at each evaluated inhibitor concentration. Each point represents the mean (±SD) of four independent experiments. The inhibitory concentrations required to reduce enzymatic activity by half (IC50) were derived from these data and are presented in Table 14.

4.2.10 Influence of pre-incubation on the inhibitory potency of CYP2B11 (IC_{50} shift)

To evaluate whether the inhibition by LIN, LINAct, and lavender oil of CYP2B11-mediated drug metabolism in pDLMs is time-dependent, these compounds were preincubated for 20 min before starting the reaction with the addition of tramadol or methadone to the incubation. Graphic 11a shows that preincubation increased the inhibitory potency of LIN against tramadol N-demethylation by 2.3-fold (p=0.021). On the other hand, pre-incubation reduced the inhibitory potency of LINAct against tramadol N-demethylation by 2.2-fold (p=0.002) and did not change the inhibitory potency of lavender oil. When CYP2B11-mediated N-demethylation of methadone was evaluated (Graphic 11b), preincubation decreased inhibitory potencies of LINAct by 3-fold (p=0.001) and lavender oil by 1.6-fold (p=0.026), but the inhibitory potency of LIN was not affected.

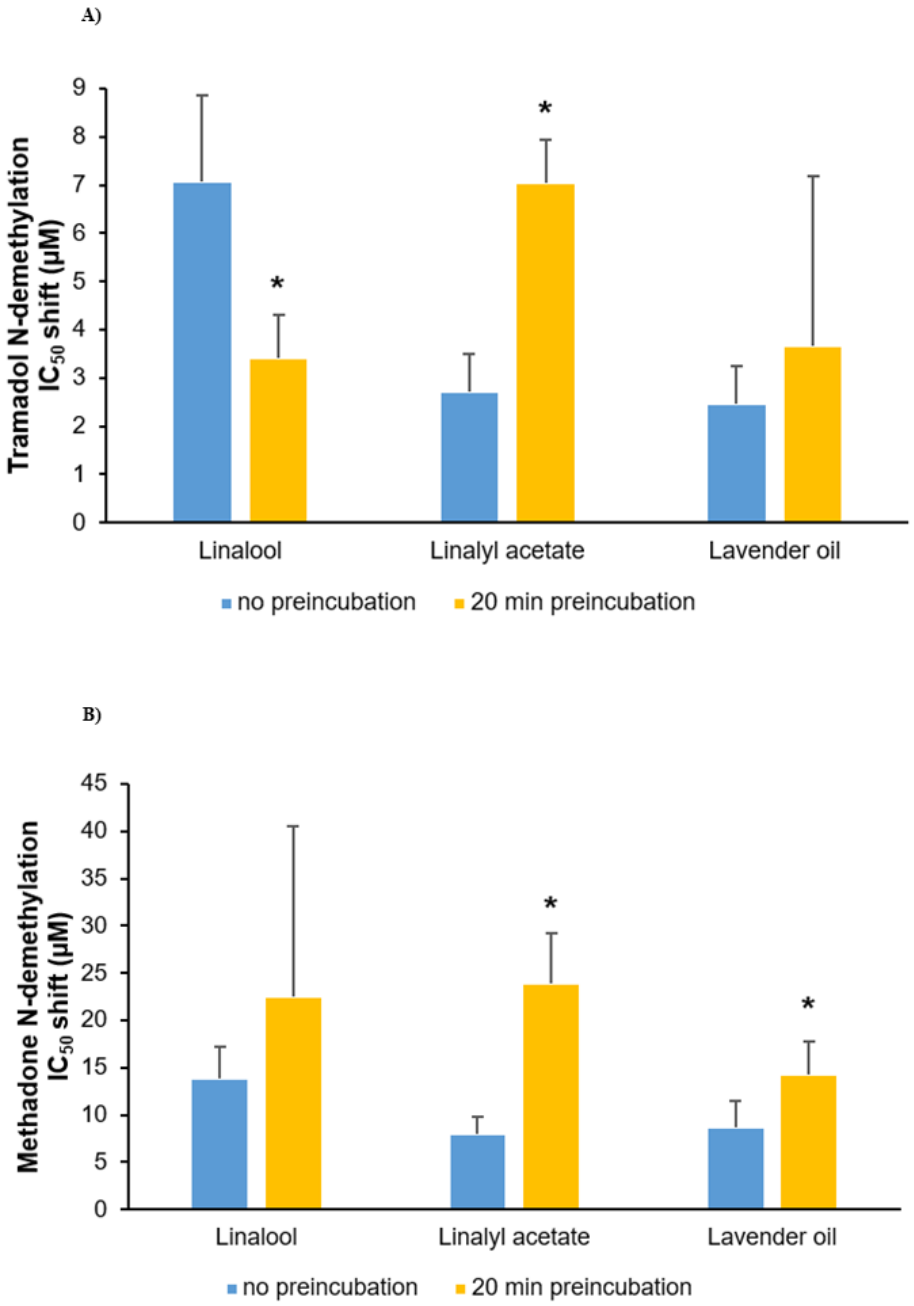

Figure 33 Effect of preincubation on the inhibitory potency of linalool, linalyl acetate, and lavender oil of CYP2B11 (IC50 shift). (a) Half-maximum inhibitory concentration (IC_{50}) shifts in N-demethylation of tramadol. (b) IC_{50} shifts in N-demethylation of methadone. Each bar represents the mean (±SD) of four independent experiments. Data were analyzed using the t-test, and $p<0.05$ was considered statistically significant. "*" significant, $p<0.05$.

4.2.11 In vitro – in vivo extrapolation of P450 inhibition by linalool, linalyl acetate, and lavender oil

The in vitro determined ratio between the maximum plasma concentration (C_{max}) and the IC_{50} after a single oral dose of the drug was used as a metric to indicate the likelihood of a clinically relevant in vivo drug interaction involving these terpenoids. A C_{max}/IC_{50} ratio greater than 1.0 suggests that an in vivo drug interaction is likely, values between 0.1 and 1.0 suggest that an interaction is possible, whereas values below 0.1 indicate that an interaction is remote (Bjornsson et al., 2003). Table 14 presents the C_{max}/IC_{50} ratios calculated using C_{max} values reported in human and rat plasma and rat liver and IC_{50} values determined in this study for LIN inhibition of tramadol N-demethylation and methadone N-demethylation in pDLMs. Based on human and rat plasma C_{max} values, a possible drug interaction (C_{max}/IC_{50} > 0.1) was predicted for tramadol N-demethylation, but not for methadone N-demethylation with 2 weeks daily oral dosing of lavender oil. A single lavender oil dose was unlikely to result in an interaction with either drug. Using rat liver C_{max} values, possible drug interactions were predicted for tramadol N-demethylation and methadone N-demethylation after a single lavender oil dose, while likely drug interactions were predicted with 2 weeks of daily oral dosing.

Table 11 Ratios between the Cmax observed in humans and rats and the concentration of linalool required to reduce CYP2B11 enzymatic activity (tramadol N-demethylation and methadone N-demethylation) by half (IC50) (Table 12). Results are presented as the mean (±SD) of four independent experiments. The plasma Cmax values used for humans were 0.1 μM (22 ng/mL) and for rats 0.5 μM (77 ng/mL) after a single dose of lavender oil (Silexan®) of 80 mg and 100 mg/kg, respectively, and 0.8 μM (131 ng/mL) and for rats 0.7 μM (108 ng/mL) after multiple doses (one dose daily for 14 days) of 160 mg and 100 mg/kg, respectively. The liver Cmax values used for rats after a single dose of lavender oil (Silexan®) (100 mg/kg) was 1.8 μM (278 ng/mL), and after multiple doses (one dose of 100 mg/kg daily for 14 days) was 13.6 μM (2095 ng/mL) (Müliner et al., 2015). According to Bjornsson et al. (2003), a Cmax/IC50 ratio greater than 1 suggests the likely clinical relevance of the compound as an inhibitor. Values between 0.1 and 1 suggest possible relevance, whereas values below 0.1 suggest remote relevance. **"*"** - likely or possible clinically relevant inhibition. “nd” – not determined.

	Plasma C_{max}/IC_{50} (ratio)		**Liver C_{max}/IC_{50} (ratio)**	
	Tramadol N-demethylation	**Methadone N-demethylation**	**Tramadol N-demethylation**	**Methadone N-demethylation**
		Single dose		
Human	0.01 ± 0.01	0.007 ± 0.02	Nd	nd
Rat	0.07 ± 0.02	0.04 ± 0.01	0.25 ± 0.09*	0.13 ± 0.04*
		Multiple doses (one dose/day, 14 days)		
Human	0.11 ± 0.15*	0.06 ± 0.02	Nd	nd
Rat	0.10 ± 0.03*	0.05 ± 0.02	1.92 ± 0.65*	0.99 ± 0.31*

5 DISCUSSION

5. DISCUSSION`

5.1 I*N SILICO* APPROACH

Molecular docking allows the prediction of interactions between two molecules, a protein structure (a target protein) and ligand (compound molecule) or structure. It allows the assessment of the structure-ligand complex and its relationship to biological systems, thereby enhancing the capacity to identify ligands with higher affinity for the target protein (FERREIRA et al., 2015; LOHNING et al., 2017; PINZI; RASTElll, 2019).

CYP2B11, essential for drug metabolism in dogs, was selected for study during the *in silico* phase. This importance is due not only to its ability to metabolize drugs in this species, but also to the variability in its expression and abundance in different dog breeds (MARTINEZ et al., 2019). The CYP2D15 enzyme was chosen because it is the most abundant enzyme in the canine liver (MARTINEZ et al., 2019) and, therefore, is important in preliminary studies involving potential drugs for use in dogs. The *in vitro* stage showed that CYP2C21 metabolizes LIN, we performed an evaluation of this enzyme in the *in silico* study, despite its lower hepatic abundance in the species. Although CYP3A12 is also one of the most abundant proteins in the liver of dogs (MARTINEZ et al., 2019), it did not demonstrate any capacity to metabolize LIN or LINAct in the *in vitro* study, so it was not included in the *in silico* stage. Furthermore, for practical reasons, this study was limited to the evaluation of only three enzymes.

The SWISS-MODEL tool (https://swissmodel.expasy.org/) was used to perform 3D modeling of the CYP enzymes, offering accessibility and ease in modeling protein complexes. This tool uses the sequence similarity of existing proteins as template and

performs homology-based techniques for protein modeling to create a new model, guided on the global model quality estimate (GMQE), which combines alignment information between the target and selected template structure. It evaluates the reliability of the target as a base protein for generating the target protein to be studied, which is expressed as absolute values from 0 to 1. The higher the value, the greater the reliability of the target for modeling (BIENERT et al., 2017; WATERHOUSE et al., 2018). The modeled target of CYP2B11 and CYP2C21 had GMQE of 0.94, whereas that of CYP2D15 had a GMQE of 0.93. These values suggest that they are near the maximum GMQE value, making them suitable targets for the next analysis.

Structural characterization of a template protein is a prerequisite for homology modeling, which requires a sufficient sequence similarity to the target protein. If a suitable structure does not exist, alternative modeling approaches, like *ab initio* or *de novo* methods, need to be employed (CHEN et al., 2024; LOHNING et al., 2017; PINZI; RASTELlI, 2019). This stage of *in silico* analysis constructs a 3D model of the target protein by using a comparable model, according to the principle that proteins with similar structures often display analogous biological functions (LOHNING et al., 2017; MUEGGE; MUKHERJEE, 2016; MUHAMMED; AKI-YALCIN, 2019). In this study, the structures of the CYP2B11, CYP2C21, and CYP2D15 enzymes were constructed from pre-existing targets of CYP450 from sheep (*Ovis aries*), North American plains bison (*Bison bison*) and Siberian tiger (*Panthera tigris altaica*), respectively. Figures 8, 9, and 10 show that, for the three enzymes, the residues are generally overlapping, indicating a high similarity between the target protein and the model created by SWISS-MODEL. Furthermore, the predominance of green color in these figures indicates that the similarity is greater than

the differences between the target and model. These data show that the modeled structures are suitable for subsequent docking and ligand-based modeling analyses. Another important piece of information extracted from Figures 8, 9, and 10 is the percentage of identity between the target structure and the model created from it. Table 8 lists the reference values and interpretations of each model. According to Lohning et al. (2017), a sequence must have more than 35% homology to be considered a reliable model. Xiang (2006) sets the minimum value at 40%, while other authors (CHOTHIA; LESK, 1986; LOHNING et al., 2017; XIANG, 2006) establish that the value must exceed 50%. Thus, the higher the percentage of identity, the lower the chance of errors in the sequential construction and orientation of the chain and in the prediction of residues involved in the bonds. According to these authors, the model created for each CYP under study is reliable as it maintains at least 79.18% identity.

Table 12 Reference values for the percentage identity between the modeled structure and the target.

Author	% identity for a reliable homology modeling	Notes
Lohning et al. (2017)	>35%	It may ignore sequences related to structural or evolutionary ties.
Xiang (2006)	>40%	**30-40%:** it is difficult to obtain a correct alignment **<30%:** it is difficult to obtain homology modeling
Chothia & Lesk (1986)	>50%	**<20%:** large structural differences and homology modeling is almost impossible

The Ramachandran plot is a useful tool for validating the model created by SWISS-MODEL. This plot shows the regions in which amino acid residues are located. If more than 90% of the residues are in favorable regions, this indicates that the conformation of the modeled protein is stereochemically acceptable, i.e., the 3D model is reliable for

performing molecular docking (LASKOWSKI et al., 1993). For the three CYPs modeled, the percentage of residues in favorable regions was >92% (Graphic 1), corroborating the other data on the reliability of the obtained 3D structures.

The residues that participate in molecular docking have chemical features that are crucial for effective biochemical interactions (Table 9). Charged residues (basic or acidic) have a positive charge and favor hydrogen bonds. Thus, in electropositive or polar environments, the interaction tends to be stronger, especially with electron donor/acceptor atoms. These residues tend to perform initial ligand recognition in a more dynamic, i.e., less stable manner. Neutral residues do not possess any electrical charge. They form strong hydrogen bonds and thus favor more stable and directed interactions. The result is the formation of more stable complexes. Aromatic residues form hydrogen bonds with hydroxyl group (-OH) and hydrophobic interactions if the ligand contains an aromatic ring in its structure. This characteristic imparts a versatile complex but is highly dependent on the orientation of the ligand (BÖHM; SCHNEIDER, 2003; IUPAC-IUB, 1984; J. R. YUNTA, 2025; KUMAR; KUMAR, 2019).

Table 13 Chemical characteristics of the residues that participate in the interactions between the enzymes CYP2B11, CYP2C21, and CYP2D15 and the ligands linalool and linalyl acetate (IUPAC-IUB, 1984; Böhm and Schneider, 2003; Kumar and Kumar, 2019; J. R. Yunta, 2025).

Residue	Chemical feature	Interactions
Lysine (LYS)	Basic	Hydrogen bonds; electrostatic
Arginine (ARG)		
Asparagine (ASN)	Neutral	Strong hydrogen bonds
Serine (SER)		
Glycine (GLN)		
Tyrosine (TYR)	Aromatic	Hydrophobic

In the present study, the molecular docking was performed (structure based and ligand based) for the CYP2B11, CYP2D15, and CYP2C21 enzymes. Their protein structures were modeled based on the homology-based approach using SWISS-MODEL program, which uses AlphaFold database to select the best template structure to generate the protein/target model based on the homology modelling.

Figure 11 shows the docking analysis of CYP2B11 using the MOE tool. In this image, the surface of the enzyme is blue, whereas LIN (A) and LINAct (B) are represented by rods. These compounds are capable of interacting through hydrogen bonds (yellow lines) with the residues ARG 126.A, LYS 122.A, and ASN 397.A, in addition to electrostatic interactions between these residues (represented in purple). These characteristics and the positions of the residues favor the stable docking of the protein (FERREIRA et al., 2015; PINZI; RASTElll, 2019), suggesting that LIN and LINActct can be metabolized by CYP2B11. By comparing the interactions between the terpenoids and the enzyme, it is possible to identify possible differences in affinity and, consequently, in the metabolization rate of each of the molecules studied. LIN, an alcohol, interacts with more superficial residues, whereas LINAct, an ester, interacts with deeper residues of the enzyme. The binding energies obtained by AutoDock Vina, as well as the amount of hydrogen bonds formed, support this interpretation. This ester showed the lowest binding energy, then it binds more strongly to CYP2B11 than LIN due to its higher affinity and increased hydrogen bonding. Consequently, the docking of this molecule to CYP2B11 is more stable, facilitating easier recognition of LINAct as a substrate. The binding energy is the energy released during binding between the ligand and the target receptor, denoting the stability of the complex. The less binding energy is, the more stable the complex and, therefore,

regarding the development of new drugs, the therapeutic (or toxic) potential of a candidate compound (KRIHARIYANI et al., 2024; ZOTHANTLUANGA; CHETIA, 2022). It is important to highlight that this does not imply improved metabolic processes or accelerated reactions. Binding affinity is related to the strength of the bond between the molecule and the enzyme active site. High affinity aids binding but can inactivate the enzyme if it is too high, reducing the metabolic rate. The Michaelis-Menten equation (Equation 1) relates the reaction rate to the Michaelis–Menten constant (K_m), which is the substrate concentration at which the reaction rate is half the maximum rate (LIU, 2017). K_m is inversely proportional to the substrate's affinity for the enzyme and, therefore, directly proportional to the binding energy, although an excessively low K_m does not guarantee a higher reaction rate because a very low K_m generates an almost irreversible binding (as occurs with the organophosphate-acetylcholinesterase complex) (MAIN, 1969; SHENOUDA; GREEN; SULTATOS, 2009; VALERO et al., 1995). This generates the phenomenon of "enzyme freezing", an enzymatic inactivation that reduces metabolic capacity, which can be time-dependent or mechanism-dependent (MAURER; TABRIZI-FARD; FUNG, 2000; YADAV et al., 2020). Furthermore, the position of the ligand in relation to the heme iron (catalytic center) of CYP also defines the velocity and efficiency of the reaction because this site is the oxidative site of this enzyme (ISIN; GUENGERICH, 2008).

Equation 3 Michaelis-Menten equation (LIU, 2017).

$$v = \frac{V_{max} \times [S]}{K_m + [S]}$$

Where:

v = velocity of reaction

V_{max}= maximum velocity of reaction

[S] = substrate concentration

K_m = Michaelis-Menten constant

SWISS-MODEL selects templates primarily from the AlphaFold database. As AlphaFold-generated templates do not include non-protein components and often exclude non-peptide entities like ligands, metal ions, and prosthetic groups, the resulting model in this study lacked the heme group typically present in CYP enzymes. Due to the absence of heme in the model, docking was performed on the apo-form (without any bound cofactors, ligands, or prosthetic groups - like metal ions or heme groups) of the protein, focusing on potential ligand-binding pockets predicted on the protein surface. In this work, our initial approach was to identify the insights into ligand compatibility, though it may not fully recapitulate heme-dependent interactions. The docking results in this work are shown as preliminary and indicative of possible binding regions. Interestingly, docking poses of LIN and LINAct were observed near the putative active site, suggesting that these compounds may interact within the functional domain. Further refinement of the model with heme incorporation would be necessary for accurate simulation of ligand interactions involving the active site. Future work will include heme integration and refined docking to better represent the catalytic pocket and assess ligand binding in the native holoenzyme context.

Lohning et al. (2017) and Ferreira et al. (2015) pointed out that different software programs are useful for predicting the positioning of the ligand in molecular docking and therefore the stability of the complex. Although different tools can be used, those study notes that the position of the residues and ligands was found to be a determinant of a successful enzymatic reaction (FERREIRA et al., 2015; LOHNING et al., 2017). An incorrectly positioned ligand can inactivate the reaction.

The interactions between terpenoids and CYP2C21 present some differences in relation to CYP2B11. With CYP2B11, LINAct interacts with a more internalized chain of CYP. Regarding to CYP2C21, this ester binds in a region as superficial as LIN. Furthermore, both interact with the protein through two hydrogen bonds, suggesting similar binding strengths. Together, these data suggest that the CYP2C21 enzyme is capable of metabolizing both LIN and LINAct, although possibly with a lower capacity compared to CYP2B11. Considering the binding energy, LINAct appeared to have slightly more affinity for the catalytic site of CYP2C21 than LIN. Unlike CYP2B11, binding to terpenoids occurs at the same residues, suggesting that the binding pattern occurs in an equivalent way, whereas this pattern is different in the binding of LIN and LINAct to CYP2B11.

When evaluating the interaction between LIN and CYP2D15 (Figure 14A), we observed four hydrogen bonds with the ASN 85.A and SER 62.A residues, showing favorable docking for the interaction between this alcohol and the enzyme. LINAct forms three hydrogen bonds with the TYR 200.A residue, showing that this affinity may be due to weaker interactions, such as hydrophobic interactions or Van der Waals forces. Unlike the other CYPs evaluated, LIN therefore presents greater binding stability with CYP2D15

than LINAct, despite having binding energies with similar values. Near the binding region of the LINAct, there is an electronegative region that favors docking, but compared to the other interactions under analysis, this region appears to be further from the binding zone, suggesting a lower affinity of the molecule for CYP2D15.

Data from molecular docking (Table 10) suggests LINAct has a slightly higher affinity for CYP enzymes than LIN. LINAct shows the highest affinity for CYP2C21, while LIN has the lowest for CYP2B11. When comparing the number of hydrogen bonds, LIN had the highest number of hydrogen bonds with CYP2D15, suggesting that the LIN-CYP2D15 complex was the most stable among those evaluated. The LINAct-CYP2C21 complex exhibited more favorable interactions, characterized by strong polar interactions and affinity. These data show that the presence of more bonds does not necessarily indicate better affinity, as exemplified by the LIN-CYP2D15 interaction. CYP enzymes have a heme group with iron (Fe^{2+}) in the center, which is the catalytic site. The reaction occurs between the substrate, iron, and oxygen. This catalytic site has a hydrophobic characteristic, which facilitates its interaction with xenobiotics, especially when they have a more nonpolar character (GUENGERICH, 2008; KIRTON; BAXTER; SUTCLIFFE, 2002). The metabolizing potential of CYP depends on its affinity for the substrate, its binding strength, and the nature of the residues, which therefore define the stability of the complex. As mentioned previously, substrate-enzyme binding alone is insufficient for metabolism. In fact, the substrate-enzyme interaction must be ideal for catalysis; the position of the substrate, binding energy, and the binding region determine if biotransformation will occur (NAIR; MCKINNON; MINERS, 2016; PETERSON; GRAHAM, 1998; WERCK-REICHHART; FEYEREISEN, 2000). When examining the effect on

metabolism, more stable complexes will enhance metabolic efficiency only if the substrate is favorably positioned relative to the catalytic center (heme iron).

Table 14 Molecular docking with interacted residues of enzymes CYP2B11, CYP2C21 e CYP2D15 with ligand compound linalool and linalyl acetate (GUENGERICH, 2008; KIRTON; BAXTER; SUTCLIFFE, 2002).

Complex	Binding Affinity (Kcal/mol)	Complex stability	Metabolization potential*	Notes
CYP2B11-linalool	-4.096	Moderate	Intermediate	Fewer H-bonds, basic residues.
CYP2B11-linalyl acetate	-4.643	Good	Good	Better affinity and + H bonds but depends on the position in relation to the heme iron.
CYP2C21-linalool	-4.487	Good	Good	Polar residues favor stability; good affinity.
CYP2C21-linalyl acetate	-4.998	Very good	Very good	Best affinity among all pairs; may indicate greater propensity for metabolization if correctly positioned.
CYP2D15-linalool	-4.144	Good	Intermediate to good	More H-bonds (4), which may favor the stability of the complex.
CYP2D15-linalyl acetate	-4.199	Good	Intermediate to good	Fewer residues involved (only TYR 200), despite good affinity.

**Note: Consider binding affinity, number of hydrogen bonds, and nature of residues.*

Paul Ehrlich (1909) defined "pharmacophore" as "that which carries the essential characteristics responsible for the biological activity of a drug". In 2002, Guner updated the concept, defining pharmacophore as being "a set of structural characteristics in a molecule that is recognized at a receptor site and is responsible for its biological activity". According to the International Union of Pure and Applied Chemistry (IUPAC), the pharmacophoric properties of a ligand "is the set of steric and electronic characteristics necessary to ensure ideal supramolecular interactions with a specific biological target structure and to trigger (or block) its biological response" (EHRLICH, 1909; GUNER, 2002; WERMUTH et al., 1998). LIN and LINAct were studied here due to their potential biological activities in dogs; thus, this study analyzed their pharmacophoric properties.

Knowledge of the pharmacophoric features of a ligand is essential for predicting how and where it may interact with a target protein. The number and diversity of these features often reflect a ligand's potential to bind with multiple regions of the active site, influencing both its binding affinity and specificity (GAY; ROBERTS; HALPERT, 2010). In general, a greater number of pharmacophoric features correspond to a greater potential for stabilizing interactions. For LIN, five pharmacophoric features were identified, whereas LINAct exhibited seven, suggesting that the ester form may have enhanced capacity to interact with diverse regions within the enzyme's active site. LIN contains two hydrophobic regions, whereas LINAct contains five, which may favor its binding to the predominantly nonpolar environment near the heme group of CYP enzymes (GAY; ROBERTS; HALPERT, 2010). Although LIN possesses a dual region capable of both donating and accepting hydrogen bonds, LINAct features a region limited to hydrogen-bond acceptance, indicating different interaction dynamics with the binding site that can affect complex stability. Additionally, LIN has two AtomQ regions (associated with non-classical interactions such as van der Waals forces) while LINAct has only one. Although these interactions are weaker, they can still contribute to the overall stability and specificity of ligand-enzyme complexes, because they influence the positioning and orientation of the ligand at the active site. The presence of GLN and TYR residues are particularly important because of their chemical characteristic (GAY; ROBERTS; HALPERT, 2010; SARKHEL; DESIRAJU, 2004). Together, these pharmacophoric differences suggest distinct binding behaviors between the two molecules rather than a prediction of metabolic susceptibility. The metabolic potential of a compound is determined not only by its pharmacophoric properties but also by its orientation and proximity to the catalytic site (GAY; ROBERTS; HALPERT, 2010). In the present study, pharmacophoric analysis was performed in

combination with molecular docking, dynamics simulations, and *in vitro* studies to comprehensively define the metabolic profiles of these terpenoids in dogs.

The Generalized-Born Volume Integral/Weighted Surface Area (GBVI/WSA) is a scoring function, which estimates the free energy of binding ligand from a given pose. For all scoring functions, lower scores indicate more favorable poses. In molecular docking studies, binding energies and docking score are the primary bases for the selection of active and non-active compounds. Molecular docking analysis showed LIN has a better binding affinity with CYP2B11, with a more favorable docking score and BGVI/WSA energy. The more negative the value, the stronger and more stable the binding becomes (LABUTE, 2008). The two hydrogen bonds formed with the GLN and ASP residues (polars) contributed to greater structural stability at the binding site, in addition to favoring better and firm positioning of the molecule within the protein, compared to the single hydrogen bond formed between LINAct and the HIS residue (slightly polar) (CHAN; LASKOWSKI; SELWOOD, 2010). The binding energies presented in Tables 5, 6, and 7 indicate that both LIN and LINAct can be metabolized by the CYPs under study, and the lower the binding energy, the greater the enzymatic selectivity of the CYPs. Clinically, this may impact the bioavailability of drugs used concomitantly with LEO, since the enzymatic selectivity for the oil compounds, if greater, may lead to toxicity and/or therapeutic ineffectiveness of the drug.

Upon comparing the molecular docking results of the three CYPs and the terpenoids, LIN was found to have better affinity and more specific interactions in general, with emphasis on CYP2B11 and CYP2C21. In practical terms, this indicates that LIN may exhibit a higher biotransformation rate, favoring its rapid elimination from the body.

Clinically, this may translate into a shorter duration of pharmacological action, requiring more frequent doses to maintain the therapeutic effect. In contrast, LINAct, which exhibited lower affinity and specificity in interactions, may be metabolized more slowly, resulting in a longer half-life, potential accumulation with repeated administrations, or even differences in the adverse effect profile, depending on the metabolic pathway involved. This may occur due to the lower molecular weight of LIN, greater polarity and flexibility, and chemical grouping (alcohol), which facilitates the docking and formation of more interactions (NGUYEN et al., 2017). The more nonpolar character and the greater conformational rigidity of LINAct, owing to the presence of the ester group, reduces rotational freedom and it may limit its ability to adapt to the 3D microenvironment of CYP active sites. In other words, the molecule has less flexibility to adopt conformations that favor ideal interactions with catalytic residues, which can compromise both enzymatic recognition and binding efficiency of the drug., especially with CYP2D15 (ERICKSON et al., 2004; NGUYEN et al., 2017). Thus, LIN exhibited greater binding stability to the studied CYPs.

A study conducted with the monoterpene α-terpinyl acetate, a compound present in several essential oils, demonstrated that this substance is capable of strongly binding to the human isoform CYP2B6, the ortholog of canine CYP2B11. Furthermore, molecular docking analyses confirmed the direct interaction of this terpene with the active site of the enzyme (Lee *et al.*, 2018). Although this study was conducted in humans, it suggests that structurally similar compounds, such as linalool, may exhibit comparable metabolic behaviors and binding patterns in dogs. These data strengthen the plausibility of the results observed in the present study, in which linalool demonstrated greater consistency

and stability of binding to CYP2B11 than linalyl acetate. In rodent studies, exposure to monoterpenes such as camphor, menthol, and α-pinene resulted in a significant induction of CYP2B subtype enzymes, with up to six-fold increases in the mRNA and protein expression of these hepatic isoforms (Austin *et al.*, 1988). Because the CYP2B subfamily in rodents is functionally analogous to CYP2B11 in dogs, these data indicate that terpenoid compounds have the potential to modulate the activity and expression of CYP enzymes in mammals, including in vivo. These findings support the plausibility of the results of this study, suggesting that LIN, owing to its similar structure, may also interact with and be preferentially metabolized by isoforms such as CYP2B11 and CYP2C21 in dogs, compared to bulkier and less polar compounds such as linalyl acetate.

The findings indicate that ligands with a higher affinity for CYP enzymes and increased interaction potential, such as LIN, are more likely to undergo metabolic transformation. This study found that CYP2B11 and CYP2C21 enzymes showed a higher ability to interact with LIN, which suggests their potential role in the biotransformation of this monoterpene. These results are predictive and act as a preliminary stage for *in vitro* studies that can evaluate metabolic depletion and drug interaction profiles at a cellular level. However, the *in silico* approach has limitations such as differences between modeled and native enzymes, treating proteins as rigid in docking simulations, and calculated binding energies not fully representing cellular or physiological complexity. Future research may involve molecular modeling of CYP3A12, the major hepatic enzyme in dogs, as well as docking analyses focused on ligand positioning relative to the heme iron to better predict metabolic relevance. Furthermore, *in silico* screening of potential enzyme inducers or inhibitors can improve the prediction of drug interaction risks.

5.2 *IN VITRO* APPROACH

EOs and their constituents are increasingly used to treat psychiatric disorders in humans and behavioral disorders in animals (McCaskill, 2021; Tan *et al.*, 2023b; Haverbeke *et al.*, 2024). However, no studies to date have investigated the pharmacokinetic behavior of linalool (LIN), linalyl acetate (LINAct), or lavender essential oil (LEO) in dogs. This study provides, for the first time, preliminary information regarding the metabolism of these compounds in this species, focusing mainly on the participation of CYP isoforms. In general, patients who are being treated for behavioral disorders, such as anxiety and depression, use polypharmacy, thereby becoming susceptible to drug interactions (Sarkar, 2017). Given the increased use of EOs as adjuvants in these treatments, it is crucial to evaluate how these compounds are processed in canine livers to provide data on their safety and potential drug interactions. The results of this study also provide, for the first time, important information regarding not only the metabolism of terpenoids in dogs, but also about drug interactions involving LIN, LINAct, and lavender oil in patients who may be taking medications prescribed for anxiety and anxiety-related pain control. Furthermore, this study highlights the participation of CYP enzymes in the metabolism of these molecules in dogs and is, therefore, a basis for further studies in the area.

In vitro assays using pDLMs and enzymatic cofactors showed that both LIN and LINAct, as well as their mixture (lavender oil), are degraded by enzymatic action. The observed more rapid depletion of LIN in the presence of NADPH but not UDPGA suggests that biotransformation of LIN in pDLMs is mediated by CYPs, but not by UDP-glucuronosyltransferases (Graphic 2a). In contrast, depletion of LINAct by pDLMs occurred with or without the addition of NADPH or UDPGA (Graphic 2b), suggesting that

CYPs and UGTs are not primarily involved in LINAct metabolism. Depletion of LINAct in pDLMs was accompanied by time-dependent formation of LIN (Graphic 2c). Interestingly, when NADPH was added to the pDLMs, LIN concentrations peaked at 20 minutes and then decreased, suggesting CYP-dependent biotransformation of LIN formed from LINAct.

Evaluation of changes of LIN and LINAct concentrations from pDLMs after addition of lavender oil was similar to changes observed after adding each compound separately, except that depletion of LIN was slower with lavender oil (Graphic 3a versus graphic 2a) probably because there was simultaneous formation of LIN (from LINAct) and depletion of LIN in the lavender oil incubations.

Since conversion of LINAct to LIN could be either enzyme mediated (via esterases present in pDLMs) or spontaneous (chemical instability), the effect by boiling the pDLMs on pure LINAct and lavender oil was evaluated. Heating by boiling irreversibly inactivates enzymes through their denaturation. Comparing the production of LIN from pure LINAct in boiled and unboiled microsomes (Graphic 4b), it was noted that LIN formation was entirely dependent on heat-labile enzymatic activity. After denaturation of these proteins by heat, no LIN was produced. However, it was also observed that there was substantial depletion of LINAct in incubations with boiled pDLMs versus unboiled pDLMs, although depletion was less extensive in the boiled pDLMs (Graphic 4a). The reason for LINAct depletion in boiled pDLMs is unclear, although it does not involve conversion to LIN. Possible causes include biotransformation to another compound either spontaneously or by a heat-stable enzyme. Other possibilities include time-dependent binding of LINAct to pDLMs or to the incubation tube. These possibilities need further investigation to resolve.

The results of the assay using lavender oil as the terpenoid source showed that LINAct is depleted from the incubation with both boiled and unboiled pDLMs, irrespective of whether this terpenoid is produced from EOs or as an isolated compound. The LIN concentration in lavender oil showed minimal variation with incubation time, but it slightly increased in the unboiled pDLMs incubation probably from formation from LINAct. Together, these results reinforce the hypothesis that hepatic esterases participate in the biotransformation of LINAct to LIN, but this only accounts for a proportion of the depletion of LINAct from incubations.

Human and rat liver microsomes may degrade LIN and LINAct (Chadha and Madyastha, 1982, 1984; NOSKOVÁet al., 2016; Mondal et al., 2023), which indicates that there is some similarity between the metabolic processes of mammalian species, including dogs, and LINAct could be converted into LIN and possibly other metabolites. Figure 21 presents a possible mechanism of biotransformation of LIN and LINAct. Briefly, hepatic metabolism occurs in two phases: a catabolic reaction (e.g., oxidation) and an anabolic phase (e.g., glucuronidation). In this study, we used liver microsomes as a source of CYP enzymes. This is a well-established method for *in vitro* substrate depletion assays (Knights *et al.*, 2016). Furthermore, CYP enzymes may convert a biologically inactive molecule (prodrug) into an active molecule (Chillistone and Hardman, 2023). Our results suggest that LINAct is converted into LIN in the presence of pDLMs enriched with the CYP cofactor NADPH, although it may also be biotransformed to LIN through the action of esterases. In the same way, Müliner et al. (2015) showed that only LIN was detected in human plasma, rat plasma, and rat liver under the conditions of their experiment. We found that the rate of depletion of LINAct was more pronounced than that of LIN, whereas

LIN was produced during LINAct depletion. Together, these data suggest that LINAct is a prodrug that, in the presence of NADPH-CYP, is converted to LIN, a biologically active molecule. Also, LINAct could be converted to LIN mainly due to hepatic esterases.

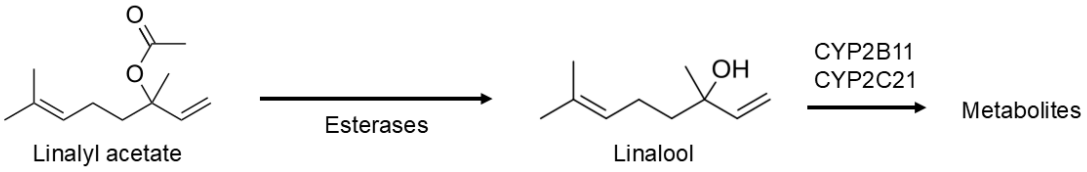

Figure 34 Possible mechanisms of biotransformation of linalool and linalyl acetate in pooled dog liver microsomes.

Carboxylesterases (CES) hydrolyze several types of xenobiotics in humans and animals (Taketani *et al.*, 2007). These esterases metabolize approximately 35% of the metabolism of drugs used in clinical practice, and bioactivate most of prodrugs of the ester and amides classes prescribed (Yoshida *et al.*, 2018). Although there are several subfamilies of CES, the main ones responsible for drug metabolism are CES1 and CES2. CES1 has a greater affinity for large alkyl groups and small alcohols and amines. CES2 prefers large-chain alcohol and amines and small alkyl groups. Dogs express both CES1 and CES2 in the liver but not the intestine (Taketani *et al.*, 2007; Kurokawa *et al.*, 2016; Wang *et al.*, 2020). LINAct is an ester formed by an acetate group, which is a small alkyl group and a derivative of linalool (linalyl), with a large and branched terpene chain, and is therefore a large alcohol. Based on substrate preferences, CES2 is likely the predominant isoform involved in LINAct hydrolysis in dogs. According to Huggins and Moulton (1948), nonspecific esterases could be found in several tissues in dogs, with the highest concentration in the liver, followed by the tracheal mucosa, bladder mucosa, and gastric mucosa, besides, pancreas, and lungs (Huggins and Moulton, 1948). This indicates that,

whether orally or by inhalation, LINAct is capable of being metabolized. Although LEO could be applied topically (Komiya *et al.*, 2009), the activity of cutaneous esterases in dogs has not been described. However, in other species, such as humans, rats, and pigs, esterase activity in the skin has been described (William Montagna and Victor R Formisano, 1955; Prusakiewicz *et al.*, 2006; Jewell *et al.*, 2007). Thus, LINAct may also be metabolized in dogs. There is still little characterization of esterases in dogs in various tissues, in addition to a few specific studies on the metabolism of LINAct in this species, thus representing a promising area for future research.

The use of *in vitro* metabolism to predict hepatic elimination is a widely used method in drug development (Obach, 1999; Obach and Reed-Hagen, 2002; Sodhi and Benet, 2021). The *in vitro* and *in vivo* pharmacokinetic correlations were first described by Rane et al. (1977) in rats. The kinetic parameters V_{max} and k_m were defined for the analysis of the enzymatic behavior (Obach, 1999). In our work, we used the *in vitro* approach by performing incubations with the substrate (linalool), canine liver microsomes, and the cofactor NADPH; each incubation was performed with different concentrations of LIN and microsomal proteins. Results showed a clear positive correlation ($R^2 = 0.94$) between the protein concentration and the rate of LIN depletion. The first-order rate constant of an enzyme is most accurately estimated when the substrate is present at low concentrations in the system (less than 10% of the Km value) and could be used with the protein concentration to calculate the CLint of this compound *in vitro* (Wagner, 1973; Obach, 1999; Johnson and Goody, 2011; Srinivasan, 2022). However, when increasing LIN concentrations at a fixed proteins concentration, the elimination rate became saturated (nonlinear), similar to that observed earlier for other monoterpenes that are metabolized

by CYPs (Khojasteh-Bakht *et al.*, 1999; Miyazawa *et al.*, 2001; Duisken *et al.*, 2005; Miyazawa and Gyoubu, 2007; Abass *et al.*, 2011). This nonlinear kinetics could be mathematically represented by the Michaelis-Menten equation, which relates the substrate concentration, the velocity of depletion by the enzyme, and a constant called the Michaelis-Menten constant (k_m), which is the substrate concentration at which the enzyme has half of its maximum catalytic rate (Wagner, 1973; Obach and Reed-Hagen, 2002; Johnson and Goody, 2011; Srinivasan, 2022). These are valuable parameters for describing the metabolic capacity of enzymes. Considering that typical Km values for xenobiotics range around 100 μM, with high-affinity substrates displaying values as low as 0.1 μM (Bar-Even *et al.*, 2011), it could be suggested that LIN exhibits a high k_m value of 50 μM. This indicates that at this concentration, CYP enzymes begin to exhibit saturation or partial saturation when all protein binding sites are occupied, and hepatic clearance begins to decrease. In this study, the estimated k_m value for LIN, under the experimental conditions presented, was 52 ± 11 μM. This k_m value reflects the LIN concentration at which the elimination rate reaches 50% of its maximum (V_{max}), providing an estimate of the enzyme's affinity for the substrate. k_m may also indicate the range in which the plasma concentration is proportional to the elimination, in other words, a first-order kinetics. Because the C_{max} value of LIN in dogs has not been described, it is necessary to use data from other species. In humans, for example, the C_{max} of LIN after a single oral dose of Silexan® is 74–145 ng/mL (0.48 - 0.95 μM), and for rats, this value is approximately 77 ng/mL (0.5 μM), values much lower than those found in our experiments. For clinical interpretation, it is necessary to calculate the C_{max}/k_m ratio. This ratio indicates the probability of substrate accumulation in tissues based on metabolic saturation. Here,

for CYP2B11, this ratio could be estimated using an average of the C_{max} values found in humans and rats, as these are the data available in the literature, and the k_m values found in this experiment (Table 15). Considering the lack of data in the literature, it is reasonable to suggest that therapeutic oral doses for dogs are similar to those species and, therefore, the C_{max}/k_m ratio remains below 1, maintaining first-order LIN metabolism, thus providing predictable and dose-dependent pharmacokinetics for this terpene. It is important to emphasize that the values presented in table 15 are only estimates, indicating the need for specific dog data. The higher the k_m value, the lower the saturation probability is. In addition, k_m reflects the affinity of the enzyme for the substrate (Wagner, 1973; Obach and Reed-Hagen, 2002; Johnson and Goody, 2011). Given the high concentration of LIN, this suggests the moderate affinity of CYP enzymes for it and, consequently, the need for a greater quantity of molecules for saturation to actually occur. One of the clinical consequences of these parameters is that the k_m value could be used to define the dose-proportionality of a drug. Drugs with low k_m values generally have a nonproportional blood concentrations and elimination kinetics, such as ethanol (Wilkinson, 1980). On the other hand, drugs with proportional blood concentrations and elimination kinetics are accompanied by high k_m (Obach and Reed-Hagen, 2002), as is the case with LIN. From this equation, it is possible to obtain the substrate depletion constant rate (k_{dep}), which represents the basal enzymatic activity in the absence of saturation, if the measurements are under first-order conditions. This helps to scale the *in vitro* data and apply it to *in vivo* models to predict drug clearance rates (Obach *et al.*, 1997; Obach, 1999; Obach and Reed-Hagen, 2002). Although the Michaelis-Menten equation is widely used to describe classical enzyme kinetics, it has significant limitations. It assumes a simplified system with only one

substrate, no allosteric effects, and a constant steady-state equilibrium between the free enzyme, substrate, and enzyme-substrate complex. Therefore, it fails to consider phenomena common to more complex biological systems, such as competitive inhibition, regulation by cofactors, interactions with multiple substrates, or enzyme conformational variations (Hold and Panke, 2009; Schnell, 2014; Leow and Chan, 2019) Therefore, the parameters obtained from this model must be interpreted within a simplified and idealized context.

Table 15 The ratio between Cmax and the plasma concentration of linalool found in Silexan® necessary to reduce CYP2B11 enzyme activity in humans, rats, and dogs.

Species	Cmax (μM)	Cmax/Km Ratio
Single dose		
Humans	0.1	0.002
Rats	0.5	0.010
Dogs (estimated)	0.3	0.006
Multiple doses		
Humans	0.8	0.015
Rats	0.7	0.014
Dogs (estimated)	0.75	0.014

LIN has a substrate depletion constant rate of 0.050 μM/min, indicating that 0.050 μM of LIN was reduced from the dog's liver every minute in the absence of saturation (Nath and Atkins, 2006). This is an important parameter to predict the time needed to metabolize LIN by the liver. The data found in this study suggest that LIN may have the potential for dose-dependent pharmacokinetics *in vivo*. Thus, metabolic capacity

decreases at high LIN concentrations, providing valuable information for anxiety treatment, which is generally performed in a multiple-dose regimen (Locke *et al.*, 2015). In a canine patient, it is also necessary to consider the possible accidental ingestion of drugs containing LIN.

In this study, recombinant enzymes were used to determine the CLint of LIN and extrapolated to values in pDLMs. This approach allowed us to determine the relative importance of different CYP isoforms in LIN metabolism. The CLint of the enzymes that were shown to metabolize LIN was CYP2B11 > CYP2C21 > CYP2C41, with CYP2B11 having a 1.6-fold higher metabolizing capacity compared with CYP2C21 and 7-fold higher compared with CYP2C41. The participation of CYP2B11 was dominant, having 7 times more LIN depletion capacity than the other recombinant enzymes tested. Thus, the variability in the expression of this isoform may significantly influence the hepatic clearance of LIN in dogs because it plays a significant role in drug metabolism (Mills *et al.*, 2010b; Court, 2013a; Gagliardi *et al.*, 2015). Mutations in this enzyme May lead to drug toxicity. For example, some dog breeds, such as Greyhounds, are deficient in this enzyme, and drugs that are dependent on it may accumulate in the plasma (Court, 2013a; Martinez *et al.*, 2020, 2024). This particularity provides evidence that this isoform is important for these species.

Considering the complexity of treatment for anxiety, which increases the probability of the patient receiving multiple medications and the chance of interactions between them (Griffiths, 1988; Corrie and Hardman, 2017; Watson et al., 2018b), the second part of this study focused in analyze the possibility that LIN, LINAct and lavender oil may interfere with the pharmacokinetics of other drugs that are often prescribed for anxiety and anxiety-

related pain. One type of drug interaction involves enzyme induction. With induction, the concentration of metabolizing enzymes present in the microsomes increases, resulting in increased substrate depletion, which was confirmed by using different pDLMs concentrations. This may result in a decrease in the therapeutic efficacy of the affected drug because hepatic clearance is increased. The process of enzyme induction in a dog is time-consuming (Griffiths, 1988; Corrie and Hardman, 2017), so microsomes from dogs previously treated with CYP-selective inducing compounds were used for this study, including phenobarbital (induces CYP2B11 and CYP2C21) (Ohno *et al.*, 2009; Court, 2013a; Martinez *et al.*, 2020; Cantiello *et al.*, 2022), rifampicin (induces CYP3A12) (Nishibe Y *et al.*, 1998; Shin *et al.*, 2022), clofibric acid (induces CYP4A) (Bars *et al.*, 1993; Roman *et al.*, 1993) and β-naphthoflavone (induces CYP1A1 and CYP1A2) (Muntané-Relat J *et al.*, 1995; Xiao *et al.*, 2009), as well as their respective vehicles.

Phenobarbital treatment led to a 5-fold increase in LIN depletion, likely due to upregulation of CYP isoforms responsible for LIN metabolism, particularly CYP2B11. It is well known that phenobarbital enhances the transcription of enzymes responsible for metabolism of xenobiotics, including the CYPs. This is mediated by the activation of the constitutive androstane receptor (CAR). Phenobarbital may also activate phosphorylation and dephosphorylation cycles that favor CYP synthesis (Zelko and Negishi, 2000; Blättler *et al.*, 2007; Brodie *et al.*, 2013). Blättler et al. (2007) showed that AMP-activated protein kinase (AMPK) activity also participates in hyperregulation, and this occurs in a dose-dependent manner. It is feasible to speculate that an adjustment in the dose and/or frequency of LIN administration might be necessary in dogs that are taking phenobarbital or another CYP2B11- or CYP2C21-inducing drug.

In vitro inhibition assays are a key step in the development of new drugs (Maeda *et al.*, 2021), and the results of this type of interaction have important implications for clinical and therapeutic practice. In the present study, the inhibitory capacity of the tested terpenoids was evaluated using canine liver microsomes and recombinant CYP enzymes. The results demonstrate that CYP2B11 was inhibited by these compounds, but CYP2C21 and CYP3A12 were not.

All terpenoids herein tested inhibited CYP2B11-mediated reactions in pDLMs, with LIN having the lowest inhibitory potency among the two compounds and the mixture tested. In human liver microsomes, LINAct may inhibit the enzymes CYP3A4 (Mondal *et al.*, 2023), whose orthologs in dogs are, respectively, CYP3A12 (Court, 2013a). Regarding LIN, however, similar results were found in the present study and in that of Mondal et al. (2023), evidencing once again the complexity of herb-drug interactions. The difference between the results of LIN and LINAct suggests that the chemical structure of the molecules may be involved in this process (van Rossum, 1963). The reduced inhibitory activity of LIN appears to be linked to its lower affinity or stability in the CYP2B11 catalytic site when compared to LINAct. Furthermore, considering that lavender oil is a mixture of LINAct, LIN, and other molecules (Kıvrak, 2018; Pokajewicz *et al.*, 2021; Kozuharova *et al.*, 2023), the intermediate inhibitory capacity of the oil may be associated with the antagonistic behaviors of both LIN and LINAct. The inhibitory results of lavender oil found by Mondal et al. (2023) showed a higher capacity than that of LINAct alone, which corroborates the expected results based on the antagonistic behavior between LIN and LINAct. Further studies related to the chemistry of these compounds and their interactions are required.

Unexpectedly, the results obtained using pDLMs were not like those found in experiments with recombinant enzymes. Neither LIN nor LINAct inhibited the activity of the enzymes rCYP2B11, rCYP2C21, and rCYP3A12 under the experimental conditions applied. Because CYP3A12 was not inhibited in the experiments with pDLMs, it was expected that it would not be inhibited when evaluated alone. However, rCYP2B11 (mainly) and rCYP2C21 inhibition were expected, but it did not occur. According to Fujiwara et al. (2008), the results for enzymes found in hepatocytes may be different from those found when studying recombinant enzymes. This could be explained by the fact that the same compound is, at the same time, a substrate of one enzyme and an inhibitor of another in the same system. In the cited study, 1-naphthol is a substrate of the enzyme UGT1A6 and an inhibitor of UGT1A9, both of which belong to the human hepatic microsomal system. When evaluating the recombinant UGT1A9 enzyme, it was observed that the inhibition was more pronounced than in the microsomal system because there was probably no decrease in the concentration of substrate resulting from UGT1A6 metabolism (Fujiwara *et al.*, 2008; Parkinson *et al.*, 2010). In our study, LIN was metabolized by both CYP2B11 and CYP2C21 and did not inhibit rCYP2B11 nor rCYP2C21. One explanation for this phenomenon is the presence of a potential metabolite formed from the biotransformation of LIN in the microsomal system that is capable of inhibiting CYP2B11, but not CYP2C21. To investigate this hypothesis, additional experiments similar to this one could be performed using the main metabolite of LIN, 8-hydroxylinalool, as a test compound to evaluate its inhibitory potential for rCYP2B11 and rCYP2C21. These results demonstrate the importance of this type of analysis in predicting drug interactions in living organisms. An earlier experiment using buprenorphine also revealed a discrepancy between the IC50 values of human microsomes and recombinant enzymes.

The inhibition of reactions catalyzed by the CYP2D6 enzyme in human microsomes was significantly high, whereas the inhibition of rCYP2D6 was comparatively low (Umeda *et al.*, 2005). This divergence reinforces the limitations of using recombinant enzymes in isolation for predicting *in vivo* metabolism and highlights the complexity of enzyme-substrate-metabolite interactions in full microsomal systems.

Some inhibitors are time dependent. This phenomenon is also called mechanism-based inhibition and may be clinically relevant to drug interactions. The most common in vitro approach involves pre-incubation of the inhibitor in a system containing microsomes or recombinant enzymes, and cofactors. The substrate is added after pre-incubation. If the IC50 is significantly lower (inhibition is more potent) than that of the system without pre-incubation, then the inhibition is time dependent. The change in IC50 is referred to as the IC50 shift and is a measure of time-dependent inhibition potency (Burt *et al.*, 2010). This information is important because it may indicate whether the inhibitor-enzyme interaction is reversible or not. A large IC50 shift suggests that the reaction has the potential for irreversibility, which may generate toxicity and accumulation of the substrate in the plasma until new enzymes are synthesized (Burt *et al.*, 2010; Riley and Wilson, 2015). When assessing whether CYP2B11 inhibition is time-dependent (IC50 shift), the results revealed that pre-incubation increases the inhibitory potency of N-demethylation of tramadol by LIN (2.3-fold), highlighting the time-dependence of inhibition. On the other hand, the opposite effect was observed for LINAct. Pre-incubation of this terpenoid reduced its inhibitory potency, especially the N-demethylation of methadone (3 times). Once again, lavender oil had values closer to those of LINAct, and this may have occurred because this mixture had a higher concentration of LINAct (42%) than LIN (40%). These

findings underscore the complex pharmacodynamic profiles of terpenoids and their potential to alter drug metabolism in a time- and compound-dependent manner. Therefore, this information should be considered in clinical practice.

The relationship between inhibitor C_{max} and IC_{50} is an important parameter for assessing the clinical relevance of a drug. The values obtained were used to predict whether the drug is an effective inhibitor (Bjornsson *et al.*, 2003). Because there was a limitation due to the lack of data on the C_{max} of LIN or LINAct (pure or from lavender oil) in dogs after oral administration, it was necessary to extrapolate the values from the results in humans and rats. Silexan® is a drug developed to control anxiety in humans that consists of standardized lavender oil (Müliner et al., 2015). LIN C_{max} in rats and humans was measured after the oral administration of single or multiple doses of Silexan®. In rats, the maximum concentration of LIN in the liver was also measured after a single dose and after multiple doses. When comparing the values found by Müliner et al. (2015) and those found in the present study, a significant relationship was noted, suggesting that if similar concentrations are found in dogs, there is a risk of potential clinically relevant inhibition of CYP2B11. Table 14 shows the ratio between C_{max} and the plasma concentration of LIN found in Silexan® necessary to reduce CYP2B11 enzyme activity in humans, rats, and dogs. For humans, the C_{max} was estimated to be 0.1 µM (22 ng/mL) (single dose = 80 mg) and 0.8 µM (131 ng/mL) (daily doses = 160 mg, 14 days). For rats, the C_{max} considered was estimated at 0.5 µM (77 ng/mL, single dose = 100 mg/kg) and 0.7 µM (108 ng/mL, daily doses = 100 mg/kg, 14 days). The k_m considered was the one presented in this work (52 µM). The C_{max}/k_m ratios were calculated for single and multiple doses. Due to the absence of data on dogs in the literature, C_{max} values for humans and rats were used to

estimate the C_{max} for dogs, assuming that therapeutic doses for this species are lower than those for humans and similar to those for rats. According to Bjornsson et al. (2003), a Cmax/Km ratio greater than 1.000 suggests a likely clinically relevant interaction; values between 0.100 and 1.000 indicate possible relevance; and ratios below 0.100 suggest a low likelihood of clinically relevant enzyme inhibition. Therefore, further studies are needed to investigate the pharmacokinetics of LIN and LINAct in dogs.

In the present study, LIN, LINAct and their mixture (in lavender oil) inhibited the metabolism of tramadol and methadone. These two opioids are widely used in veterinary medicine to treat moderate to severe pain of various etiologies (Kerr and Swanton, 2023; Soares-Santos *et al.*, 2024). Consequently, co-administration of terpenoids, particularly LINAct, with opioids such as tramadol and methadone may require caution due to the risk of reduced clearance and consequent drug accumulation. It is expected that dosing LIN and LINAct may reduce the metabolism of opioids, leading to their accumulation in plasma. In addition to the persistence of therapeutic effects, it may cause the appearance and persistence of side or even toxic effects. There is a need for further investigations on the metabolism of LIN and LINAct, and drug interactions involving these terpenoids in dogs. The use of canine animal models may be useful for exploring the pharmacokinetics of these drugs and provide more robust information for the oral administration of LEO in this species.

6 CONCLUSIONS

6 CONCLUSIONS

This study integrated *in silico* and *in vitro* approaches to characterize the hepatic metabolism of linalool, linalyl acetate, and lavender essential oil in dogs, with an emphasis on the involvement of cytochrome P450 enzymes in this process. Each approach has distinct advantages and limitations. However, when used in a complementary manner, they offer a more comprehensive and refined understanding of biotransformation mechanisms and potential drug-drug interactions.

The *in silico* simulations included 3D modeling of the canine isoforms CYP2B11, CYP2C21, and CYP2D15, followed by molecular docking with LIN and LINAct molecules. The results indicated different binding affinities between the compounds and the isoforms tested, with a strong interaction between LIN and CYP2B11. This favorable energetic affinity suggests a greater propensity for interaction between this monoterpene and this isoform, corroborating the *in vitro* findings that identified CYP2B11 as the main enzyme involved in LIN metabolism. This convergence between the approaches strengthens the hypothesis that CYP2B11 plays a central role in LIN biotransformation in dogs.

However, molecular modeling has several significant limitations. By itself, it does not allow for the prediction of kinetic parameters (such as Km or Vmax) or discrimination of the type of metabolic reaction involved (e.g., oxidation, hydrolysis, conjugation). It also does not consider dynamic phenomena, such as enzyme induction, substrate competition, time-dependent inhibition, or the formation of active metabolites. Therefore, *in vitro* data is essential for elucidating these aspects. Our experiments with canine liver microsomes demonstrated that LIN undergoes NADPH-dependent metabolism, indicating the

involvement of CYPs, while LINAct appears to be converted to LIN through the action of hepatic esterases, a process not considered in the *in silico* modeling, as the computational study design was limited to evaluating interactions with CYPs.

Furthermore, the behavior of LIN as a potential CYP2B11 inhibitor varied between the approaches. Although docking suggested a strong binding affinity, assays with recombinant enzymes did not demonstrate direct inhibition of rCYP2B11 by LIN. Conversely, in liver microsomes, a significant inhibition of CYP2B11 activity was observed, particularly after incubation with LIN. This suggests that the inhibitory effect may be mediated by metabolites formed during biotransformation or specific conformational changes in the microsomal system. This finding reinforces the limitations of both recombinant and *in silico* models in reproducing the complexity of metabolic interactions *in vivo*.

Another relevant aspect concerns LINAct. The conversion of this ester to LIN has been consistently observed *in vitro*, primarily through the action of hepatic esterases, reinforcing the hypothesis that LINAct may act as a prodrug. However, this possibility has not been evaluated *in silico*, as the modeling focused exclusively on interactions with CYPs. Therefore, the concept of a prodrug emerged only from the functional interpretation of *in vitro* data and could not have been predicted using the computational data used in this study.

Despite these limitations, docking has proven valuable for predicting the initial interactions between substrates and enzymes, allowing for the prioritization of compounds for functional assays. The combined analysis of the data identified the predominant role

of CYP2B11, followed by CYP2C21 in the metabolism of LIN and LINAct in dogs. Furthermore, the induction and inhibition effects observed *in vitro* suggest that these enzymes can be modulated in polypharmacy contexts, which has significant clinical implications. Because CYP2B11 exhibits genetic variations across dog breeds, its activity may directly affect the pharmacokinetics of LEO and co-administered drugs.

Therefore, the integration of *in silico* and *in vitro* approaches allowed us to construct a more robust and physiologically relevant model of the metabolism of the main components of LEO in dogs. This strategy reinforces the importance of the combined use of computational and experimental methods in veterinary pharmacology, especially when predicting metabolic interactions, clarifying the role of specific isoforms, and supporting evidence-based therapeutic decisions.

Figure 33 shows a summary of experimental findings presented in this work.

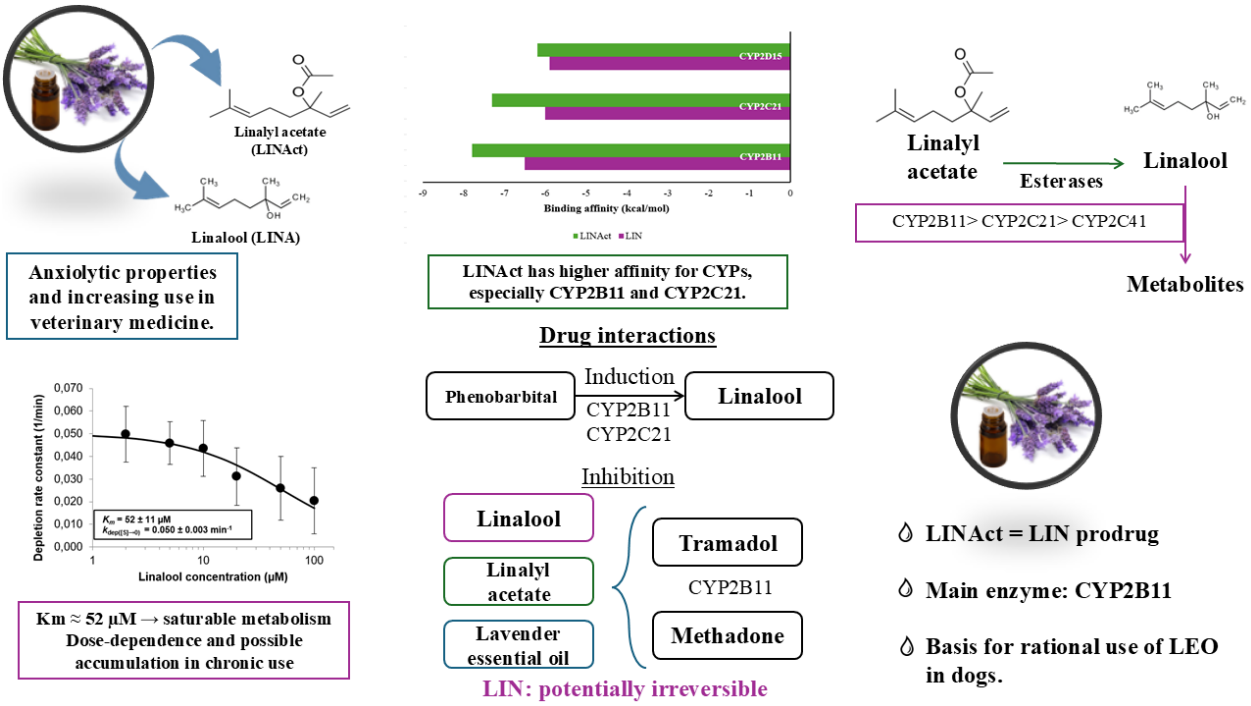

Figure 35 Summary of experimental findings presented in this work.

7 PERSPECTIVES

7 PERSPECTIVES

Further *in silico* approaches are necessary to study molecular dynamics in computational models, in addition to a study focused on the active sites of CYP2B11 and CYP2C21 to evaluate substrate-enzyme interactions more specifically targeting the heme group of each of them. In the *in vitro* context, quantifying the metabolites generated from the metabolism of LIN and how these metabolites act in the modulation of canine CYPs are suggested to characterize in greater depth the drug interaction between LEO and other drugs used in the therapy of anxiety. As the main future step, an *in vivo* pharmacokinetic study is planned with the aim of validating the data obtained in the previous steps. Furthermore, this study is essential to quantify the real clearance of LIN and LINAct, bioavailability, half-life, maximum plasma concentration, and the time to reach this concentration considering physiological and environmental factors, being the next step in the objective of outlining an adequate and safe dosage of LEO for dogs, thus contributing to effective therapy.

8 REFERENCES

8 REFERENCES

Abass K, Reponen P, Mattila S, and Pelkonen O (2011) Metabolism of α-thujone in human hepatic preparations *in vitro*. *Xenobiotica* **41**:101–111.

AFNOR (2000) *Huiles Essentielles, Tome 2, Monographies Relatives Aux Huiles Essentielles*, 6th ed., AFNOR, Association Française de Normalisation, Paris, France.

Anderson IB (1996) Pennyroyal Toxicity: Measurement of Toxic Metabolite Levels in Two Cases and Review of the Literature. *Ann Intern Med* **124**:726.

Arnold K, Bordoli L, Kopp J, and Schwede T (2006) The SWISS-MODEL workspace: a web-based environment for protein structure homology modelling. *Bioinformatics* **22**:195–201.

Austin CA, Shephard EA, Pike SF, Rabin BR, and Phillips IR (1988) The effect of terpenoid compounds on cytochrome P-450 levels in rat liver. *Biochem Pharmacol* **37**:2223–2229.

Baldinger P, Hoflich AS, Mitterhauser M, Hahn A, Rami-Mark C, Spies M, Wadsak W, Lanzenberger R, and Kasper S (2015) Effects of Silexan on the Serotonin-1A Receptor and Microstructure of the Human Brain: A Randomized, Placebo-Controlled, Double-Blind, Cross-Over Study with Molecular and Structural Neuroimaging. *International Journal of Neuropsychopharmacology* **18**:pyu063–pyu063.

Bampidis V, Azimonti G, Bastos M de L, Christensen H, Dusemund B, Durjava MF, Kouba M, López-Alonso M, López Puente S, Marcon F, Mayo B, Pechová A, Petkova M, Ramos F, Sanz Y, Villa RE, Woutersen R, Brantom P, Chesson A, Dierick N, Martelli G, Westendorf J, Anguita M, Galobart J, and Manini P (2020) Safety of 31 flavouring compounds belonging to different chemical groups when used as feed additives for all animal species. *EFSA Journal* **18**.

Baratta MT, Zaya MJ, White JA, and Locuson CW (2010) Canine CYP2B11 metabolizes and is inhibited by anesthetic agents often co-administered in dogs. *J Vet Pharmacol Ther* **33**:50–55.

Bar-Even A, Noor E, Savir Y, Liebermeister W, Davidi D, Tawfik DS, and Milo R (2011) The Moderately Efficient Enzyme: Evolutionary and Physicochemical Trends Shaping Enzyme Parameters. *Biochemistry* **50**:4402–4410.

Bars RG, Bell DR, and Elcombe CR (1993) Induction of cytochrome p450 and peroxisomal enzymes by clofibric acid in vivo and in VITRO. *Biochem Pharmacol* **45**:2045–2053.

Bartova L, Dold M, Fugger G, Weidenauer A, Rujescu D, and Kasper S (2023) Silexan for treatment of anxiety and depression in the context of COVID-19. *European Neuropsychopharmacology* **70**:47–48.

Batista PA, de Paula Werner MF, Oliveira EC, Burgos L, Pereira P, da Silva Brum LF, Story GM, and Santos ARS (2010) The Antinociceptive Effect of (-)-Linalool in Models of Chronic Inflammatory and Neuropathic Hypersensitivity in Mice. *J Pain* **11**:1222–1229.

Berman HM (2000) The Protein Data Bank. *Nucleic Acids Res* **28**:235–242.

Bjornsson TD, Callaghan JT, Einolf HJ, Fischer V, Gan L, Grimm S, Kao J, King SP, Miwa G, Ni L, Kumar G, McLeod J, Obach RS, Roberts S, Roe A, Shah A, Snikeris F, Sullivan JT, Tweedie D, Vega JM, Walsh J, and Wrighton SA (2003) THE CONDUCT OF IN VITRO AND IN VIVO DRUG-DRUG INTERACTION STUDIES: A PHARMACEUTICAL RESEARCH AND MANUFACTURERS OF AMERICA (PhRMA) PERSPECTIVE. *Drug Metabolism and Disposition* **31**:815–832.

Blättler SM, Rencurel F, Kaufmann MR, and Meyer UA (2007) In the regulation of cytochrome P450 genes, phenobarbital targets LKB1 for necessary activation of AMP-activated protein kinase. *Proceedings of the National Academy of Sciences* **104**:1045–1050.

Böhm H-J, and Schneider G (2003) *Protein-Ligand Interactions: From Molecular Recognition to Drug Design*, Wiley-VCH Verlag GmbH & Co. KGaA.

Brito RG, Santos PL, Prado DS, Santana MT, Araújo AAS, Bonjardim LR, Santos MR V., de Lucca Júnior W, Oliveira AP, and Quintans-Júnior LJ (2013) Citronellol Reduces Orofacial Nociceptive Behaviour in Mice – Evidence of Involvement of Retrosplenial Cortex and Periaqueductal Grey Areas. *Basic Clin Pharmacol Toxicol* **112**:215–221.

Brnawi WI, Hettiarachchy NS, Horax R, Kumar-Phillips G, Seo H, and Marcy J (2018) Comparison of Cinnamon Essential Oils from Leaf and Bark with Respect to Antimicrobial Activity and Sensory Acceptability in Strawberry Shake. *J Food Sci* **83**:475–480.

Brodie MJ, Mintzer S, Pack AM, Gidal BE, Vecht CJ, and Schmidt D (2013) Enzyme induction with antiepileptic drugs: Cause for concern? *Epilepsia* **54**:11–27.

Burt HJ, Galetin A, and Houston JB (2010) IC 50-based approaches as an alternative method for assessment of time-dependent inhibition of CYP3A4. *Xenobiotica* **40**:331–343.

Cantiello M, Carletti M, Giantin M, Gardini G, Capolongo F, Cascio P, Pauletto M, Girolami F, Dacasto M, and Nebbia C (2022) Induction by Phenobarbital of Phase I and II Xenobiotic-Metabolizing Enzymes in Bovine Liver: An Overall Catalytic and Immunochemical Characterization. *Int J Mol Sci* **23**:3564.

Cederbaum AI (2012) Alcohol Metabolism. *Clin Liver Dis* **16**:667–685.

Chadha A, and Madyastha KM (1984) Metabolism of geraniol and linalool in the rat and effects on liver and lung microsomal enzymes. *Xenobiotica* **14**:365–374.

Chadha A, and Madyastha KM (1982) ω-Hydroxylation of acyclic monoterpene alcohols by rat lung microsomes. *Biochem Biophys Res Commun* **108**:1271–1277.

Chemical Computing Group ULC (2025) Molecular Operating Environment (MOE)., Montreal.

Chen L, Li Q, Nasif KFA, Xie Y, Deng B, Niu S, Pouriyeh S, Dai Z, Chen J, and Xie CY (2024) AI-Driven Deep Learning Techniques in Protein Structure Prediction. *Int J Mol Sci* **25**:8426.

Chillistone S, and Hardman JG (2023) Modes of drug elimination and bioactive metabolites. *Anaesthesia & Intensive Care Medicine* **24**:482–485.

Chopra B, and Dhingra AK (2021) Natural products: A lead for drug discovery and development. *Phytotherapy Research* **35**:4660–4702.

Corrie K, and Hardman JG (2017) Mechanisms of drug interactions: pharmacodynamics and pharmacokinetics. *Anaesthesia & Intensive Care Medicine* **18**:331–334.

Court MH (2007) A Pharmacogenomics Primer. *The Journal of Clinical Pharmacology* **47**:1087–1103.

Court MH (2013a) Canine Cytochrome P-450 Pharmacogenetics. *Veterinary Clinics of North America: Small Animal Practice* **43**:1027–1038.

Court MH (2013b) Feline Drug Metabolism and Disposition. *Veterinary Clinics of North America: Small Animal Practice* **43**:1039–1054.

Court MH, Mealey KL, Burke NS, Jimenez TP, Zhu Z, and Wakshlag JJ (2024) Cannabidiol and cannabidiolic acid: Preliminary in vitro evaluation of metabolism and drug–drug interactions involving canine cytochrome P-450, UDP-glucuronosyltransferase, and P-glycoprotein. *J Vet Pharmacol Ther* **47**:1–13.

Court MH, Von Moltke LL, Shader RI, and Greenblatt DJ. (1997) Biotransformation of Chlorzoxazone by Heptatic Microsomes from Humans and Ten Other Mammalian Species. *Biopharm Drug Dispos* **18**:213–226.

Crișan I, Ona A, Vârban D, Muntean L, Vârban R, Stoie A, Mihăiescu T, and Morea A (2023) Current Trends for Lavender (Lavandula angustifolia Mill.) Crops and Products with Emphasis on Essential Oil Quality. *Plants* **12**:357.

Currie GM (2018) Pharmacology, Part 2: Introduction to Pharmacokinetics. *J Nucl Med Technol* **46**:221–230.

Dalgaard L (2015) Comparison of minipig, dog, monkey and human drug metabolism and disposition. *J Pharmacol Toxicol Methods* **74**:80–92.

Dattani S, Rodés-Guirao L, Ritchie H, Ortiz-Ospina E, and Roser M (2023) Life Expectancy.

Davanço MG, Campos DR, and Carvalho P de O (2020) In vitro – In vivo correlation in the development of oral drug formulation: A screenshot of the last two decades. *Int J Pharm* **580**:119210.

de Melo Alves Silva LC, de Oliveira Mendes F de C, de Castro Teixeira F, de Lima Fernandes TE, Barros Ribeiro KR, da Silva Leal KC, Dantas DV, and Neves Dantas RA (2023) Use of Lavandula angustifolia essential oil as a complementary therapy in adult health care: A scoping review. *Heliyon* **9**:e15446.

de Sousa DP, Damasceno ROS, Amorati R, Elshabrawy HA, de Castro RD, Bezerra DP, Nunes VR V., Gomes RC, and Lima TC (2023) Essential Oils: Chemistry and Pharmacological Activities. *Biomolecules* **13**:1144.

Do TKT, Francis Hadji-Minaglou, Sylvain Antoniotti, and Xavier Fernandez (2015) Authenticity of essential oils. *TrAC Trends in Analytical Chemistry* **66**:146–157.

Doroshyenko O, Rokitta D, Zadoyan G, Klement S, Schläfke S, Dienel A, Gramatté T, Lück H, and Fuhr U (2013) Drug Cocktail Interaction Study on the Effect of the Orally

Administered Lavender Oil Preparation Silexan on Cytochrome P450 Enzymes in Healthy Volunteers. *Drug Metabolism and Disposition* **41**:987–993.

Duisken M, Sandner F, Blömeke B, and Hollender J (2005) Metabolism of 1,8-cineole by human cytochrome P450 enzymes: identification of a new hydroxylated metabolite. *Biochimica et Biophysica Acta (BBA) - General Subjects* **1722**:304–311.

Ediriweera MK, Tennekoon KH, and Samarakoon SR (2019) In vitro assays and techniques utilized in anticancer drug discovery. *Journal of Applied Toxicology* **39**:38–71.

Eguchi K, Nishibe Y, Baba T, and Ohno K (1996) Quantitation of cytochrome P450 enzymes (CYP1A1/2, 2B11, 2C21 and 3A12) in dog liver microsomes by enzyme-linked immunosorbent assay. *Xenobiotica* **26**:755–763.

EPC, EDQM, and HC (2009) *European Pharmacopoeia*, 10th ed., European Directorate for the Quality of Medicines & HealthCare of the Council of Europe, Strasbourg, France.

Fernández-Quintero ML, Ljungars A, Waibl F, Greiff V, Andersen JT, Gjølberg TT, Jenkins TP, Voldborg BG, Grav LM, Kumar S, Georges G, Kettenberger H, Liedl KR, Tessier PM, McCafferty J, and Laustsen AH (2023) Assessing developability early in the discovery process for novel biologics. *MAbs* **15**.

Ferreira L, Dos Santos R, Oliva G, and Andricopulo A (2015) Molecular Docking and Structure-Based Drug Design Strategies. *Molecules* **20**:13384–13421.

Fitzi J, Fürst-Jucker J, Wegener T, Saller R, and Reichling J (2002) Phytotherapy of chronic dermatitis and pruritus of dogs with a topical preparation containing tea tree oil (Bogaskin®). *Schweiz Arch Tierheilkd* **144**:223–231.

Fujiwara R, Nakajima M, Yamanaka H, Katoh M, and Yokoi T (2008) Product Inhibition of UDP-Glucuronosyltransferase (UGT) Enzymes by UDP Obfuscates the Inhibitory Effects of UGT Substrates. *Drug Metabolism and Disposition* **36**:361–367.

Gagliardi R, Llambí S, and Arruga MV (2015) SNP genetic polymorphisms of MDR-1, CYP1A2 and CYPB11 genes in four canine breeds upon toxicological evaluation. *J Vet Sci* **16**:273–280, The Korean Society of Veterinary Science.

Graham RA, Tyler LO, Krol WL, Silver IS, Webster LO, Clark P, Chen L, Banks T, and LeCluyse EL (2006) Temporal kinetics and concentration–response relationships for induction of CYP1A, CYP2B, and CYP3A in primary cultures of beagle dog hepatocytes. *J Biochem Mol Toxicol* **20**:69–78.

Griffiths JP (1988) Drug Interactions. *Veterinary Clinics of North America: Small Animal Practice* **18**:1243–1265.

Gronkiewicz KM, Giuliano EA, Kuroki K, Bunyak F, Sharma A, Teixeira LBC, Hamm CW, and Mohan RR (2016) Development of a novel in vivo corneal fibrosis model in the dog. *Exp Eye Res* **143**:75–88.

Guengerich FP, Waterman MR, and Egli M (2016) Recent Structural Insights into Cytochrome P450 Function. *Trends Pharmacol Sci* **37**:625–640.

Haller S, Schuler F, Lazic SE, Bachir-Cherif D, Krämer SD, Parrott NJ, Steiner G, and Belli S (2012) Expression Profiles of Metabolic Enzymes and Drug Transporters in the Liver and along the Intestine of Beagle Dogs. *Drug Metabolism and Disposition* **40**:1603–1611.

Hameduh T, Haddad Y, Adam V, and Heger Z (2020) Homology modeling in the time of collective and artificial intelligence. *Comput Struct Biotechnol J* **18**:3494–3506.

Haverbeke A, Uccheddu S, Reinert C, Tertemiz S, Arnouts H, and Sannen A (2024) Dose-dependent responses: a preliminary investigation into the olfactory effects of essential oil concentrations on canine behavior. *Vet Res Commun*, doi: 10.1007/s11259-024-10466-1.

Hay Kraus BL, Greenblatt DJ, Venkatakrishnan K, and Court MH (2000) Evidence for propofol hydroxylation by cytochrome P4502B11 in canine liver microsomes: breed and gender differences. *Xenobiotica* **30**:575–588.

Heger-Mahn D, Pabst G, Dienel A, Schläfke S, and Klipping C (2014) No Interacting Influence of Lavender Oil Preparation Silexan on Oral Contraception Using an Ethinyl Estradiol/Levonorgestrel Combination. *Drugs R D* **14**:265–272.

Hoffmann KH (2020) Essential oils. *Zeitschrift für Naturforschung C* **75**:177–177.

Hold C, and Panke S (2009) Towards the engineering of in vitro systems. *J R Soc Interface* **6**.

Huggins C, and Moulton SH (1948) ESTERASES OF TESTIS AND OTHER TISSUES. *Journal of Experimental Medicine* **88**:169–179.

Hytönen MK, Arumilli M, Lappalainen AK, Owczarek-Lipska M, Jagannathan V, Hundi S, Salmela E, Venta P, Sarkiala E, Jokinen T, Gorgas D, Kere J, Nieminen P, Drögemüller C, and Lohi H (2016) Molecular Characterization of Three Canine Models of Human Rare Bone Diseases: Caffey, van den Ende-Gupta, and Raine Syndromes. *PLoS Genet* **12**:e1006037.

Igarashi M, Song C, Ikei H, Ohira T, and Miyazaki Y (2014) Effect of Olfactory Stimulation by Fresh Rose Flowers on Autonomic Nervous Activity. *The Journal of Alternative and Complementary Medicine* **20**:727–731.

IUPAC-IUB JC on BN (JCBN) (1984) Nomenclature and symbolism for amino acids and peptides. *Biochemical Journal* **219**:345–373.

J. R. Yunta M (2025) Docking and Ligand Binding Affinity: Uses and Pitfalls. *American Journal of Modeling and Optimization* **4**:74–114, Science and Education Publishing.

Jade DD, Pandey R, Kumar R, and Gupta D (2022) Ligand-based pharmacophore modeling of TNF-α to design novel inhibitors using virtual screening and molecular dynamics. *J Biomol Struct Dyn* **40**:1702–1718.

Jenner PM, Hagan EC, Taylor JM, Cook EL, and Fitzhugh OG (1964) Food flavourings and compounds of related structure I. Acute oral toxicity. *Food Cosmet Toxicol* **2**:327–343.

Jewell C, Prusakiewicz JJ, Ackermann C, Payne NA, Fate G, and Williams FM (2007) The distribution of esterases in the skin of the minipig. *Toxicol Lett* **173**:118–123.

Jiang R, Yamaori S, Takeda S, Yamamoto I, and Watanabe K (2011) Identification of cytochrome P450 enzymes responsible for metabolism of cannabidiol by human liver microsomes. *Life Sci* **89**:165–170.

Jimenez JF, Brown AL, Arnold WC, and Byrne WJ (1983) Chronic camphor ingestion mimicking Reye's syndrome. *Gastroenterology* **84**:394–8.

Jimenez TEP, Mealey KL, Schnider D, Grubb TL, Greene SA, and Court MH (2018) Identification of canine cytochrome P- 450s (CYPs) metabolizing the tramadol (+)- M1 and (+)- M2 metabolites to the tramadol (+)- M5 metabolite in dog liver microsomes. *J Vet Pharmacol Ther* **41**:815–824.

Johnson Afonne O, and Chinedu Ifediba E (2022) Natural Does Not Mean Safe, in *Medicinal Plants* p, IntechOpen.

Johnson KA, and Goody RS (2011) The Original Michaelis Constant: Translation of the 1913 Michaelis–Menten Paper. *Biochemistry* **50**:8264–8269.

Jumper J, Evans R, Pritzel A, Green T, Figurnov M, Ronneberger O, Tunyasuvunakool K, Bates R, Žídek A, Potapenko A, Bridgland A, Meyer C, Kohl SAA, Ballard AJ, Cowie A, Romera-Paredes B, Nikolov S, Jain R, Adler J, Back T, Petersen S, Reiman D, Clancy E, Zielinski M, Steinegger M, Pacholska M, Berghammer T, Bodenstein S, Silver D, Vinyals O, Senior AW, Kavukcuoglu K, Kohli P, and Hassabis D (2021) Highly accurate protein structure prediction with AlphaFold. *Nature* **596**:583–589.

Kamimura H (2006) Genetic polymorphism of cytochrome P450s in beagles: possible influence of CYP1A2 deficiency on toxicological evaluations. *Arch Toxicol* **80**:732–738.

Kar S, and Chatterjee S (2021) In Silico Meets In Vitro Techniques in ADMET Profiling of Drug Discovery (Part II). *Curr Drug Metab* **22**:502–502.

Karakus E, Prinzinger C, Leiting S, and Geyer J (2021) Sequencing of the Canine Cytochrome P450 CYP2C41 Gene and Genotyping of Its Polymorphic Occurrence in 36 Dog Breeds. *Front Vet Sci* **8**.

Kasper S, Gastpar M, Müller WE, Volz H-P, Möller H-J, Dienel A, and Schläfke S (2010) Silexan, an orally administered Lavandula oil preparation, is effective in the treatment of 'subsyndromal' anxiety disorder: a randomized, double-blind, placebo controlled trial. *Int Clin Psychopharmacol* **25**:277–287.

Kasper S, Müller WE, Volz H-P, Möller H-J, Koch E, and Dienel A (2018) Silexan in anxiety disorders: Clinical data and pharmacological background. *The World Journal of Biological Psychiatry* **19**:412–420.

Kawai E, Takeda R, Ota A, Morita E, Imai D, Suzuki Y, Yokoyama H, Ueda S, Nakahara H, Miyamoto T, and Okazaki K (2020) Increase in diastolic blood pressure induced by fragrance inhalation of grapefruit essential oil is positively correlated with muscle sympathetic nerve activity. *The Journal of Physiological Sciences* **70**:2.

Kerr CL, and Swanton WE (2023) Anesthesia update - Incorporating methadone into companion animal anesthesia and analgesic protocols: A narrative review. *Can Vet J* **64**:1058–1065.

Khojasteh SC, Oishi S, and Nelson SD (2010) Metabolism and Toxicity of Menthofuran in Rat Liver Slices and in Rats. *Chem Res Toxicol* **23**:1824–1832.

Khojasteh-Bakht SC, Chen W, Koenigs LL, Peter RM, and Nelson SD (1999) Metabolism of (R)-(+)-Pulegone and (R)-(+)-Menthofuran by Human Liver Cytochrome P-450s: Evidence for Formation of a Furan Epoxide. *Drug Metabolism and Disposition* **27**:574.

Kıvrak Ş (2018) Essential oil composition and antioxidant activities of eight cultivars of Lavender and Lavandin from western Anatolia. *Ind Crops Prod* **117**:88–96.

Knights KM, Stresser DM, Miners JO, and Crespi CL (2016) In Vitro Drug Metabolism Using Liver Microsomes. *Curr Protoc Pharmacol* **74**.

Komiya M, Sugiyama A, Tanabe K, Uchino T, and Takeuchi T (2009) Evaluation of the effect of topical application of lavender oil on autonomic nerve activity in dogs. *Am J Vet Res* **70**:764–769.

Kozuharova E, Simeonov V, Batovska D, Stoycheva C, Valchev H, and Benbassat N (2023) Chemical composition and comparative analysis of lavender essential oil samples from Bulgaria in relation to the pharmacological effects. *Pharmacia* **70**:395–403.

KuKanich B, and Hubin M (2010) The pharmacokinetics of ketoconazole and its effects on the pharmacokinetics of midazolam and fentanyl in dogs. *J Vet Pharmacol Ther* **33**:42–49.

Kumar Shivani, and Kumar Suresh (2019) Molecular Docking: A Structure-Based Approach for Drug Repurposing, in *In Silico Drug Design* pp 161–189, Elsevier.

Kuntz ID, Blaney JM, Oatley SJ, Langridge R, and Ferrin TE (1982) A geometric approach to macromolecule-ligand interactions. *J Mol Biol* **161**:269–288.

Kurokawa T, Fukami T, Yoshida T, and Nakajima M (2016) Arylacetamide Deacetylase is Responsible for Activation of Prasugrel in Human and Dog. *Drug Metabolism and Disposition* **44**:409–416.

Lascelles BDX, Court MH, Hardie EM, and Robertson SA (2007) Nonsteroidal anti-inflammatory drugs in cats: a review. *Vet Anaesth Analg* **34**:228–250.

Lee J, Yoo H-D, Bae J-W, Lee S, and Shin K-H (2019) Population pharmacokinetic analysis of tramadol and O-desmethyltramadol with genetic polymorphism of CYP2D6 . *Drug Des Devel Ther* **Volume 13**:1751–1761.

Lee Y, Park H-G, Kim V, Cho M-A, Kim H, Ho T-H, Cho KS, Lee I-S, and Kim D (2018) Inhibitory effect of α-terpinyl acetate on cytochrome P450 2B6 enzymatic activity. *Chem Biol Interact* **289**:90–97.

Leow JWH, and Chan ECY (2019) Atypical Michaelis-Menten kinetics in cytochrome P450 enzymes: A focus on substrate inhibition. *Biochem Pharmacol* **169**:113615.

Locke AB, Kirst N, and Shultz CG (2015) Diagnosis and management of generalized anxiety disorder and panic disorder in adults. *Am Fam Physician* **91**:617–24.

Lohning AE, Levonis SM, Williams-Noonan B, and Schweiker SS (2017) A Practical Guide to Molecular Docking and Homology Modelling for Medicinal Chemists. *Curr Top Med Chem* **17**.

Loiodice S, Nogueira da Costa A, and Atienzar F (2019) Current trends in in silico , in vitro toxicology, and safety biomarkers in early drug development. *Drug Chem Toxicol* **42**:113–121.

López V, Nielsen B, Solas M, Ramírez MJ, and Jäger AK (2017) Exploring pharmacological mechanisms of lavender (Lavandula angustifolia) essential oil on central nervous system targets. *Front Pharmacol* **8**:280, Frontiers Media SA.

Lu P, Singh SB, Carr BA, Fang Y, Xiang CD, Rushmore TH, Rodrigues AD, and Shou M (2005) Selective Inhibition of Dog Hepatic CYP2B11 and CYP3A12. *Journal of Pharmacology and Experimental Therapeutics* **313**:518–528.

Ma C, Peng Y, Li H, and Chen W (2021) Organ-on-a-Chip: A New Paradigm for Drug Development. *Trends Pharmacol Sci* **42**:119–133.

Mackenzie PI, Somogyi AA, and Miners JO (2017) Advances in drug metabolism and pharmacogenetics research in Australia. *Pharmacol Res* **116**:7–19.

Maeda K, Hisaka A, Ito K, Ohno Y, Ishiguro A, Sato R, and Nagai N (2021) Classification of drugs for evaluating drug interaction in drug development and clinical management. *Drug Metab Pharmacokinet* **41**:100414.

Mag P, Nemes-Terényi M, Jerzsele Á, and Mátyus P (2024) Some Aspects and Convergence of Human and Veterinary Drug Repositioning. *Molecules* **29**:4475.

Marnett LJ, Cohen SM, Fukushima S, Gooderham NJ, Hecht SS, Rietjens IMCM, Smith RL, Adams TB, Bastaki M, Harman CL, McGowen MM, and Taylor S V. (2014) GRASr2 Evaluation of Aliphatic Acyclic and Alicyclic Terpenoid Tertiary Alcohols and Structurally Related Substances Used as Flavoring Ingredients. *J Food Sci* **79**.

Martignoni M, Groothuis GMM, and de Kanter R (2006a) Species differences between mouse, rat, dog, monkey and human CYP-mediated drug metabolism, inhibition and induction. *Expert Opin Drug Metab Toxicol* **2**:875–894.

Martignoni M, Groothuis GMM, and de Kanter R (2006b) Species differences between mouse, rat, dog, monkey and human CYP-mediated drug metabolism, inhibition and induction. *Expert Opin Drug Metab Toxicol* **2**:875–894.

Martinez MN, Antonovic L, Court M, Dacasto M, Fink-Gremmels J, Kukanich B, Locuson C, Mealey K, Myers MJ, and Trepanier L (2013) Challenges in exploring the cytochrome P450 system as a source of variation in canine drug pharmacokinetics. *Drug Metab Rev* **45**:218–230.

Martinez MN, Court MH, Fink-Gremmels J, and Mealey KL (2018) Population variability in animal health: Influence on dose–exposure–response relationships: Part I: Drug metabolism and transporter systems. *J Vet Pharmacol Ther* **41**.

Martinez MN, Mochel JP, Neuhoff S, and Pade D (2021) Comparison of Canine and Human Physiological Factors: Understanding Interspecies Differences that Impact Drug Pharmacokinetics. *AAPS J* **23**:59.

Martinez SE, Andresen MC, Zhu Z, Papageorgiou I, and Court MH (2020) Pharmacogenomics of poor drug metabolism in Greyhounds: Cytochrome P450 (CYP) 2B11 genetic variation, breed distribution, and functional characterization. *Sci Rep* **10**:69.

Martinez SE, Pandey A V., Perez Jimenez TE, Zhu Z, and Court MH (2024) Pharmacogenomics of poor drug metabolism in greyhounds: Canine P450 oxidoreductase genetic variation, breed heterogeneity, and functional characterization. *PLoS One* **19**:e0297191.

Martinez SE, Shi J, Zhu H-J, Perez Jimenez TE, Zhu Z, and Court MH (2019) Absolute Quantitation of Drug-Metabolizing Cytochrome P450 Enzymes and Accessory Proteins in Dog Liver Microsomes Using Label-Free Standard-Free Analysis Reveals Interbreed Variability. *Drug Metabolism and Disposition* **47**:1314–1324.

Matos A, Bain KT, Bankes DL, Furman A, Skalski B, Verzicco J, and Turgeon J (2020) Cytochrome P450 (CYP450) Interactions Involving Atypical Antipsychotics Are Common in Community-Dwelling Older Adults Treated for Behavioral and Psychological Symptoms of Dementia. *Pharmacy* **8**:63.

McCaskill L (2021) The Use of Essential Oils in Traditional Chinese Veterinary Medicine: Small Animal Practice. *American Journal of Traditional Chinese Veterinary Medicine* 67–78.

Mealey KL, Jabbes M, Spencer E, and Akey JM (2008) Differential expression of CYP3A12 and CYP3A26 mRNAs in canine liver and intestine. *Xenobiotica* **38**:1305–1312.

Mealey KL, Martinez SE, Villarino NF, and Court MH (2019) Personalized medicine: going to the dogs? *Hum Genet* **138**:467–481.

Meesters RJW, Duisken M, and Hollender J (2007) Study on the cytochrome P450-mediated oxidative metabolism of the terpene alcohol linalool: Indication of biological epoxidation. *Xenobiotica* **37**:604–617.

Mekonnen A, Tesfaye S, Christos SG, Dires K, Zenebe T, Zegeye N, Shiferaw Y, and Lulekal E (2019) Evaluation of Skin Irritation and Acute and Subacute Oral Toxicity of Lavandula angustifolia Essential Oils in Rabbit and Mice. *J Toxicol* **2019**.

Miastkowska M, Kantyka T, Bielecka E, Kałucka U, Kamińska M, Kucharska M, Kilanowicz A, Cudzik D, and Cudzik K (2021) Enhanced Biological Activity of a Novel Preparation of Lavandula angustifolia Essential Oil. *Molecules* **26**:2458.

Mills BM, Zaya MJ, Walters RR, Feenstra KL, White JA, Gagne J, and Locuson CW (2010a) Current Cytochrome P450 Phenotyping Methods Applied to Metabolic Drug-Drug Interaction Prediction in Dogs. *Drug Metabolism and Disposition* **38**:396–404.

Mills BM, Zaya MJ, Walters RR, Feenstra KL, White JA, Gagne J, and Locuson CW (2010b) Current Cytochrome P450 Phenotyping Methods Applied to Metabolic Drug-Drug Interaction Prediction in Dogs. *Drug Metabolism and Disposition* **38**:396–404.

Miranda GMD, Mendes A da CG, and Silva ALA da (2016) Population aging in Brazil: current and future social challenges and consequences. *Revista Brasileira de Geriatria e Gerontologia* **19**:507–519.

Miyazawa M, and Gyoubu K (2007) Roles of human CYP2A6 and rat CYP2B1 in the oxidation of (**+**)-fenchol by liver microsomes. *Xenobiotica* **37**:943–953.

Miyazawa M, Shindo M, and Shimada T (2001) Roles of cytochrome P450 3A enzymes in the 2-hydroxylation of 1,4-cineole, a monoterpene cyclic ether, by rat and human liver microsomes. *Xenobiotica* **31**:713–723.

Mohebbi A (2023) Ligand-based 3D pharmacophore modeling, virtual screening, and molecular dynamic simulation of potential smoothened inhibitors. *J Mol Model* **29**:143.

Mondal G, Dale OR, Wang Y-H, Khan SI, Khan IA, and Yates CR (2023) In Vitro Metabolism and CYP-Modulating Activity of Lavender Oil and Its Major Constituents. *Molecules* **28**:755.

Montibeler J, Domingos T da S, Braga EM, Gnatta JR, Kurebayashi LFS, and Kurebayashi AK (2018) Efetividade da massagem com aromaterapia no estresse da equipe de enfermagem do centro cirúrgico: estudo-piloto. *Revista da Escola de Enfermagem da USP* **52**.

Morofuji Y, and Nakagawa S (2020) Drug Development for Central Nervous System Diseases Using In vitro Blood-brain Barrier Models and Drug Repositioning. *Curr Pharm Des* **26**:1466–1485.

Mössner LD, Schmitz A, Theurillat R, Thormann W, and Mevissen M (2011) Inhibition of cytochrome P450 enzymes involved in ketamine metabolism by use of liver microsomes and specific cytochrome P450 enzymes from horses, dogs, and humans. *Am J Vet Res* **72**:1505–1513.

Muegge I, and Mukherjee P (2016) An overview of molecular fingerprint similarity search in virtual screening. *Expert Opin Drug Discov* **11**:137–148.

Mueller RS, and Olivry T (2017) Critically appraised topic on adverse food reactions of companion animals (4): can we diagnose adverse food reactions in dogs and cats with in vivo or in vitro tests? *BMC Vet Res* **13**:275.

Muhammed MT, and Aki-Yalcin E (2019) Homology modeling in drug discovery: Overview, current applications, and future perspectives. *Chem Biol Drug Des* **93**:12–20.

Müller WE, Schuwald A, Nöldner M, Kasper S, and Friedland K (2015) Pharmacological basis of the therapeutic use of Silexan (Lasea®). *Psychopharmakotherapie* **22**:3–14.

Muntané-Relat J, Ourlin JC, Domergue J, and Maurel P (1995) Differential effects of cytokines on the inducible expression of cyp1a1, CYP1A2, and CYP3A4 in human hepatocytes in primary culture*1. *Hepatology* **22**:1143–1153.

Nath A, and Atkins WM (2006) A Theoretical Validation of the Substrate Depletion Approach to Determining Kinetic Parameters. *Drug Metabolism and Disposition* **34**:1433–1435.

Nicolas J-M, Chanteux H, Mancel V, Dubin G-M, Gerin B, Staelens L, Depelchin O, and Kervyn S (2014) N-Alkylprotoporphyrin Formation and Hepatic Porphyria in Dogs After Administration of a New Antiepileptic Drug Candidate: Mechanism and Species Specificity. *Toxicological Sciences* **141**:353–364.

Nishibe Y, Wakabayashi M, Harauchi T, and Ohno K (1998) Characterization of cytochrome P450 (CYP3A12) induction by rifampicin in dog liver. *Xenobiotica* **28**:549–557.

Nishimuta H, Nakagawa T, Nomura N, and Yabuki M (2013) Species differences in hepatic and intestinal metabolic activities for 43 human cytochrome P450 substrates between humans and rats or dogs. *Xenobiotica* **43**:948–955.

Nosková K, Dovrtělová G, Zendulka O, Řemínek R, and Juřica J (2016) The Effect of (-)-Linalool on the Metabolic Activity of Liver CYP Enzymes in Rats. *Physiol Res* S499–S504.

Obach RS (1999) Prediction of human clearance of twenty-nine drugs from hepatic microsomal intrinsic clearance data: An examination of in vitro half-life approach and nonspecific binding to microsomes. *Drug Metab Dispos* **27**:1350–9.

Obach RS, Baxter JG, Liston TE, Silber BM, Jones BC, Macintyre F, Rance DJ, and Wastall P (1997) The Prediction of Human Pharmacokinetic Parameters from Preclinical and In Vitro Metabolism Data. *Journal of Pharmacology and Experimental Therapeutics* **283**:46.

Obach RS, and Reed-Hagen AE (2002) Measurement of Michaelis Constants for Cytochrome P450-Mediated Biotransformation Reactions Using a Substrate Depletion Approach. *Drug Metabolism and Disposition* **30**:831–837.

Ohno M, Motojima K, Okano T, and Taniguchi A (2009) Induction of Drug-Metabolizing Enzymes by Phenobarbital in Layered Co-culture of a Human Liver Cell Line and Endothelial Cells. *Biol Pharm Bull* **32**:813–817.

Parkinson A, Kazmi F, Buckley DB, Yerino P, Ogilvie BW, and Paris BL (2010) System-Dependent Outcomes during the Evaluation of Drug Candidates as Inhibitors of Cytochrome P450 (CYP) and Uridine Diphosphate Glucuronosyltransferase (UGT) Enzymes: Human Hepatocytes versus Liver Microsomes versus Recombinant Enzymes. *Drug Metab Pharmacokinet* **25**:16–27.

Perez TE, Mealey KL, Grubb TL, Greene SA, and Court MH (2016) Tramadol Metabolism to O -Desmethyl Tramadol (M1) and N -Desmethyl Tramadol (M2) by Dog Liver Microsomes: Species Comparison and Identification of Responsible Canine Cytochrome P450s. *Drug Metabolism and Disposition* **44**:1963–1972.

Piñero J, Furlong LI, and Sanz F (2018) In silico models in drug development: where we are. *Curr Opin Pharmacol* **42**:111–121.

Pinzi L, and Rastelli G (2019) Molecular Docking: Shifting Paradigms in Drug Discovery. *Int J Mol Sci* **20**:4331.

Pokajewicz K, Białoń M, Svydenko L, Fedin R, and Hudz N (2021) Chemical Composition of the Essential Oil of the New Cultivars of Lavandula angustifolia Mill. Bred in Ukraine. *Molecules* **26**:5681.

Pokajewicz K, Białoń M, Svydenko L, Hudz N, Balwierz R, Marciniak D, and Wieczorek PP (2022) Comparative Evaluation of the Essential Oil of the New Ukrainian Lavandula angustifolia and Lavandula x intermedia Cultivars Grown on the Same Plots. *Molecules* **27**:2152.

Prusakiewicz JJ, Ackermann C, and Voorman R (2006) Comparison of Skin Esterase Activities from Different Species. *Pharm Res* **23**:1517–1524.

Qiao X, Wu X, Chen S, Niu M-M, Hua H, and Zhang Y (2024) Discovery of novel and potent dual-targeting AXL/HDAC2 inhibitors for colorectal cancer treatment via structure-based pharmacophore modelling, virtual screening, and molecular docking, molecular dynamics simulation studies, and biological evaluation. *J Enzyme Inhib Med Chem* **39**.

Rai VK, Sinha P, Yadav KS, Shukla A, Saxena A, Bawankule DU, Tandon S, Khan F, Chanotiya CS, and Yadav NP (2020) Anti-psoriatic effect of Lavandula angustifolia essential oil and its major components linalool and linalyl acetate. *J Ethnopharmacol* **261**:113127.

Ramirez Rozzi F, and Froment A (2018) Earliest Animal Cranial Surgery: from Cow to Man in the Neolithic. *Sci Rep* **8**:5536.

Ramos CAF, Sá R de C da S, Alves MF, Benedito RB, de Sousa DP, Diniz M de FFM, Araújo MST, and de Almeida RN (2015) Histopathological and biochemical assessment of d -limonene-induced liver injury in rats. *Toxicol Rep* **2**:482–488.

Rane A, Wilkinson GR, and Shand DG (1977) Prediction of hepatic extraction ratio from in vitro measurement of intrinsic clearance. *Journal of Pharmacology and Experimental Therapeutics* **200**:420–424, ASPET.

Rang R, Ritter JM, Flower RJ, and Henderson G (2011) *Rang & Dale Farmacologia*, 7th ed., Elsevier Brasil, Rio de Janeiro.

Rebehmed J, de Brevern AG, Sowdhamini R, and Joseph AP (2022) Editorial: Advances in Molecular Docking and Structure-Based Modelling. *Front Mol Biosci* **9**.

Relling M V., and Evans WE (2015) Pharmacogenomics in the clinic. *Nature* **526**:343–350.

Renganathan V, and Madyastha KM (1983) Linalyl Acetate Is Metabolized by Pseudomonas incognita with the Acetoxy Group Intact. *Appl Environ Microbiol* **45**:6–15.

Riley RJ, and Wilson CE (2015) Cytochrome P450 time-dependent inhibition and induction: advances in assays, risk analysis and modelling. *Expert Opin Drug Metab Toxicol* **11**:557–572.

Ring CS, Sun E, McKerrow JH, Lee GK, Rosenthal PJ, Kuntz ID, and Cohen FE (1993) Structure-based inhibitor design by using protein models for the development of

antiparasitic agents. *Proceedings of the National Academy of Sciences* **90**:3583–3587.

Roden DM, McLeod HL, Relling M V, Williams MS, Mensah GA, Peterson JF, and Van Driest SL (2019) Pharmacogenomics. *The Lancet* **394**:521–532.

Roman LJ, Palmer CNA, Clark JE, Muerhoff AS, Griffin KJ, Johnson EF, and Masters BSS (1993) Expression of Rabbit Cytochromes P4504A Which Catalyze the ω-Hydroxylation of Arachidonic Acid, Fatty Acids, and Prostaglandins. *Arch Biochem Biophys* **307**:57–65.

Roussel F, Duignan DB, Lawton MP, Obach RS, Strick CA, and Tweedie DJ (1998) Expression and Characterization of Canine Cytochrome P450 2D15. *Arch Biochem Biophys* **357**:27–36.

Sakkas H, and Papadopoulou C (2017) Antimicrobial Activity of Basil, Oregano, and Thyme Essential Oils. *J Microbiol Biotechnol* **27**:429–438.

Samojlik I, Petković S, Mimica-Dukić N, and Božin B (2012) Acute and Chronic Pretreatment with Essential Oil of Peppermint (Mentha × piperita L., Lamiaceae) Influences Drug Effects. *Phytotherapy Research* **26**:820–825.

Samojlik I, Petković S, Stilinović N, Vukmirović S, Mijatović V, and Božin B (2016) Pharmacokinetic Herb-Drug Interaction between Essential Oil of Aniseed (Pimpinella anisum L., Apiaceae) and Acetaminophen and Caffeine: A Potential Risk for Clinical Practice. *Phytotherapy Research* **30**:253–259.

Sampathkumar K, and Kerwin BA (2024) Roadmap for Drug Product Development and Manufacturing of Biologics. *J Pharm Sci* **113**:314–331, Elsevier.

Sarkar S (2017) Psychiatric Polypharmacy, Etiology and Potential Consequences. *Curr Psychopharmacol* **6**:12–26.

Sattayakhom A, Wichit S, and Koomhin P (2023) The Effects of Essential Oils on the Nervous System: A Scoping Review. *Molecules* **28**:3771.

Sayed AM, Morsy S, Tawfik GM, Naveed S, Minh-Duc NT, Hieu TH, Ali ZA, Shinkar A, Doheim MF, Hashan MR, and Huy NT (2020) The best route of administration of lavender for anxiety: a systematic review and network meta-analysis. *Gen Hosp Psychiatry* **64**:33–40.

Schlacher A, Stanzer T, Osprian I, Mischitz M, Klingsbichel E, Faber K, and Schwab H (1998) Detection of a new enzyme for stereoselective hydrolysis of linalyl acetate using simple plate assays for the characterization of cloned esterases from Burkholderia gladioli. *J Biotechnol* **62**:47–54.

Schnell S (2014) Validity of the Michaelis–Menten equation – steady-state or reactant stationary assumption: that is the question. *FEBS J* **281**:464–472.

Seangseerattanakulchai K, and Piratae S (2021) Drug resistance in blood parasitic infections in cattle: a review. *Ann Parasitol* **67**:583–590.

Sharer JE, Shipley LA, Vandenbranden MR, Binkley SN, and Wrighton SA (1995) Comparisons of phase I and phase II in vitro hepatic enzyme activities of human, dog, rhesus monkey, and cynomolgus monkey. *Drug Metab Dispos* **23**:1231–41.

Shin Y, Choi C, Oh ES, Kim CO, Park K, and Park MS (2022) Effect of Rifampicin on the Pharmacokinetics of Evogliptin in Healthy Volunteers. *Drug Des Devel Ther* **Volume 16**:4301–4310.

Shou M, Norcross R, Sandig G, Lu P, Li Y, Lin Y, Mei Q, Rodrigues AD, and Rushmore TH (2003) SUBSTRATE SPECIFICITY AND KINETIC PROPERTIES OF SEVEN HETEROLOGOUSLY EXPRESSED DOG CYTOCHROMES P450. *Drug Metabolism and Disposition* **31**:1161–1169.

Sim DS, and Kauser K (2015) In Vivo Target Validation Using Biological Molecules in Drug Development, in pp 59–70.

Soares-Santos RR, Machado DP, Romero TL, and Duarte IDG (2024) Nitric oxide and potassium channels but not opioid and cannabinoid receptors mediate tramadol-induced peripheral antinociception in rat model of paw pressure withdrawal. *Can J Physiol Pharmacol* **102**:218–227.

Sodhi JK, and Benet LZ (2021) Successful and Unsuccessful Prediction of Human Hepatic Clearance for Lead Optimization. *J Med Chem* **64**:3546–3559.

Srinivasan B (2022) A guide to the Michaelis–Menten equation: steady state and beyond. *FEBS J* **289**:6086–6098.

Starkey ES, and Sammons HM (2015) Practical pharmacokinetics: what do you really need to know? *Arch Dis Child Educ Pract Ed* **100**:37–43.

Taketani M, Shii M, Ohura K, Ninomiya S, and Imai T (2007) Carboxylesterase in the liver and small intestine of experimental animals and human. *Life Sci* **81**:924–932.

Tan L, Liao F, Long L, Ma X, Peng Y, Lu J, Qu H, and Fu C (2023a) Essential oils for treating anxiety: a systematic review of randomized controlled trials and network meta-analysis. *Front Public Health* **11**.

Tan L, Liao F, Long L, Ma X, Peng Y, Lu J, Qu H, and Fu C (2023b) Essential oils for treating anxiety: a systematic review of randomized controlled trials and network meta-analysis. *Front Public Health* **11**.

Tasaki T, Nakamura A, Itoh S, Ohashi K, Yamamoto Y, Masuda M, Iwata H, Kazusaka A, Kamataki T, and Fujita S (1998) Expression and Characterization of Dog CYP2D15 Using Baculovirus Expression System. *J Biochem* **123**:162–168.

Tenmizu D, Endo Y, Noguchi K, and Kamimura H (2004) Identification of the novel canine CYP1A2 1117 C>;T SNP causing protein deletion. *Xenobiotica* **34**:835–846.

Trepanier LA (2006) Cytochrome P450 and Its Role in Veterinary Drug Interactions. *Veterinary Clinics of North America: Small Animal Practice* **36**:975–985.

Turner M (2011) Call to curb lab tests on dogs. *Nature* **474**:551–551.

Turpeinen M, Ghiciuc C, Opritoui M, Tursas L, Pelkonen O, and Pasanen M (2007) Predictive value of animal models for human cytochrome P450 (CYP)-mediated metabolism: A comparative study in vitro. *Xenobiotica* **37**:1367–1377.

Uehleke B, Schaper S, Dienel A, Schlaefke S, and Stange R (2012) Phase II trial on the effects of Silexan in patients with neurasthenia, post-traumatic stress disorder or somatization disorder. *Phytomedicine* **19**:665–671.

Umeda S, Harakawa N, Yamamoto M, and Ueno K (2005) Effect of Nonspecific Binding to Microsomes and Metabolic Elimination of Buprenorphine on the Inhibition of Cytochrome P4502D6. *Biol Pharm Bull* **28**:212–216.

Vamathevan JJ, Hall MD, Hasan S, Woollard PM, Xu M, Yang Y, Li X, Wang X, Kenny S, Brown JR, Huxley-Jones J, Lyon J, Haselden J, Min J, and Sanseau P (2013) Minipig and beagle animal model genomes aid species selection in pharmaceutical discovery and development. *Toxicol Appl Pharmacol* **270**:149–157.

van den Anker J, Reed MD, Allegaert K, and Kearns GL (2018) Developmental Changes in Pharmacokinetics and Pharmacodynamics. *The Journal of Clinical Pharmacology* **58**.

van Rossum JM (1963) THE RELATION BETWEEN CHEMICAL STRUCTURE AND BIOLOGICAL ACTIVITY.

Vercelli C, Pasquetti M, Giovannetti G, Visioni S, Re G, Giorgi M, Gambino G, and Peano A (2021) In vitro and in vivo evaluation of a new phytotherapic blend to treat acute externa otitis in dogs. *J Vet Pharmacol Ther* **44**:910–918.

Villa RE, Azimonti G, Bonos E, Christensen H, Durjava M, Dusemund B, Gehring R, Glandorf B, Kouba M, López-Alonso M, Marcon F, Nebbia C, Pechová A, Prieto-Maradona M, Röhe I, Theodoridou K, Bastos M de L, Brantom P, Chesson A, Schlatter J, Westendorf J, and Manini P (2024) Safety and efficacy of a feed additive consisting of an essential oil derived from the flowering tops of Lavandula angustifolia Mill. (lavender oil) for use in all animal species (FEFANA asbl). *EFSA Journal* **22**.

Visser M, Zaya MJ, Locuson CW, Boothe DM, and Merritt DA (2019) Comparison of predicted intrinsic hepatic clearance of 30 pharmaceuticals in canine and feline liver microsomes. *Xenobiotica* **49**:177–186.

Volpe DA, Xu Y, Sahajwalla CG, Younis IR, and Patel V (2018) Methadone Metabolism and Drug-Drug Interactions: In Vitro and In Vivo Literature Review. *J Pharm Sci* **107**:2983–2991.

Vora LK, Gholap AD, Hatvate NT, Naren P, Khan S, Chavda VP, Balar PC, Gandhi J, and Khatri DK (2024) Essential oils for clinical aromatherapy: A comprehensive review. *J Ethnopharmacol* **330**:118180.

Wagner JG (1973) Properties of the Michaelis-Menten equation and its integrated form which are useful in pharmacokinetics. *J Pharmacokinet Biopharm* **1**:103–121.

Wang Y, Huang J, Lin X, Su W, Zhu P, Yang N, and Adams E (2024) Recent progress in the extraction of terpenoids from essential oils and separation of the enantiomers by GC–MS. *J Chromatogr A* **1730**:465118.

Wang Y, Li L, Chen T, Chen W, and Xu Y (2013) Microsecond molecular dynamics simulation of Aβ42 and identification of a novel dual inhibitor of Aβ42 aggregation and BACE1 activity. *Acta Pharmacol Sin* **34**:1243–1250.

Wang Y-Q, Shang X-F, Wang L, Zhang P, Zou L-W, Song Y-Q, Hao D-C, Fang S-Q, Ge G-B, and Tang H (2020) Interspecies variation of clopidogrel hydrolysis in liver microsomes from various mammals. *Chem Biol Interact* **315**:108871.

Ward KW, Nagilla R, and Jolivette LJ (2005) Comparative evaluation of oral systemic exposure of 56 xenobiotics in rat, dog, monkey and human. *Xenobiotica* **35**:191–210.

Waring RH (2020) Cytochrome P450: genotype to phenotype. *Xenobiotica* **50**:9–18.

Watson F, Rusbridge C, Packer RMA, Casey RA, Heath S, and Volk HA (2018) A review of treatment options for behavioural manifestations of clinical anxiety as a comorbidity in dogs with idiopathic epilepsy. *The Veterinary Journal* **238**:1–9.

Webb B, and Sali A (2016) Comparative Protein Structure Modeling Using MODELLER. *Curr Protoc Bioinformatics* **54**.

Wermuth CG, Ganellin CR, Lindberg P, and Mitscher LA (1998) Glossary of terms used in medicinal chemistry (IUPAC Recommendations 1998). *Pure and Applied Chemistry* **70**:1129–1143.

Wilkinson PaulK (1980) Pharmacokinetics of Ethanol: A Review. *Alcohol Clin Exp Res* **4**:6–21.

William Montagna, and Victor R Formisano (1955) Esterase activity in the skin of mammals. *J Anat* **89**:425–9.

Woelk H, and Schläfke S (2010) A multi-center, double-blind, randomised study of the Lavender oil preparation Silexan in comparison to Lorazepam for generalized anxiety disorder. *Phytomedicine* **17**:94–99.

Wohlleben W, Mast Y, Stegmann E, and Ziemert N (2016) Antibiotic drug discovery. *Microb Biotechnol* **9**:541–548.

Wolber G, and Langer T (2005) LigandScout: 3-D Pharmacophores Derived from Protein-Bound Ligands and Their Use as Virtual Screening Filters. *J Chem Inf Model* **45**:160–169.

Xia S, Chen E, and Zhang Y (2023) Integrated Molecular Modeling and Machine Learning for Drug Design. *J Chem Theory Comput* **19**:7478–7495.

Xiao Y, Xue X, Wu Y, Xin G, Qian Y, Xie T, Gong L, and Ren J (2009) β-Naphthoflavone protects mice from aristolochic acid-I-induced acute kidney injury in a CYP1A dependent mechanism. *Acta Pharmacol Sin* **30**:1559–1565.

Xing J (2021) Development in Drug Metabolite Profiling (Part-I). *Curr Drug Metab* **22**:836–837.

Xiong G, Wu Z, Yi J, Fu L, Yang Z, Hsieh C, Yin M, Zeng X, Wu C, Lu A, Chen X, Hou T, and Cao D (2021) ADMETlab 2.0: an integrated online platform for accurate and comprehensive predictions of ADMET properties. *Nucleic Acids Res* **49**:W5–W14.

Yang J, Patel M, Nikanjam M, Capparelli E V., Tsunoda SM, Greenberg HE, Penzak SR, Aubrey Stoch S, Bertino JS, Nafziger AN, and Ma JD (2018) Midazolam Single Time Point Concentrations to Estimate Exposure and Cytochrome P450 (CYP) 3A Constitutive Activity Utilizing Limited Sampling Strategy With a Population Pharmacokinetic Approach. *The Journal of Clinical Pharmacology* **58**:1205–1213.

Yoshida T, Fukami T, Kurokawa T, Gotoh S, Oda A, and Nakajima M (2018) Difference in substrate specificity of carboxylesterase and arylacetamide deacetylase between dogs and humans. *European Journal of Pharmaceutical Sciences* **111**:167–176.

You J, Shin YK, and Seol GH (2024) Alleviating effect of lavender (Lavandula angustifolia) and its major components on postherpetic pain: a randomized blinded controlled trial. *BMC Complement Med Ther* **24**:54.

Yuan X, and Xu Y (2018) Recent Trends and Applications of Molecular Modeling in GPCR–Ligand Recognition and Structure-Based Drug Design. *Int J Mol Sci* **19**:2105.

Zárybnický T, Boušová I, Ambrož M, and Skálová L (2018) Hepatotoxicity of monoterpenes and sesquiterpenes. *Arch Toxicol* **92**:1–13.

Zelko I, and Negishi M (2000) Phenobarbital-Elicited Activation of Nuclear Receptor CAR in Induction of Cytochrome P450 Genes. *Biochem Biophys Res Commun* **277**:1–6.

Zeng W, Gui L, Tan X, Zhu P, Hu Y, Wu Q, Li X, Yang L, Jia W, Liu C, and Lan K (2021) Tertiary Oxidation of Deoxycholate Is Predictive of CYP3A Activity in Dogs. *Drug Metabolism and Disposition* **49**:369–378.

Zhang Y, Long Y, Yu S, Li D, Yang M, Guan Y, Zhang D, Wan J, Liu S, Shi A, Li N, and Peng W (2021) Natural volatile oils derived from herbal medicines: A promising therapy way for treating depressive disorder. *Pharmacol Res* **164**:105376.

Zhang Z, Schwartz S, Wagner L, and Miller W (2000) A Greedy Algorithm for Aligning DNA Sequences. *Journal of Computational Biology* **7**:203–214.

Zhao J, Jin X, Yang C, Quinto M, Shang H, and Li D (2020) Gas purge micro solvent extraction: A rapid and powerful tool for essential oil chromatographic fingerprints. *J Pharm Biomed Anal* **187**:113339.

Zhu Y, Xiao T, Lei S, Zhou F, and Wang M-W (2015) Application of chemical biology in target identification and drug discovery. *Arch Pharm Res* **38**:1642–1650.